\\

Analysis of the IMS Velocity Prediction Program
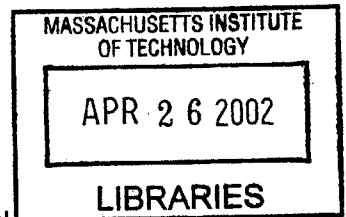
by

Claudio Cairoli

M.S. Mechanical and Aerospace Engineering
University of Virginia, 2000

SUBMITTED TO THE DEPARTMENT OF OCEAN ENGINEERING IN PARTIAL
FULFILLMENT OF THE REQUIREMENTS FOR THE DEGREE OF

MASTER OF SCIENCE
IN
NAVAL ARCHITECTURE AND MARINE ENGINEERING
AT THE
MASSACHUSETTS INSTITUTE OF TECHNOLOGY

FEBRUARY 2002

Signature of the Author:_____⟨

Department of Ocean Engineering
January 18, 2002

Certified by:_____   —

⟨⟩   Prof. Jerome H. Milgram
Professor of Ocean Engineering
Thesis Supervisor

Accepted by:_____

Prof. Henrik Schmidt
Chairman, Departmental Committee of Graduate Studies
Department of Ocean Engineering

Analysis of the IMS Velocity Prediction Program

by

Claudio Cairoli

Submitted to the Department of Ocean Engineering
on January 18, 2002 in Partial Fulfillment of the
Requirements for the Degree of Master of Science in
Naval Architecture and Marine Engineering

ABSTRACT

Experimentally measured values of resistance of different models were compared with prediction from the IMS Velocity Prediction Program (VPP) with the intent of determining the accuracy of the hydrodynamic model contained in the program. Each component of the resistance has been analyzed separately in order to determine the major sources of error. Results show that all the components are predicted by the IMS VPP with some error. However the ones with the least accuracy were found to be the upright and heeled canoe body residuary resistance. For these components a new model based on a Taylor expansion of the resistance with respect to characteristic parameters is proposed. Comparison of predictions thus obtained with experimental data show in most cases improved accuracy with respect to the current IMS formulation.

Table of Contents

List of Figures

List of Tables

1. Introduction

"It is the spirit and the intent of the rule to promote the racing of
seaworthy offshore racing yachts of various design, types and
construction on a fair and equitable basis."

Although this ambitious aim was stated in the introduction of the International Offshore Rule, or IOR, it stands as the basis of any modern racing rule. For more than a century yachting authorities in Europe and in North America have tried to devise a rule that fairly equates yachts of different sizes and speeds.

1.1 A Brief History of Offshore Racing Rules

Everything began in 1883, when the Seawanhaka Corinthian Yacht Club of Oyster Bay, Long Island, implemented a measurement formula, the *Seawanhaka Rule*, which took the boat's waterline length, added it to the square root of the sail area and then divided by two, to held level class racing, [Hodgson]. Similar developments were happening on the other side of the Atlantic, where, in England, the *Boat Racing Association Rule* was born in 1912 and adopted few years later for the Fastnet Race by the Royal Ocean Racing Club.

Despite of some weak efforts in the late 1920s, no attempts to unify the rules used in America and Europe were made until the 1960s, when rumors of a possible inclusion of an offshore racing class in 1968 Olympic Games put pressure on the yachting authorities to find a common rule. The *International Offshore Rule*, or IOR, was first presented in London at the 1968 meeting of the Offshore Rules Co-ordinating Committee, which recommended all the national authorities to adopt it for the 1969 season.

At the beginning of 1976, the Offshore Committee of US Sailing adopted a resolution calling for the development of a new "Handicapping System" to be used alongside the IOR for those yachtsmen who prefer a "handicap" rule as opposed to a "design" rule. The goal of the new rule was to protect the existing fleet from early obsolescence, in fact, because of developments in both design and construction materials, the changes that older yachts would have been required to stay truly competitive with new boats were becoming more and more numerous and expensive.

The system, then called *Measurement Handicapping System* or MHS, was based on the results of the research conducted at the Massachusetts Institute of Technology as part of the H. Irving Pratt Project. The research led to two major areas of development:

- a hull measuring device and its software companion, the Line Processing Program or LPP, made it possible to use integrated parameters rather than single point measurements, which had been previously created a lot of problems in getting accurate estimates of the parameters affecting the performance;

- a Velocity Prediction Program or VPP, based on the towing test results of series of systematically modified hull forms, predicted the yacht speed, and therefore the time allowances, for any sailing conditions using the parameters calculated by the LPP.

In 1985 the Offshore Racing Council introduced this system, renaming it the *International Measurement System* or IMS, as second international rule alongside the IOR, to provide time allowances for cruiser/racer type yachts that were not effectively rated by IOR. Finally the IMS now stands as the only internationally administered handicap rule, [ORC].

1.2 Objectives

A yacht velocity is predicted inside the VPP by finding the equilibrium of all the hydro- and aerodynamic forces acting on the boat. These forces are generally estimated using formulae derived through regression analysis of experimental data. This means that the VPP results are affected by some error. In [Milgram] it is shown that a difference of 1% in resistance affects the time to sail its normal race course by about 30 seconds, which is substantial in influencing win or loss. Although there the main reason of the example was to make the reader understand the importance of reducing the resistance of even 1%, it can be also used to show the importance of having mathematical models inside the VPP as accurate as possible.

A difference of 1% in drag is claimed to result in a difference of 0.3% in average speed and sailing time. In the 2001 Rolex IMS Offshore World Championship, held in Valencia, Spain, six of the seven races run were completed by the winner in about two hours or less (the last was a cruise race of about 12 hours). The average finish time of the winner is just shy of 100 minutes, and, in corrected time, an average of 4.6 boats finished within one minute of the winner, that is within about 1% of the total sailing time.

The objectives of this work were first to evaluate, and eventually improve, the accuracy of the VPP hydrodynamic model by comparing the prediction with experimental data. This is done using the total resistance as well as single components of it that can be isolated and analyzed individually.

Already from preliminary stages of the analysis of the data it appeared clearly that the currently used formulation of the hydrodynamic model of the VPP did not achieve a sufficient global level of accuracy. From further investigation it was found that, of all the components of resistance, only the induced drag and the viscous resistance are handled properly. The residuary resistance model for the appendages and even more the one for the canoe body were found in need of improvements. Due to the limited amount of data and to the level of accuracy, it was decided to concentrate the efforts in improving the canoe body model, leaving developments for the appendages for future work. The residuary resistance multipliers, that in the VPP are used to obtain the heeled residuary resistance from the upright value, were found to perform poorly too.

An alternative model for the bare hull, which is intended to work in both upright and heeled condition, is proposed. The idea behind it is to have a single formula for the residuary resistance, which would use upright or heeled parameters, depending on the particular condition considered.

1.3 Outline

In the next Chapter, the hydrodynamic model of the IMS Velocity Prediction Program is presented. Details are given about the formulations of the different components of the resistance. The following Chapter the boats and the corresponding models used for this work are described. It also includes an explanation of how the data measured at the towing tanks are expanded to full scale.

In Chapter 4, the current VPP formulation is analyzed. First the overall performance of the program are assessed by looking at the error in the predictions of the totals resistance, then to identify the sources of these errors, each individual component is compared with measured data.

The next Chapter opens with the description of the attempts made at trying to improve the accuracy of the appendage resistance. The main focus however is the development of a new formulation for the canoe body residuary resistance.

This thesis then ends with the conclusions and a discussion about future work.

2. IMS Velocity Prediction Program

2.1 What It Is and How It Works

The ultimate purpose of the Velocity Prediction Program, or VPP, is to provide a means of predicting the yacht speed for any prescribed sailing conditions. These are usually defined by the wind speed and the true wind angle, which is the angle between the course of the boat and the wind direction. The leeway angle is defined as the angle between the heading of the centerline of the vessel and its course. Using an iterative procedure the VPP finds the maximum boat speed V, the leeway angle λ and the heel angle ϕ at which the aerodynamic and hydrodynamic forces and moments are in equilibrium, as described by the following equations:

$$R(V,\phi,\lambda) = F_{AF}(V,\phi,\lambda)$$
$$F_{HH}(V,\phi,\lambda) = F_{AH}(V,\phi,\lambda)$$
$$M_H(V,\phi,\lambda) = M_A(V,\phi,\lambda)$$

F_{AF} and F_{AH} are the components in the direction of the course and perpendicular to the course of the sum of all the aerodynamic forces. In the same way, the resultant of the hydrodynamic forces is decomposed in the total resistance R, parallel to the yacht course, and in the hydrodynamic heel force, or side force, F_{HH}, normal to it. M_H is the hydromechanical righting moment, which counteracts the aerodynamic heeling moment M_A. Their vectors act in the direction of the boat centerline.

The use of the VPP is preceded by a run of the LPP or Line Processing Program. The LPP input is the detailed geometry of the hull, appendages, rig and sails, which are used to evaluate all the parameters, such as sailing length, prismatic coefficient, beam-draft ratio, etc., needed by the VPP.

2.2 Hydrodynamic Model

In this section the currently used hydrodynamic model is described. It has been found to be inaccurate in some parts. The research done for this thesis was aimed at improving this model.

To solve the equilibrium equations and find the boat speed, heel angle and leeway angle, it is necessary to evaluate, besides the aerodynamic forces acting on the sails, all the hydrodynamic forces acting on the hull. This is not done exactly by means of a complete numerical simulation of the boat, but approximately by modeling those forces either using simplified theories or regression analyses of experimental data.

For this scope, the resistance is decomposed into different contributions,

$$R = R_U + R_H + R_I + R_H$$

Eq. 2.1

R_U is the upright resistance, R_H is the resistance due to heel alone, R_I and R_W are respectively, the induced drag and the added resistance due to waves. Since all the boats were tested in calm water, the resistance due to waves is not described here (more on it can be found in [Claughton]). The addictive decomposition, shown in Eq. 2.1, is not exact because it neglects interactions between the different components. However, it is the best we can do at this time. Furthermore, if the estimates of these resistance components are based on experiments with large models, estimates of the interaction effects are built into the resistance components. The closer the model is to full size, the more accurate will be the modeling of interaction effects. This is an important reason for using large scale models.

2.2.1 Yacht Sailing Length

Before starting the description of how the different components of the resistance are modeled inside the VPP, it is useful to understand how the LPP calculates the yacht sailing length L (see [Claughton]). This length plays a very important role because is the characteristic length used to calculate the Froude number as well as the Reynolds number. L is not an actual physical dimension, such as the designed waterline length, but rather an average of three characteristic lengths ($L_{SM,1}$, $L_{SM,2}$ and $L_{SM,4}$), as shown in Eq. 2.2

$$L = 0.3194\left(L_{SM,1} + L_{SM,2} + L_{SM,4}\right)$$

Eq. 2.2

These characteristic lengths are calculated from the second moment of area of the sectional area curve of the immersed part of the hull, as shown in Eq. 2.3

$$L_{SM,i} = 3.932\sqrt{\left(\frac{\int x^2 \sqrt[4]{s}\,dx}{\int \sqrt[4]{s}\,dx}\right) - \left(\frac{\int x^2 \sqrt[4]{s}\,dx}{\int \sqrt[4]{s}\,dx}\right)^2}$$

Eq. 2.3

Where s is the sectional area at position x along the waterline length. The index i, instead, refers to different floatation conditions:

11

- $i = 1$ corresponds to the condition with the yacht in equilibrium at zero heel and with displacement and longitudinal position of the center of gravity corresponding to an established racing condition;

- $i = 2$ corresponds to the condition where the displacement and longitudinal position of the center of gravity are the same as in the previous condition, but the yacht is heeled 2° and trimmed for equilibrium;

- $i = 4$ corresponds to a fictitious upright condition obtained by sinking the yacht 2.5% of $L_{SM,1}$ at the forward end and 3.75% of $L_{SM,1}$ at the aft end of the waterline.

The second condition is used to prevent exploitation of the rule by line distortion, while the sunken condition is used to account for the yachts overhangs that would be immersed when the vessel is sailing fast. The skipped number, 3, in the numeration is because in the original formulation L was the weighted average of four conditions, [Kerwin].

2.2.2 The Viscous Resistance

The upright resistance is the sum of the resistance due to the canoe body and the resistance due to the appendages. These two contributions can be both divided into a viscous part and a residuary, or wavemaking, part. Inside the VPP each of these four parts is modeled in a different way.

Originally the viscous resistance of the canoe body, $R_{V,CB}$, and of the appendages were calculated using a frictional coefficient based on their wetted surface area and dynamic pressure, which was determined from the 1957 ITTC model-ship correlation line, [Kerwin]. The Reynolds number Re used in the formula is based on using 70% of the actual yacht waterline length L_{WL} as the characteristic length. This is done to keep in account the fact that not all the streamlines are as long as the waterline length. This model is still used for the canoe body, even though now the sailing length L is used in the equation for the Reynolds number, as shown in Eq. 2.4

$$\text{Re} = \frac{0.7LV}{\nu}$$

$$C_F = \frac{0.075}{\left(\log(\text{Re}) - 2\right)^2}$$

$$R_{V,CB} = \frac{1}{2}\rho V^2 C_F A_{WS}$$

Eq. 2.4

where A_{WS} is the wetted surface area of the vessel.

For the appendages a more sophisticated scheme is now applied, [IMS]. Each of the appendages is now divided into five strips in the spanwise direction. The local Re is then evaluated and used, together with the thickness chord ratio, to determine the local frictional coefficient. The value of this local coefficient is obtained through the use of three baselines, which represent the

12

values of C_F in a transitional flow as function of Re for a flat plate, a 10% and a 20% thick foil, as shown in Figure 2.1.

The viscous resistance of each strip is then the product of the appropriate coefficient, the local dynamic pressure and the strip wetted surface area.

If the keel has a bulb present at its tip, so that it occupies part of the bottom strip, the bulb is transformed to an equivalent foil section and its viscous resistance is obtained the same way as described above. In more details the characteristics of the resultant foil section are calculated as follows:

- the equivalent chord is taken as the average of the top of the bottom strip and of the maximum chord occurring in the bottom strip;

- the equivalent thickness-chord ratio is obtained by dividing the bottom strip volume by the square of the equivalent chord times 0.66;

- the reference area is equal to half the actual wetted surface area of the bottom strip.
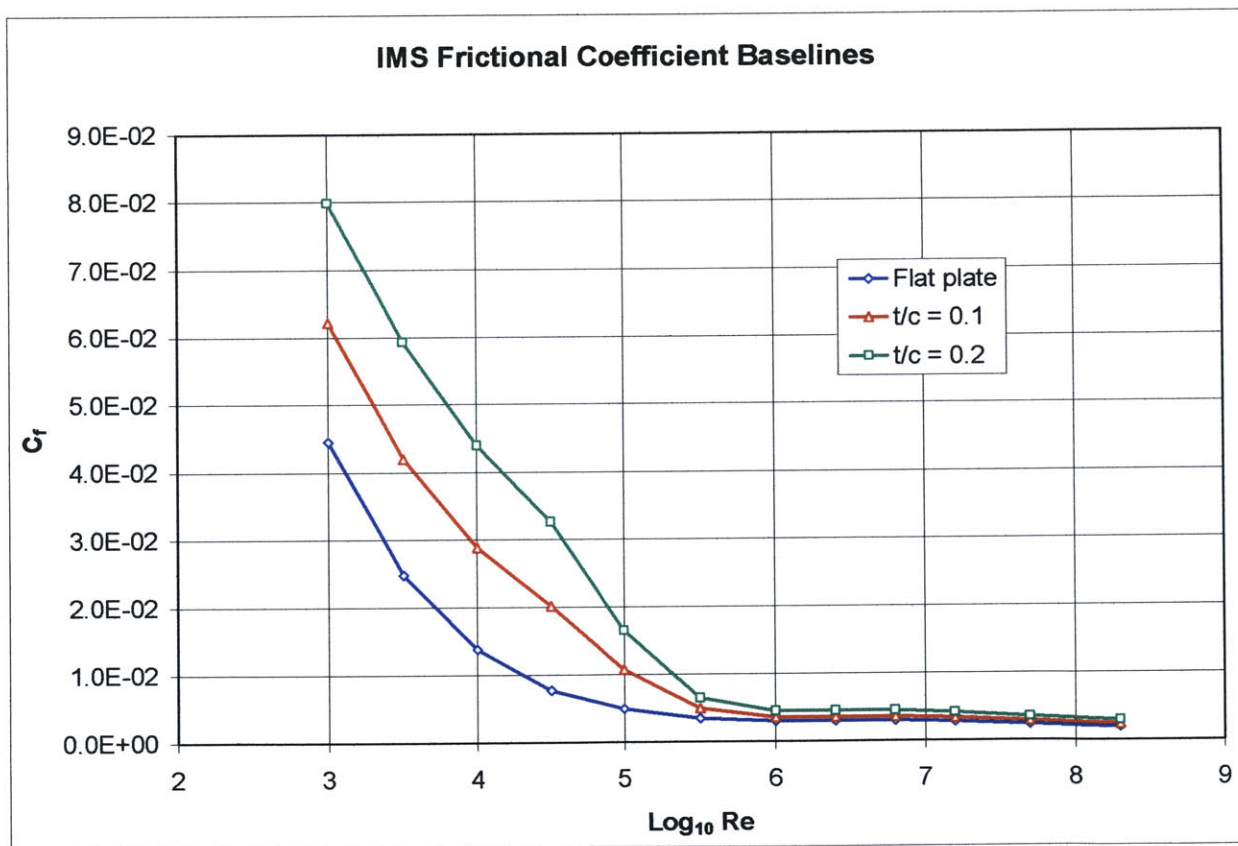
Figure 2.1 Frictional coefficient baselines for a flat plate, a 10% and a 20% thick foil.

13

2.2.3 The Residuary Resistance

Since the beginning, the determination of the residuary resistance of a sailing yacht has proven to be a very challenging task. The approach followed until now to obtain a formulation for this part of the resistance was to designed series of models of yachts with systematic variations of certain parameters and test them. Then, after determining the residuary part of the resistance through standard reduction procedures, a set of significant parameters was chosen and a regression analysis based on them was performed at different Froude numbers.

The number of parameters used has grown from three, in the original Pratt project formulation (beam-draft ratio, volumetric coefficient and displacement), to the current eight, as it can be seen from Eq. 2.5. While beam-draft ratio B/T_C, where T_C is the draft of the canoe body, and displacement Δ are still in use, the volumetric coefficient has been replaced by the length-volume ratio $L/\nabla^{1/3}$. The other parameters included are the canoe body prismatic coefficient C_P, the longitudinal position of the center of buoyancy L_{CB} and a waterplane area to canoe body volume ratio $A_{WP}/\nabla^{2/3}$. Also, at the time when the VPP was first proposed, the vast majority of boats had full keels, so that the interface between the appendages and the hull was usually difficult to identify. For this reason, the appendages were included in the total displacement in the calculations of residuary resistance. When modern designs went to more defined appendages (i.e. fin keel and separate rudder), this approach started to show its limitations, so a more sophisticated scheme, which involved separate formulations for appendages and canoe body, was introduced.

The current formulation for the canoe body is given by

$$C_R = a_0 + a_1 C_P + a_2 \frac{B}{T_C} + a_3 L_{VR} + a_4 \frac{A_{WP}}{\nabla^{2/3}} + a_5 \frac{L_{CB}}{L_{VR}} + a_6 \frac{L_{CB}^2}{L_{VR}} + a_7 L_{VR}^2$$

$$L_{VR} = \frac{L}{\nabla^{1/3}}$$

Eq. 2.5

where the residuary resistance coefficient C_R is

$$C_R = 1000 \frac{R_R}{\Delta}$$

and R_R is the residuary resistance. The coefficients a_i, with $i = 0,...,7$, are functions of the Froude number and they can be positive or negative.

The calculation for the appendages is more complicated. As for the viscous resistance, the appendages are divided into strips in the spanwise direction, then the volume and the average depth of each strip are calculated. The wavemaking resistance of a strip is based mainly on four factors:

- strip volume;

- average strip depth below the free surface;

- boat speed;

- presence of a bulb.

An algorithm for the resistance, sensitive to both volume and depth, was developed from numerical and experimental data: two baseline curves of drag per unit volume, normalized by Fr^2, vs. Fr, one for an element of fin keel at the standard depth of $0.1L$, the other for a bulb $0.2L$ deep, are now used to obtain the residuary resistance value for each strip.

2.2.4 Resistance Due to Heel

The VPP resistance predictions for the appendages are taken as independent of the heel angle, so the same formulations are used for both upright and heeled conditions. What changes with the heel are the prediction of viscous resistance for the canoe body and the presence of an extra term in the residuary part which takes into account the changes in length, and therefore in immersion, of the hull as it heels, as well as the asymmetry of it.

More precisely, the viscous resistance is still predicted using the first and second of Eq. 2.4, but now L and A_{WS} are the length and wetted surface area of the canoe body in the heeled condition.

For the residuary part, the current formulation assumes that the additional drag due to heel is someway proportional to the upright residuary drag. The multiplication factor depends on the heel angle directly, as well as on the ratio of length in heeled condition to upright length and on the length-volume ratio, as shown in the first of Eq. 2.6.

$$R_H(\phi) = \left[1 + K_H(\phi)\left(\frac{\phi}{25}\right)^2 \right] R_R(\text{Upright})$$

$$K_H(\phi) = \left\{ \left[1.25 + 2\left(0.985 - \frac{L_\phi}{L_0} \right) e^{-0.5Fr^2} \right] - 1 \right\} f_{LDR}$$

$$f_{LDR} = 0.3077 \frac{L}{\nabla^{1/3}} - 0.7692$$

Eq. 2.6

where

$$4.5 \le \frac{L}{\nabla^{1/3}} \le 8.5$$

2.2.5 Induced Drag

The induced drag R_I is the part of the resistance that is due to the fact that the appendages and the hull are producing a lifting force, which in this case is called heeling force F_H. This drag arises principally from the presence of tip vortices at the ends of keel and rudder, which shed energy into the flow. Traditionally this increase is considered to be dependent on the square of the generated lifting force. The current formulation was derived from the aerodynamic theory for a finite span, lifting surface.

15

$$R_I = \frac{F_H^2}{\pi \rho V^2 T_{EFF}}$$

where T_{EFF} is the effective draft, which was proportional to the static upright draft T_{IMS} calculated by the LPP, and V is the boat speed. It was soon found that this worked satisfactorily only at low heel angles. At higher speed and heel angles the root of the keel and rudder comes very close to the free surface, if not even out, thus affecting the wavemaking process. The magnitude of this effect was derived from tank test data and a correction factor $F(\phi, Fr, B/T)$ was introduced, as described in [IMS].

$$T_{EFF} = T_{IMS} F(\phi, Fr, B/T)$$
$$F(\phi, Fr, B/T) = \cos(\phi)^{Y-1}(0.915 - 0.105\tanh(X))G(T/L)$$
$$X = 10(Fr - (0.35 - 0.031(B/T - 5)))$$
$$Y = -0.305 + 0.77\,B/T$$

Eq. 2.7

$G(T/L)$ is an "unsteady empirical factor" added to the formulation to adjust for the fact that the performance of yachts with deeper keels, in particular in windward-leeward races, which involve a lot of tacking, seemed to be underpredicted.

3. Tank Tests

For this analysis a total of seven different models were used: four of them, Model 1, Model 4, Model 5 and Model 6, were tested at the towing tank of the Institute for Marine Dynamics (IMD) in St. John's, New Foundland, Canada. This tank is 200 *m* long, 12 *m* wide and 7 *m* deep, which allows testing of models up to 12 *m* in length, and has a high precision dynamometer developed specifically for testing sailing yachts. The remaining models, Model F, Model G and Model H were tested at the Wolfson Unit for Marine Technology and Industrial Aerodynamics at the University of Southampton, Southampton, England. This research center uses two different tanks depending on the size of the model to be tested: for models up to 2.5 *m* they use a 60 *m* long, 3.7 *m* wide, 1.8 *m* deep tank equipped with a dynamometer specifically designed for sailing vessels. For bigger models, up to 6 *m* long, the Defense Research Agency tank at Gosport, which is 258 *m* long, 12.2 *m* wide, 5.5 *m* deep, is used, again equipped with a Wolfson Unit designed towing system and dynamometer.

3.1 The Models

Model 4, Model 5 and Model 6 are a 1:2 scale beam series designed by James R. Teeters, specifically for this research project. The full-scale yachts have a waterline length (L_{WL}) of about 12.7 *m*, a displacement of about 9,100 *Kg*, with a beam-to-draft ratio (*BTR*) varying from 3.86 to 6.06. In this series Model 5 is the parent boat, Model 4 is the narrow one while Model 6 is the wide one.

In spite of the full-scale yachts for Model F, Model G and Model H being much bigger, with a waterline length in excess of 21 *m* and a displacement over 20,000 *Kg*, the models themselves are smaller, being a 1:9 scale. Designed by Langan Design, they too constitute a beam series, with beam-to-draft ratios going from 3.54 to 5.05. In this case, though, the parent boat is Model F, the narrow one is Model G while Model H is the wide boat.

Model 1 is a 1:2 scale of a yacht named NUMBERS, designed by Jim Taylor. The dimensions of NUMBERS are similar to those of the first three yachts, with a waterline length of 12.5 *m*, a displacement of 9,040 *Kg* and a beam-draft ratio of 5.19.

Table 3.1 reports the characteristic dimensions for the full-scale yachts.

Yachts Dimensions

	Model 1	Model 4	Model 5	Model 6	Model F	Model G	Model H
Waterline Length, [m]	12.494	12.47	12.465	12.438	20.806	20.794	20.796
Waterline Beam, [m]	3.413	2.92	3.294	3.73	4.11	3.716	4.512
Canoe Body Draft, [m]	0.658	0.757	0.685	0.615	0.966	0.953	0.893
Canoe Dispacement, [kg]	9039	9145	9136	9117	25956	25850	26014
Canoe Wetted Area, [m2]	39.584	36.276	38.651	40.954	80.494	77.065	83.778
Prismatic Coefficient	0.545	0.542	0.543	0.546	0.547	0.546	0.547

Table 3.1 Full scale yachts dimensions.

All the models tested at IMD have the same exact appendages, a trapezoidal fin keel and rudder. The English models, instead, have the same rudder, while the fin keels have different length and mount different bulbs. Appendages dimensions are given in Table 3.2.

Full Scale Appendages Dimensions

	IMD Models	Model F	Model G	Model H
Keel root chord	1.585	1.45	1.45	1.45
Keel tip chord	1.056	1.45	1.45	1.45
Keel span	2.45	2.819	2.708	2.96
Rudder root chord	0.688	0.75	0.75	0.75
Rudder tip chord	0.328	0.45	0.45	0.45
Rudder span	2.239	3.555	3.555	3.555
Bulb max chord		3.834	3.846	3.709
Bulb diameter		0.69	0.731	0.593

Table 3.2 All dimensions are in meters. For the IMD Models the thickness to chord ratio of the foils is 13%, for the others it is 16%.

3.2 Measured Data

All the models were tested in both appended and canoe body only configurations. In both cases, they were tested in upright position and at different heel angles, with and without leeway.

The conditions, though, were not exactly the same for all the models. The ones tested in Canada, besides in the upright condition, were tested at two different heel angles, namely 15° and 25°. At each angle, runs were made at a wide range of speeds when no leeway was used.

Five different heel angles (0°, 10°, 20°, 25° and 30°) were used in the tests conducted in England. Here, when a model was tested in the canoe body only configuration, for each heel angle, measurements were taken consistently throughout the range of speeds corresponding to reasonable sailing conditions, for the full-scale yacht. Differently, for the appended models a wide range of speeds, similar to the one used for the canoe body only configurations, was tested only in the upright condition, limiting the number of speeds tested at non-zero heel angle to as few as three.
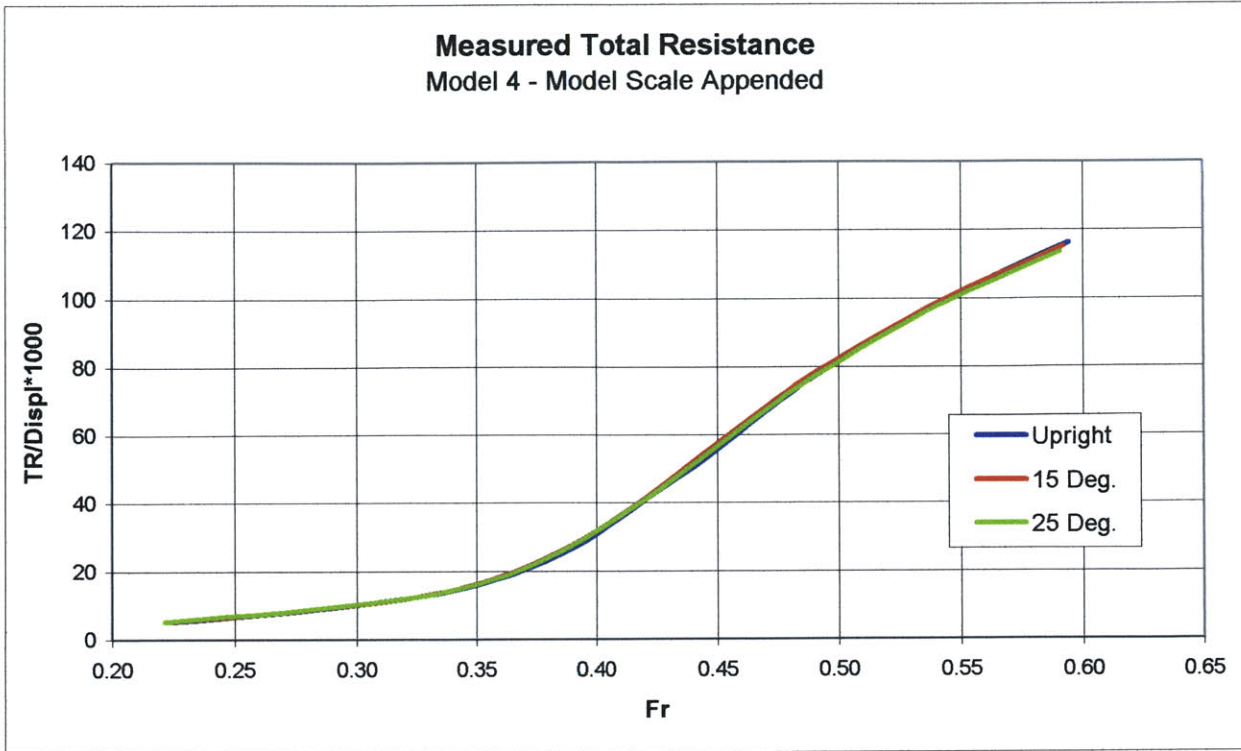
18

Figure 3.1 Measured total resistance for Model 4.
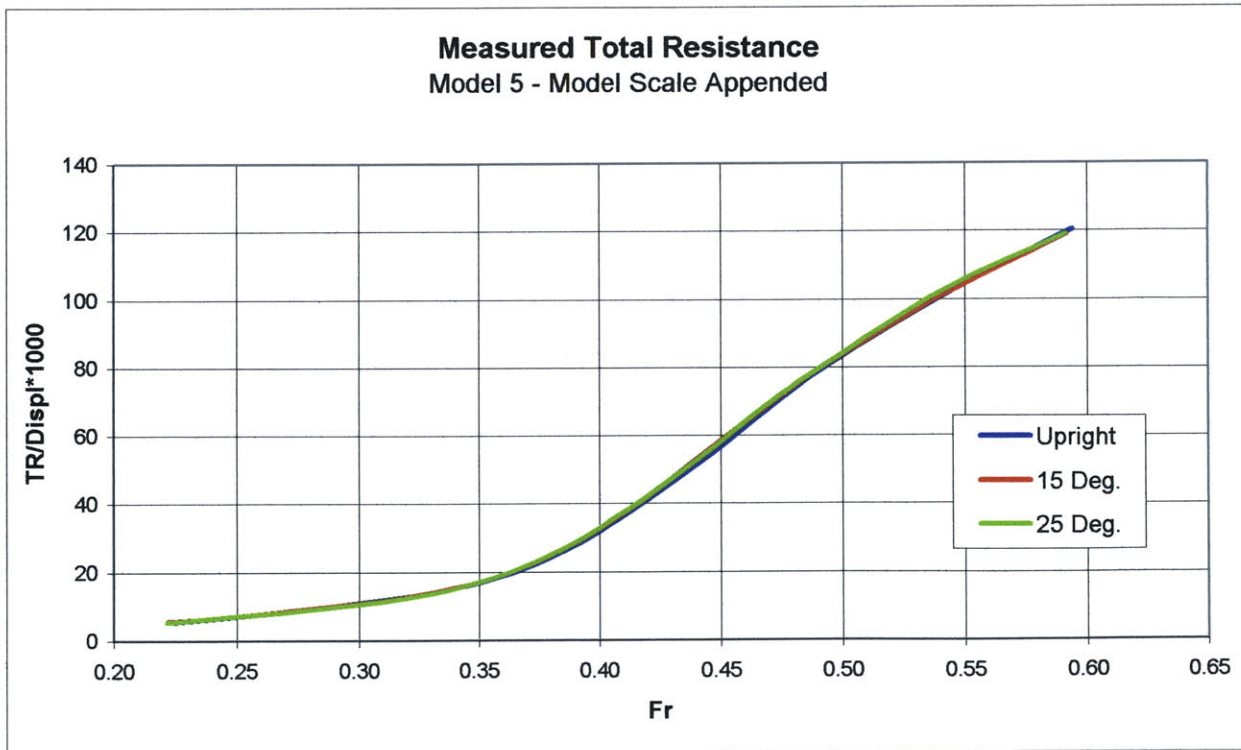

Figure 3.2 Measured total resistance for Model 5.
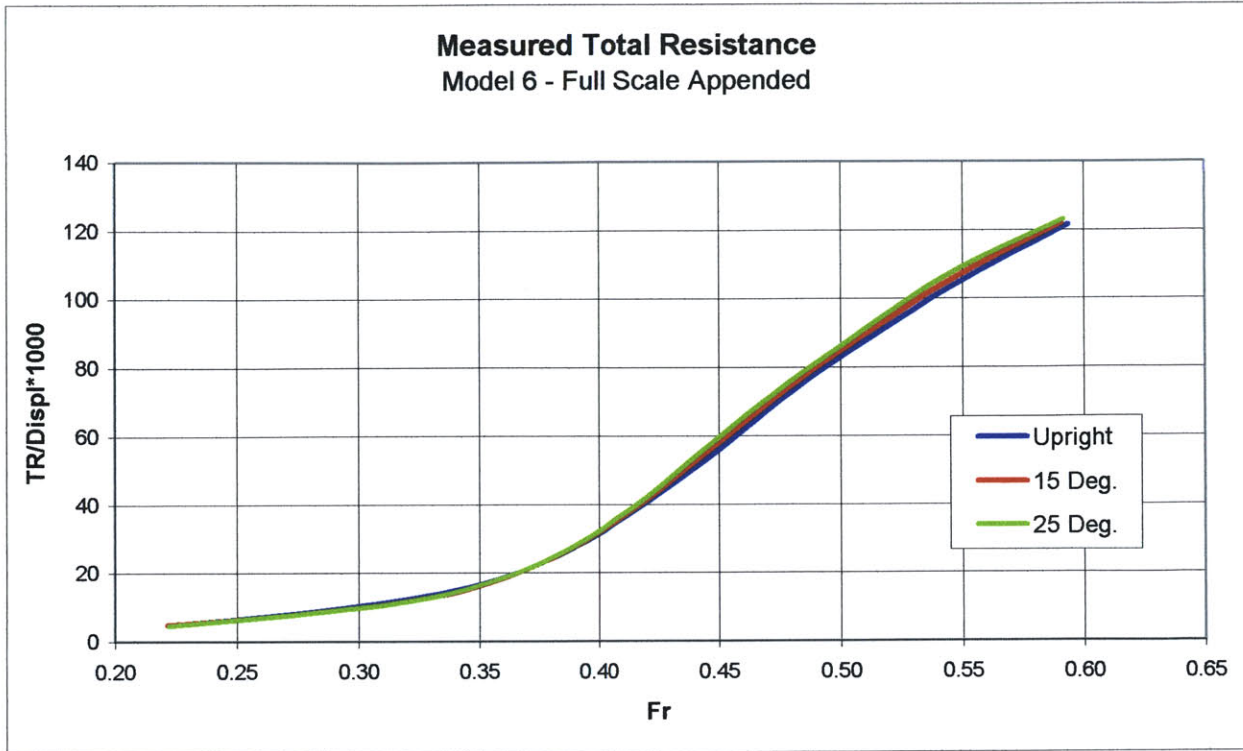
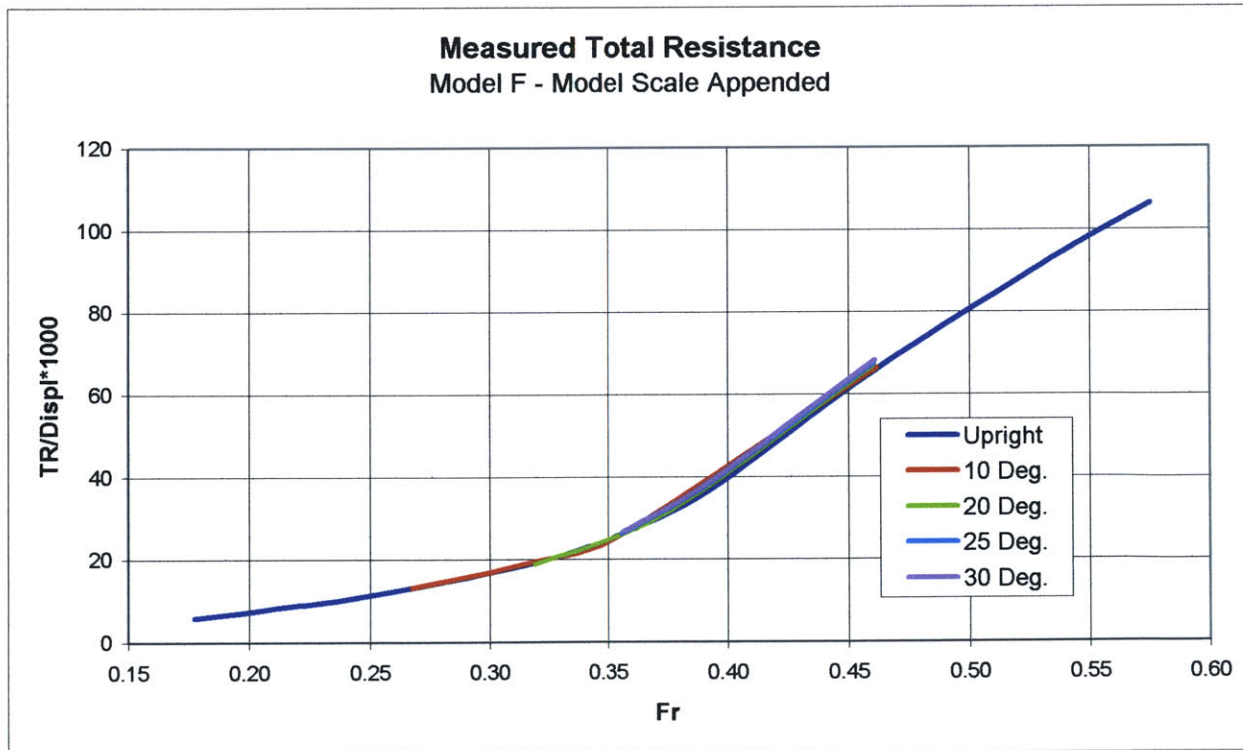**Figure 3.3 Measured total resistance for Model 6.**

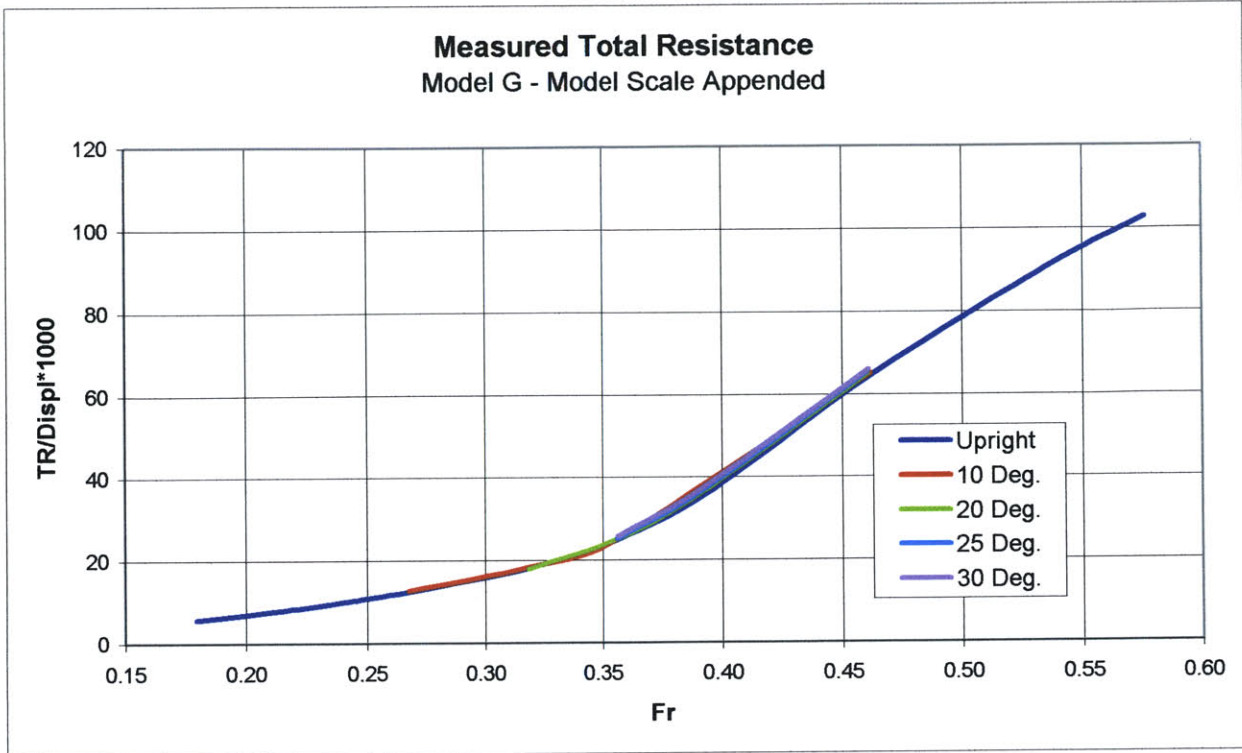**Figure 3.4 Measured total resistance for Model F.**

20

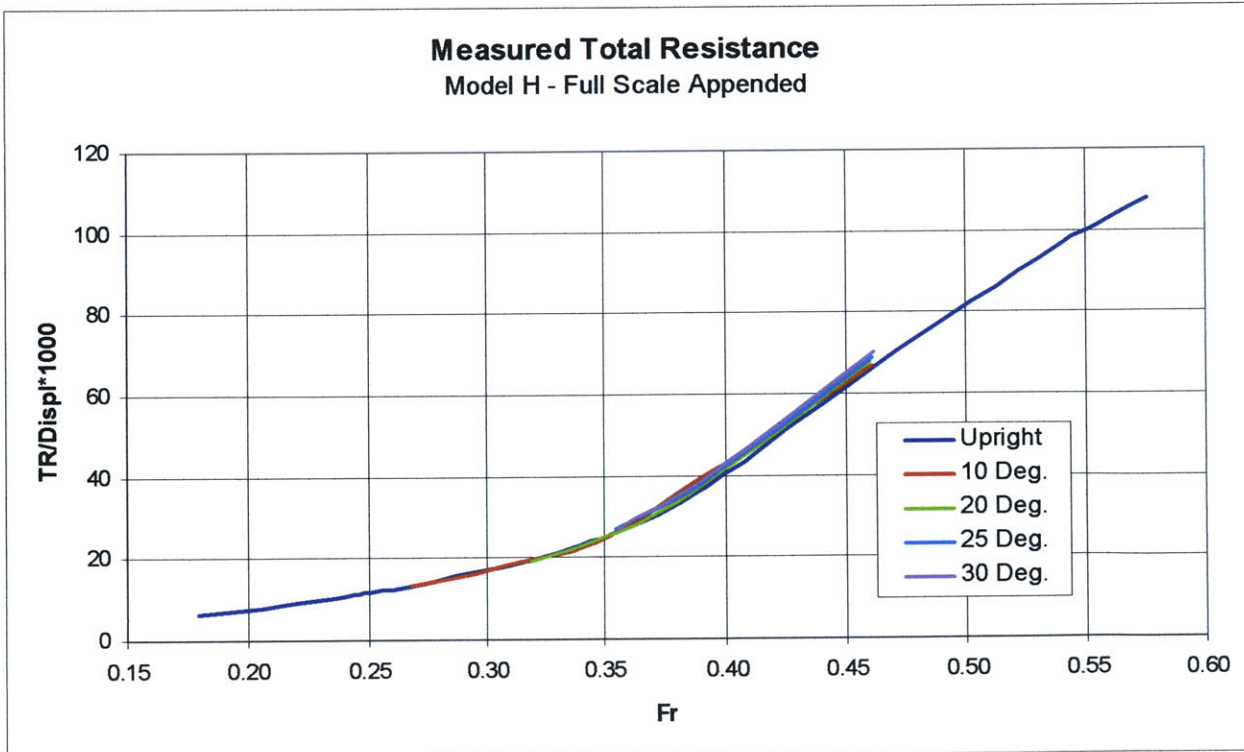**Figure 3.5 Measured total resistance for model G.**

Figure 3.6 Measured total resistance for Model H.

The data recorded and the format used by the two towing tank facilities were the same. In each run the following quantities were logged:

- model speed;

- lift and drag forces;

- roll and yaw moments;

- model sinkage and trim;

- water temperature.

Figure 3.7 shows part of the file for one of the boats provided to the author by one of the towing tank facilities.

Test	Date	Time	Heel (deg)	Yaw (deg)	Tab (deg)	Rudder (deg)	Trim Moment (N-m)	Vertical Force (N)	Vm (m/s)	Drag (N)	Lift (N)	Roll Moment (N-m)	Yaw Moment (N-m)	Sinkage (m)	Trim (deg)	Temp (deg C)
USSA04A_015	28-Mar-99	15:38:59	0	0	0	0	162	0	1.7587	68.726	1.921	3.8030	-1.7030	0.0094	0.1931	15.4
USSA04A_016	28-Mar-99	15:50:14	0	0	0	0	228	0	1.9536	86.479	-17.316	-18.6025	-3.0275	0.0120	0.1596	15.4
USSA04A_017	28-Mar-99	15:57:22	0	0	0	0	261	0	2.1496	108.437	-1.956	-0.4136	-2.3433	0.0152	0.1519	15.4
USSA04A_018	28-Mar-99	16:10:03	0	0	0	0	359	0	2.3445	133.285	-6.975	-6.2602	-3.2263	0.0186	0.0950	15.5
USSA04A_019	28-Mar-99	16:19:09	0	0	0	0	424	0	2.5402	162.934	5.037	8.2093	0.4938	0.0223	0.0559	15.5
USSA04A_020	28-Mar-99	16:28:40	0	0	0	0	554	0	2.7348	203.650	-4.061	-1.5185	-3.4423	0.0277	0.0118	15.5
USSA04A_021	28-Mar-99	16:39:47	0	0	0	0	750	0	2.9317	267.327	-2.210	1.0035	-5.0961	0.0338	0.0078	15.5
USSA04A_022	28-Mar-99	16:51:57	0	0	0	0	1076	0	3.1267	360.410	-2.628	1.2091	-8.5296	0.0405	0.0697	15.5
USSA04A_023	28-Mar-99	17:05:47	0	0	0	0	1532	0	3.3236	484.826	4.681	9.9789	-5.6058	0.0474	0.2159	15.5
USSA04A_024	28-Mar-99	17:16:52	0	0	0	0	1989	0	3.5180	626.169	0.276	5.6182	-16.2546	0.0531	0.4582	15.5
USSA04A_025	28-Mar-99	17:27:37	0	0	0	0	2510	0	3.7132	782.233	-2.664	2.6064	-17.8969	0.0574	0.7907	15.5
USSA04A_026	28-Mar-99	17:39:34	0	0	0	0	3065	0	3.9091	930.037	-0.469	6.7139	-19.8493	0.0590	1.0630	15.5
USSA04A_027	28-Mar-99	17:53:00	0	0	0	0	4010	0	4.3001	1182.240	-1.107	7.3507	-23.9392	0.0599	1.4297	15.5
USSA04A_029	28-Mar-99	18:08:54	0	0	0	0	4662	0	4.6909	1394.260	-9.234	-0.2456	-20.0107	0.0546	1.8066	15.5

Figure 3.7 Experimental log file for one of the boats tested at IMD.

The measured total resistance D_M, as defined in Sec. 3.3, for six models is reported in Figure 3.1-Figure 3.6. In these graphs a non-dimensional value of the resistance $C_{D,M}$, obtained by dividing the resistance by the displacement Δ times the acceleration of gravity g, and multiplying everything by 1000, as shown in Eq. 3.1, is plotted versus the Froude number.

$$C_{D,M} = \frac{D_M}{\Delta g}1000$$

Eq. 3.1

3.3 Expansion of Raw Tank Data to Full Scale

The procedure used to expand the data from model to full scale is very simple for the cases where the appendages were not present.

22

The measured value of drag, D_{MEAS}, was first corrected for the presence of the turbulence stimulators. These are cylinders of 0.125 *in* in diameter and 0.1 *in* in height. These stimulators are used to trip the boundary layer flow into the turbulent regime even when the experiment condition would allow for laminar flow. Since their drag is well known, the use of stimulators simplifies the estimation of viscous resistance of the models. The corrected value of drag for the model, D_M, is shown in Eq. 3.2

$$D_M = D_{MEAS} - \frac{1}{2}\rho_{FW}V_M^2 C_{D,S}A_S N_S$$

Eq. 3.2

where $C_{D,S}$ and A_S are, respectively, the drag coefficient, taken to be 0.6, and the frontal area of a single stimulator, while N_S is the number of stimulators used on the model. ρ_{FW} is the fresh water density at the recorded temperature, obtained from standard tables, and V_M is the towing velocity.
The full scale speed, V_Y, is obtained by equating the Froude numbers for the model and the full scale yacht and is given by

$$V_Y = V_M \sqrt{\lambda}$$

Eq. 3.3

λ being the scale factor, that is the ratio of a characteristic dimension of the yacht to the corresponding one of the model. For simplicity, in the comparisons all the data were reduced to salt water conditions at 15°C, since the VPP outputs are calculated at those conditions. The viscous resistance of the canoe body was estimated in the same way for both the model and the full-scale yacht. The frictional coefficient C_F was calculated using the ITTC line with the Reynolds number Re based on the 70% of the sailing length L, as defined in 2.2.1. The residuary resistance coefficient C_R was then obtained by subtracting the frictional resistance coefficient for the model from the total $C_{T,M}$. C_R is considered to be only a function of Fr and so assumes the same value for both the model and the yacht, as shown in Eq. 3.4

$$\text{Re}_i = \frac{0.7LV}{\nu}$$

$$C_{F,i} = \frac{0.075}{\left(\log(\text{Re}_i)-2\right)^2}$$

$$C_{T,M} = \frac{D_M}{\frac{1}{2}\rho_{FW}V_M^2 A_{WS,M}}$$

$$C_R = C_{T,M} - C_{F,M}$$

Eq. 3.4

where the index i is equal to M when referring to the model and to Y when referring to the full-scale yacht. The total resistance for the latter was calculated from the yacht total resistance coefficient, which is the sum of the residuary resistance and yacht frictional resistance coefficients, as in Eq. 3.5

$$C_{T,Y} = C_R + C_{F,Y}$$

$$D_Y = \frac{1}{2} \rho_{SW} V_Y^2 C_{T,Y} A_{WS,Y}$$

Eq. 3.5

The procedure used for the appended data involves a couple of extra steps. To get the residuary resistance, in fact, which in this case will be the sum of the contributions due to the hull and to the appendages, it is necessary to estimate the viscous resistance of the keel and rudder. This was done in different ways for the model scale and the full-scale yacht.

The models were tested with a great number of turbulence stimulators on the appendages and on the hull, so it is reasonable to assume that the flow on the foils was turbulent even though the Reynolds number was not too high. In this case the appendages were divided into five strips and for each strip the viscous coefficient C_V was calculated using the ITTC line with the Re based on the chordlength. To account for the fact that the foils were not flat plates, the thickness correction based on the thickness-chord ratio t/c shown in was used, as suggested in [Hoerner].

$$C_V = C_F \left(1 + 1.2 \left(\frac{t}{c} \right)^2 + 70 \left(\frac{t}{c} \right)^4 \right)$$

Eq. 3.6

C_F is the frictional coefficient as obtained from the second of Eq. 3.4, where the Re is in this case calculated using the total chordlength of the foil strip. For the full-scale appendages, the same procedure as the one contained in the IMS VPP is used.

The total resistance, expanded to full scale, for six boats is reported in Figure 3.8 to Figure 3.13 as function of the Froude number. As before, the resistance is non-dimensionalized using the displacement and the acceleration of gravity in a similar way as the one shown in Eq. 3.1. In these figures it can be seen how models of the same series have similar values of resistance, in particular at the lower speeds. Furthermore, only the two wide models, Model 6, for the first series, and Model H, for the second, show an appreciable increase in resistance as they heel.

The calculations for the appendages were performed using a Fortran 90 program specifically written for the purpose, while for the expansion to full scale, an Excel spreadsheet was developed for each model.

24
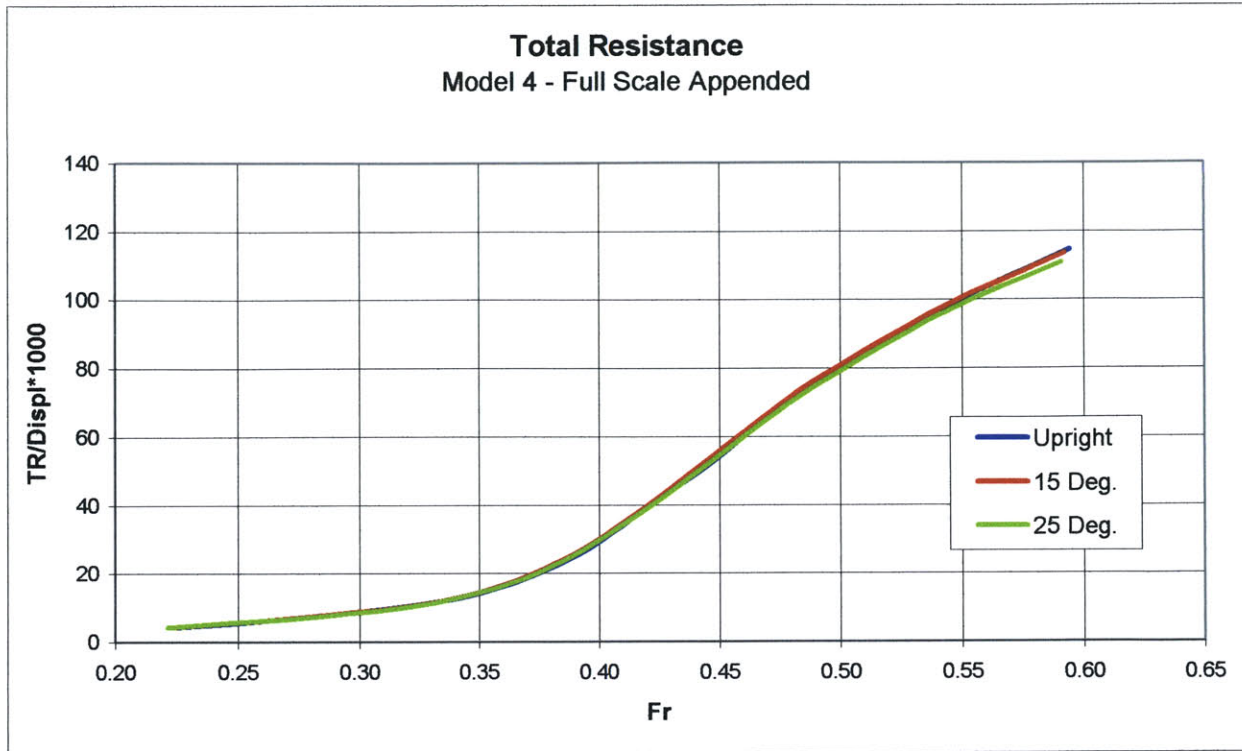
Figure 3.8 Total resistance expanded to full scale for Model 4.
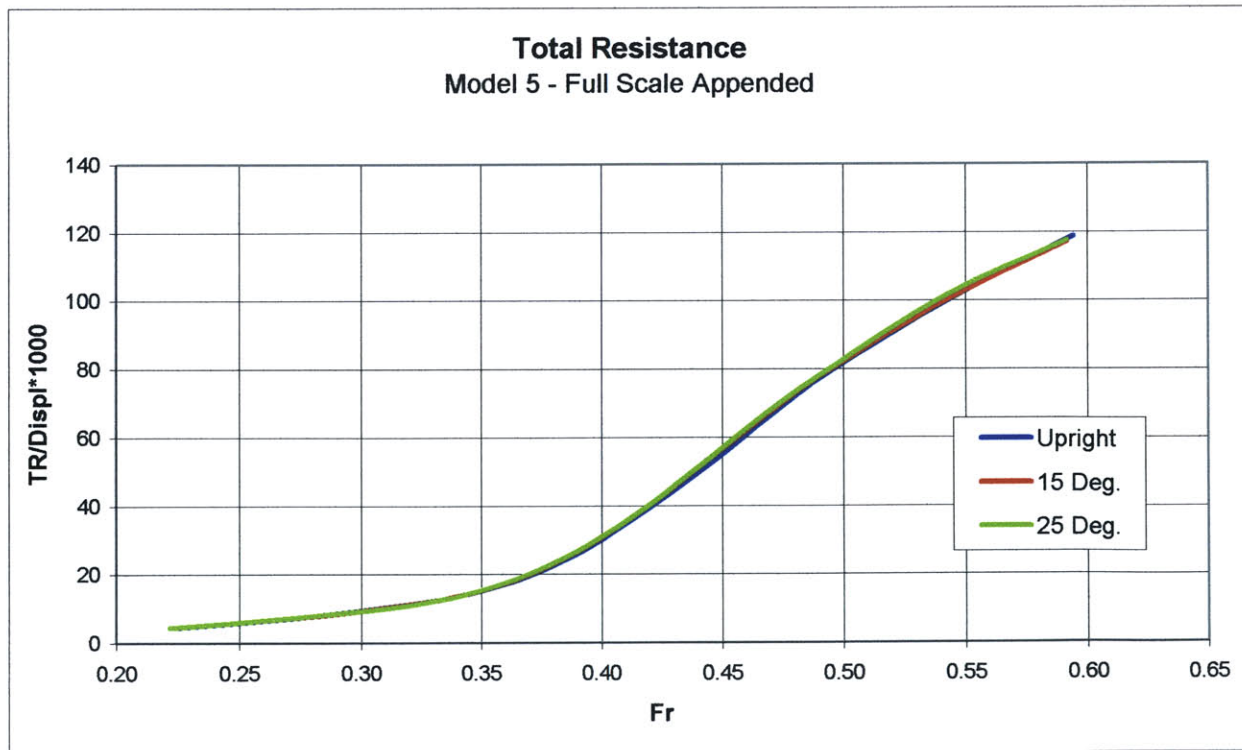
Figure 3.9 Total resistance expanded to full scale for Model 5.

Total Resistance

Model 6 - Full Scale Appended
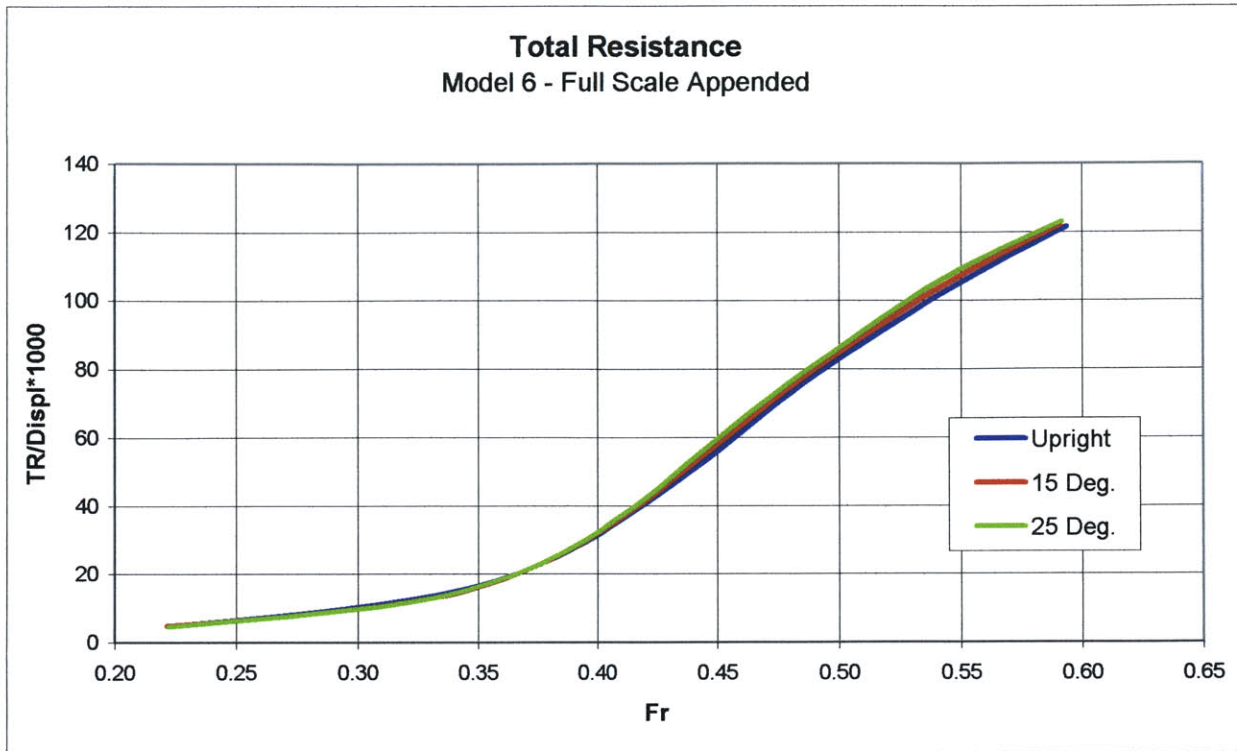
Figure 3.10 Total resistance expanded to full scale for Model 6.

Total Resistance

Model F - Full Scale Appended
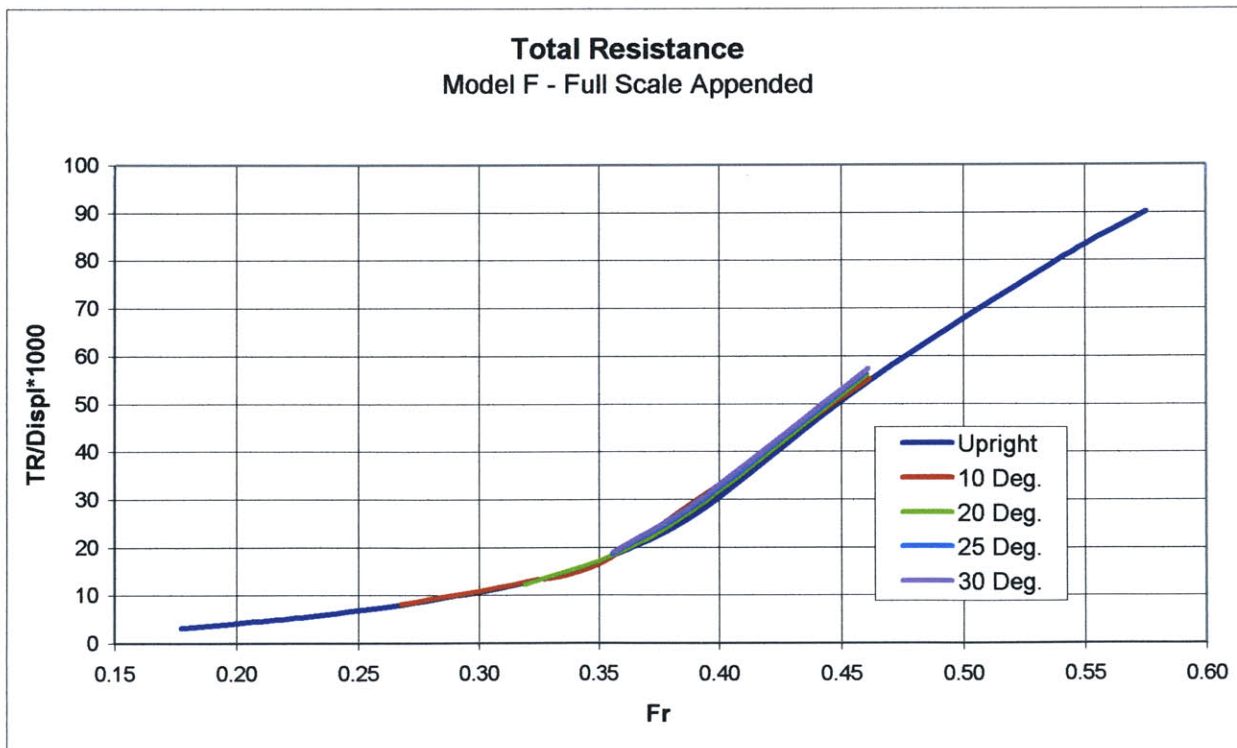
Figure 3.11 Total resistance expanded to full scale for Model F.

Total Resistance
Model G - Full Scale Appended
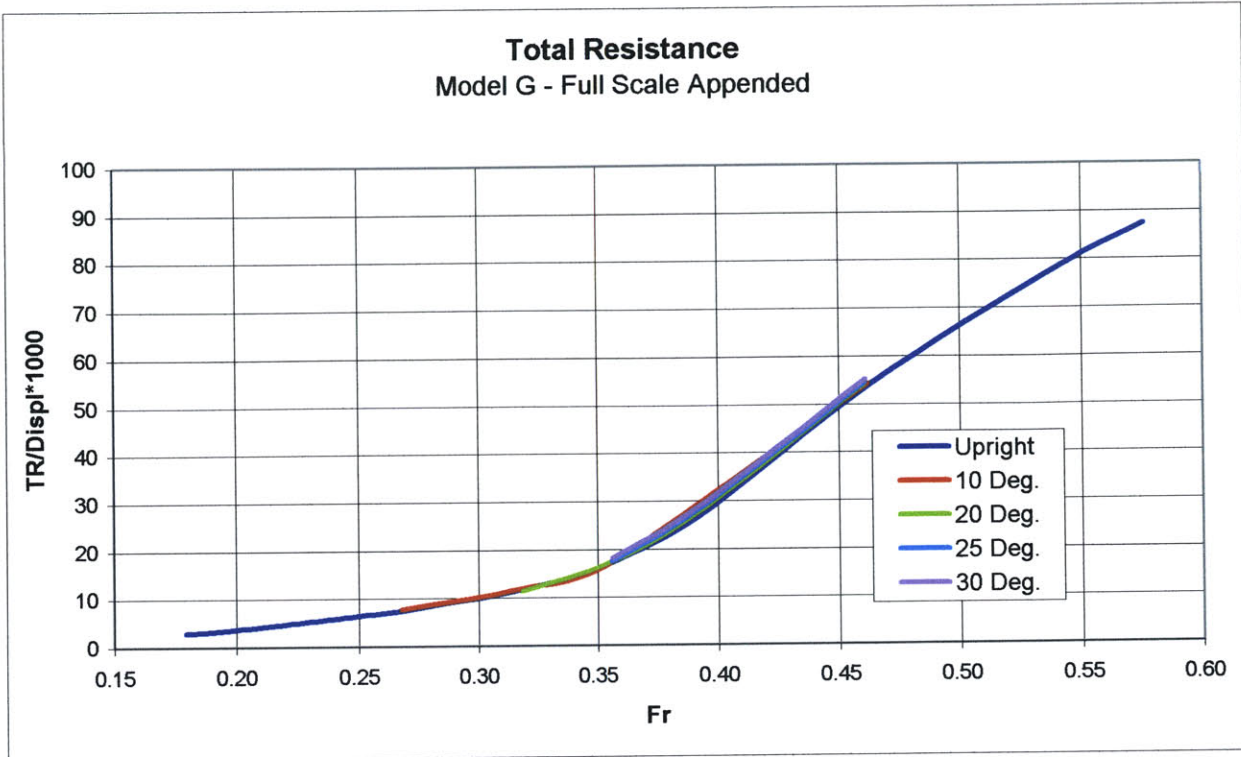
Figure 3.12 Total resistance expanded to full scale for Model G.

Total Resistance
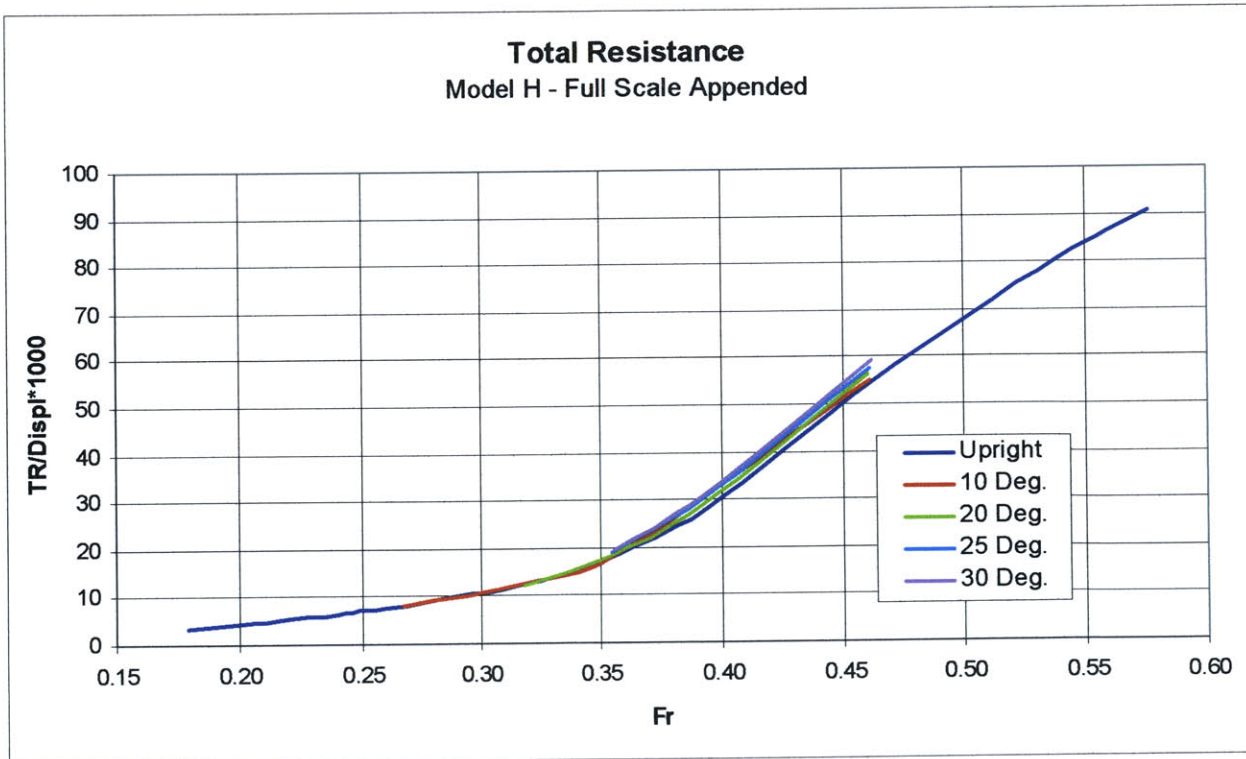Model H - Full Scale Appended

Figure 3.13 Total resistance expanded to full scale for Model H.

27

4. Analysis of the Current VPP Formulation

In this chapter the currently used hydrodynamic model is analyzed, first as a whole, then in each part separately. For this purpose predictions from the IMS VPP for the first and second set of yachts were compared to experimental data.

As said before, Model 4, Model 5 and Model 6 were specifically designed and tested for this research project. Two more sets of boats have already been designed and the tests should have already been conducted. Unfortunately, scheduling problems at the testing facility delayed the tests for these models beyond the planned end of this study, preventing the data to be part of this work. To partly compensate for this, James R. Teeters kindly made available to the author the experimental data for the second set of boats, Model F, Model G and Model H.

Model 1 was used mostly for the part of this work described in the next chapter, that is to evaluate the changes made to the VPP formulation.

4.1 Total Resistance

The first step of this work was to assess whether or not the IMS VPP, in its current formulation, was capable of accurately predicting the hydrodynamic drag of a sailing vessel.

Figure 4.1 to Figure 4.6 show the error in the IMS estimations of the total resistance as percentage of the measured value for six boats, that is

$$error = \frac{(\text{IMS Predicted Resistance}) - (\text{Measured Resistance})}{(\text{Measured Resistance})}$$

Eq. 4.1

A similar convention is maintained throughout this work, so that in any graph showing any kind of error, a positive value means that the IMS program is overpredicting that particular component of resistance, a negative value means that the measured resistance was higher than the predicted.

The solid blue lines in the above mentioned figures represent the error in the total resistance in the upright condition as a function of Fr, while the other colored lines refer to different heeled conditions. For the first set of models (Figure 4.1 to Figure 4.3), the predictions, in the upright condition, agree fairly well with experiment only at low to medium speeds, say up to $Fr = 0.35$, where the error is within about 2% of the measured value.

28

Figure 4.1 Total Resistance error for Model 4.

Figure 4.2 Total Resistance error for Model 5.

Figure 4.3 Total Resistance error for Model 6.

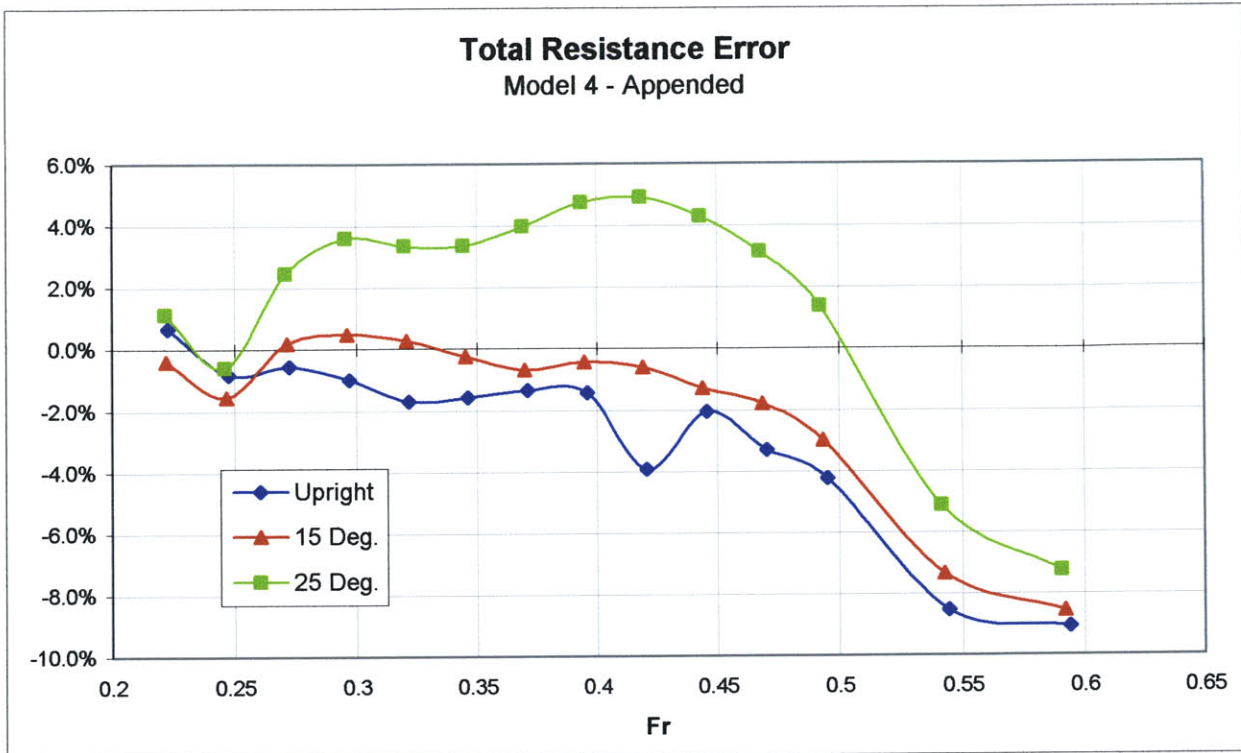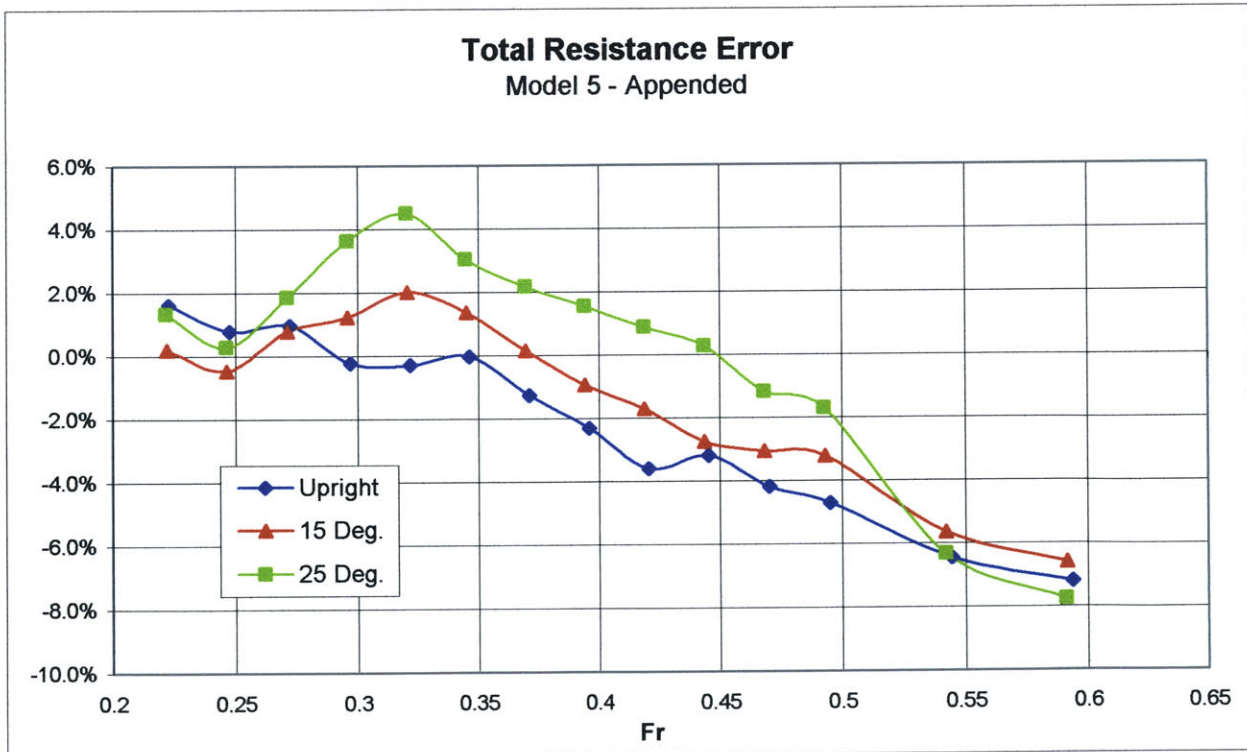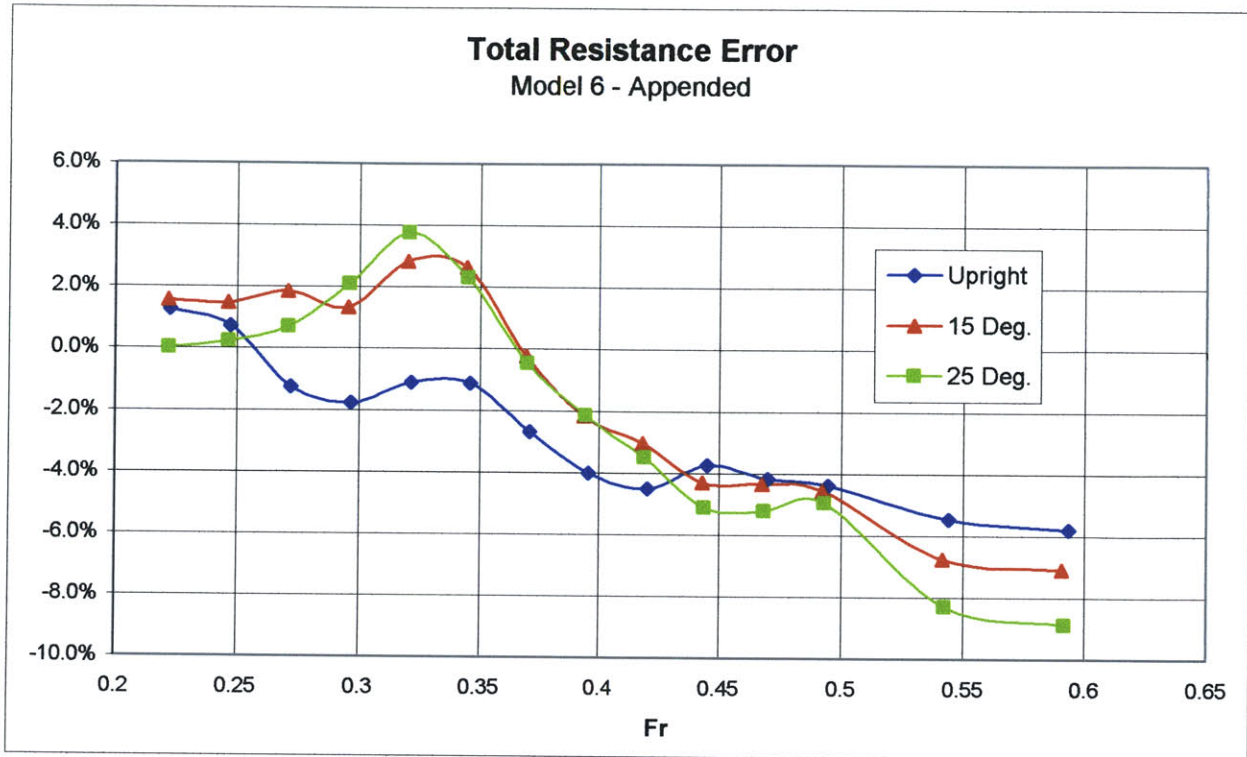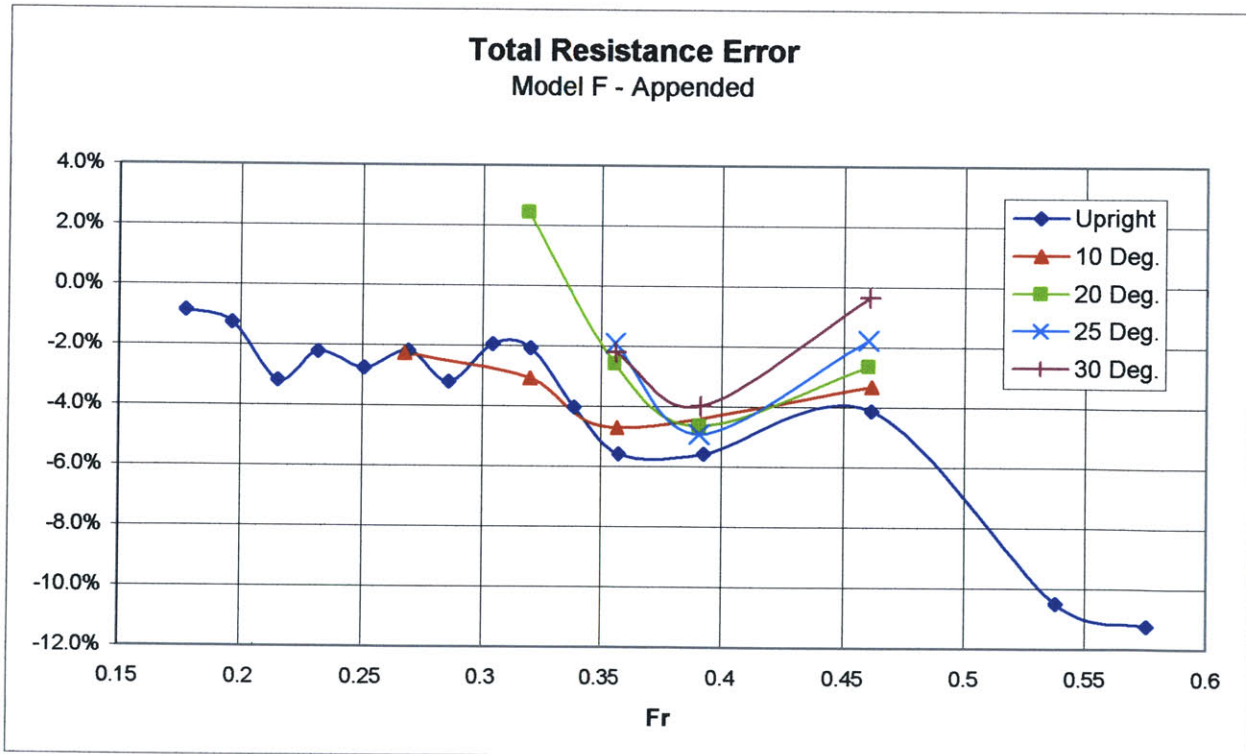**Figure 4.4 Total Resistance error for Model F.**

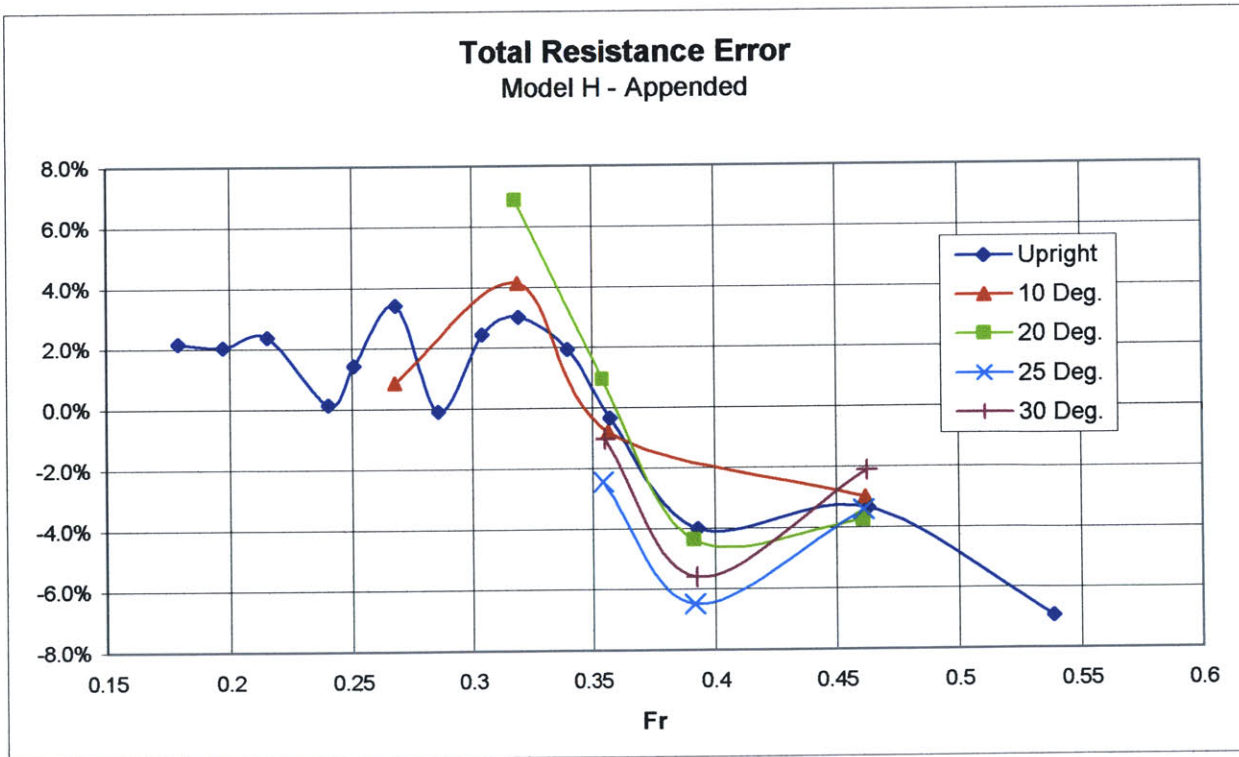**Figure 4.5 Total Resistance error for Model G.**

Figure 4.6 Total Resistance error for Model H.

31

At higher speeds the underprediction by the VPP grows considerably, in an almost linear fashion, reaching 6%-9% of the measured value around $Fr = 0.55$.

Similar general behavior is observed at 15° and 25° heel, although now there is a tendency to overpredict the resistance, with a maximum of 2-3% around a Froude number of 0.3-0.35, before the error drops to negative values. It is interesting to notice how Model 4, which is the most accurately predicted when upright (the error, with the exception of one data point, is less than 2% up to $Fr = 0.45$), is also the one for which the VPP has the worst overall performance at 25°.

The predictions for the second set of models are worse than the ones for the first. Figure 4.4 to Figure 4.6 show comparable values of error at medium-high Froude numbers, and higher value at low Fr. In this latter range of speeds, Model F, the parent boat, which is the best predicted, has a calculated value of resistance 2 to 3% lower than the measured value. The situation seems to slightly improve at non-zero angles of heel, where two models, F and G, have smaller errors than when upright. It is difficult though to draw more certain conclusions due to the limited amount of data at these conditions.

In handicap racing being able to predict accurately the absolute value of resistance for a yacht is as important as being able to estimate the difference in resistance between boats properly. For this reason, predicted differentials in resistance for the first set of boats were compared with measured values. Figure 4.7 and Figure 4.8 show the error between predictions and measurements in difference of resistance between Model 4 and Model 5 and between Model 6 and Model 5 at 0°, 15° and 25° heel, as percentage of the measured resistance of Model 5 at the particular speed.
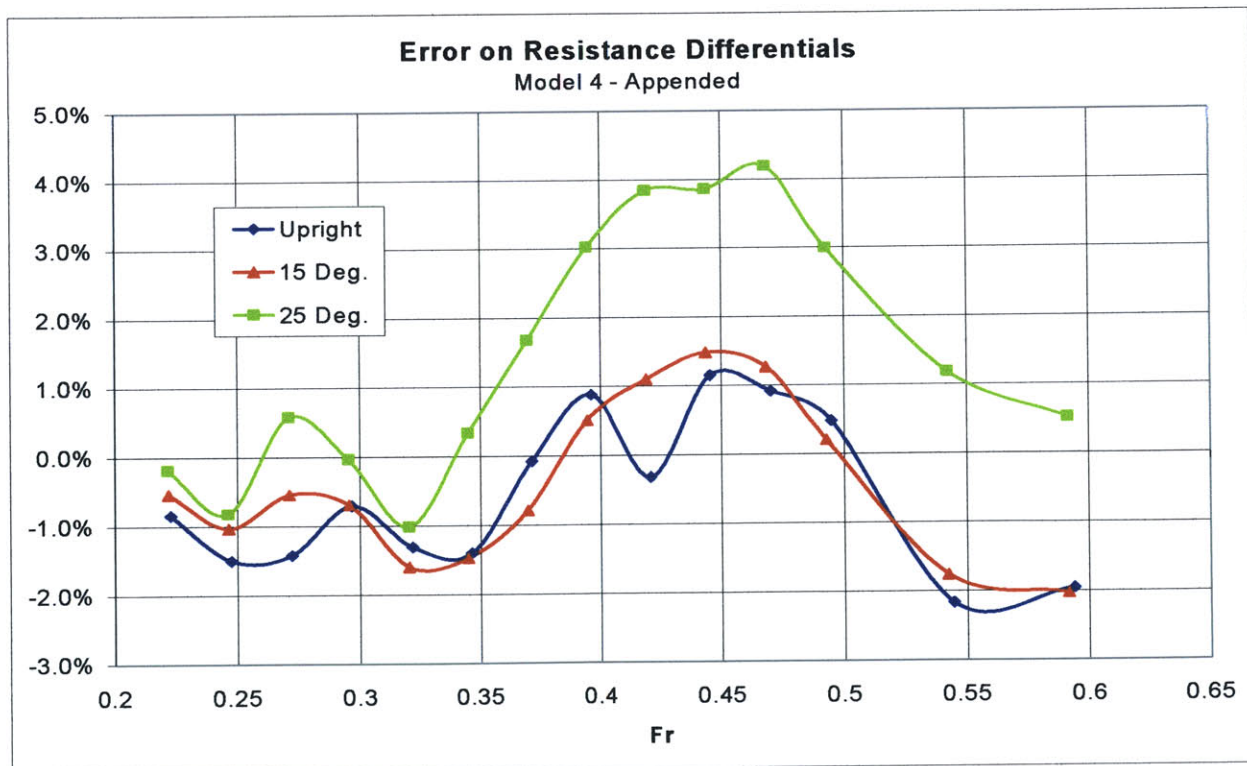
Figure 4.7 Error on differences of total resistance between Model 4 and Model 5.

To exemplify, suppose that, upright, Model 6 is found through the experiments to have a resistance of $300\,N$ higher than Model 5, which at the same speed, recorded a total resistance of $1000\,N$. Now, the IMS VPP predicts this difference to be only 1% of the measured value for Model 5, that is only $100\,N$. So the error in the differential is 2%, or more precisely −2%, since the VPP underpredicts the measured value. From the above-mentioned figures, it can be noticed that the error is similar in absolute value, although opposite in sign, for the two pairs. In the upright position, the predictions are, in both cases, for most speeds within 1% of the measured value, but as the heel angle increases, so does the error.

Although both types of error, on the absolute value of resistance and on the resistance differentials, were not as large as initially expected, it was believed that there was still margin for improvements. For this reason each component of the total resistance was analyzed separately.

4.2 Residuary Resistance

As explained in Sec. 3.3, the procedure used to expand the raw tank data to full scale involves an estimation of the viscous resistance of both appendages and canoe body, since this component of resistance cannot be separately measured. To simplify data comparison later, it was decided to use the same, reasonable approach used in the IMS VPP to estimate it. This resulted in the fact that the error in the viscous components of the resistance was of the order of one tenth of percent, and therefore the error on the residuary part to be very similar in value to the one of the total resistance.
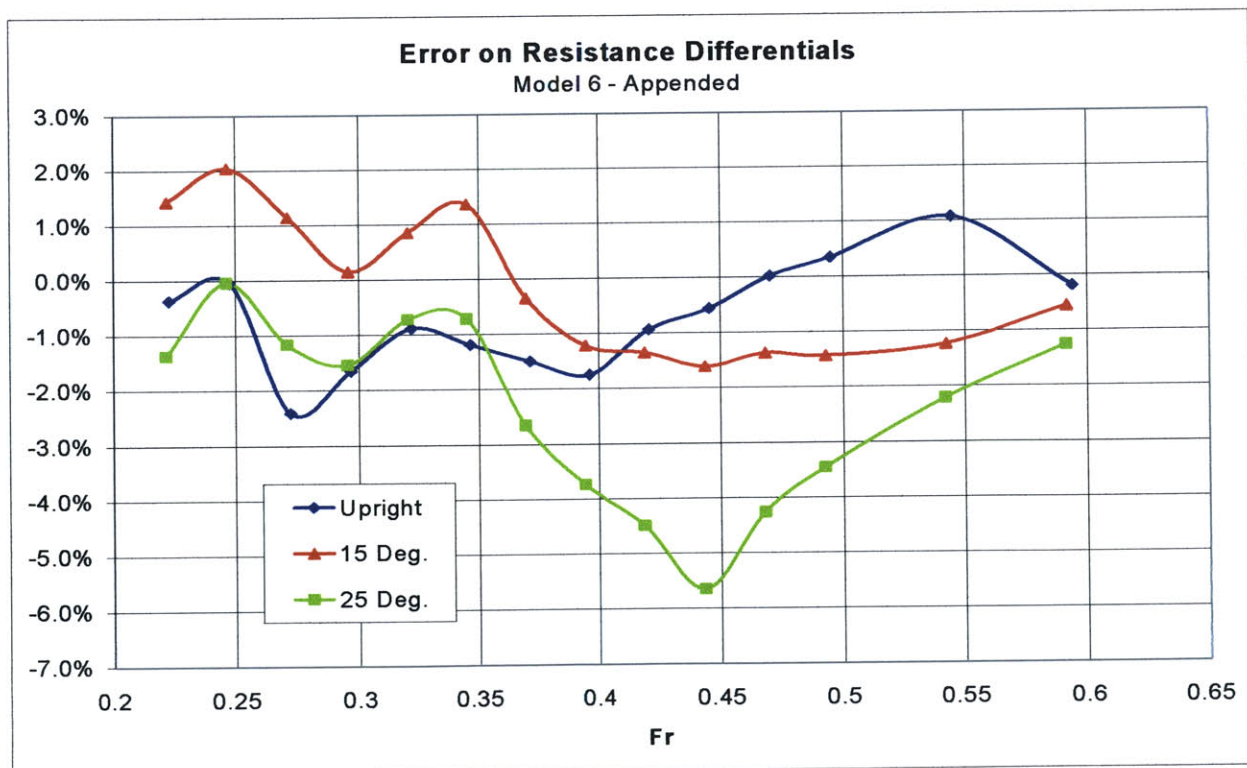

Figure 4.8 Error on differences of total resistance between Model 6 and Model 5.

The residuary resistance has two contributions: the first comes from the appendages and, in the VPP, is considered independent from the heel angle, the second comes from the canoe body and is different at each heel angle.

In the VPP model the upright canoe body residuary resistance is given by Eq. 2.5. The solid blue lines in Figure 4.9 to Figure 4.14 show how this formulation performs with respect to the experiments. Again the error is the difference in the predicted value from the measured value, expressed as percentage of the measured one.

The resistance for the models tested in Canada (Figure 4.9 to Figure 4.11) goes from being over-predicted, with a maximum around 3%, at a Froude number of about 0.2, to being under-predicted as the Froude number increases. The error, at these speeds, is different for each model: Model 4 is the most poorly predicted with a difference of about 7% from the measurements. Model 5 is better estimated with an under-prediction that never goes above 5%, while with an error of only 2.5% Model 6 has the overall best agreement with the experimental results.

For Model F and Model H (Figure 4.12 and Figure 4.14) the error exceeds 5% only at very high speeds: for the first one the resistance is always underestimated, while the second an error value oscillating around zero. Model G (Figure 4.13) is the one for which the VPP performs the worst, with values of error reaching often 7%.

It appears from these results that for both series of models the VPP canoe body residuary resistance model is less and less accurate as the beam-draft ratio of the boats is reduced. The effect of weight seems to be captured fairly well, since for boats with similar beam-draft ratios but different displacements, the error is comparable.
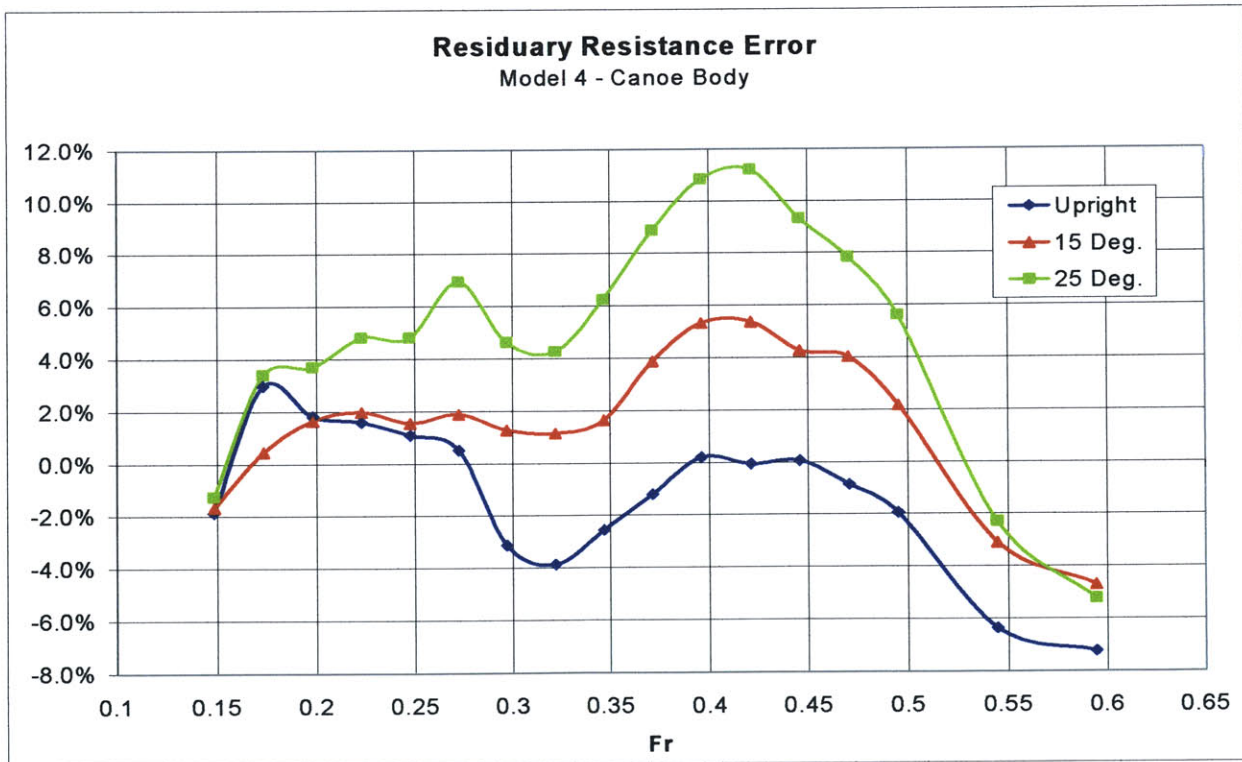

Figure 4.9 Canoe body residuary resistance error for Model 4.
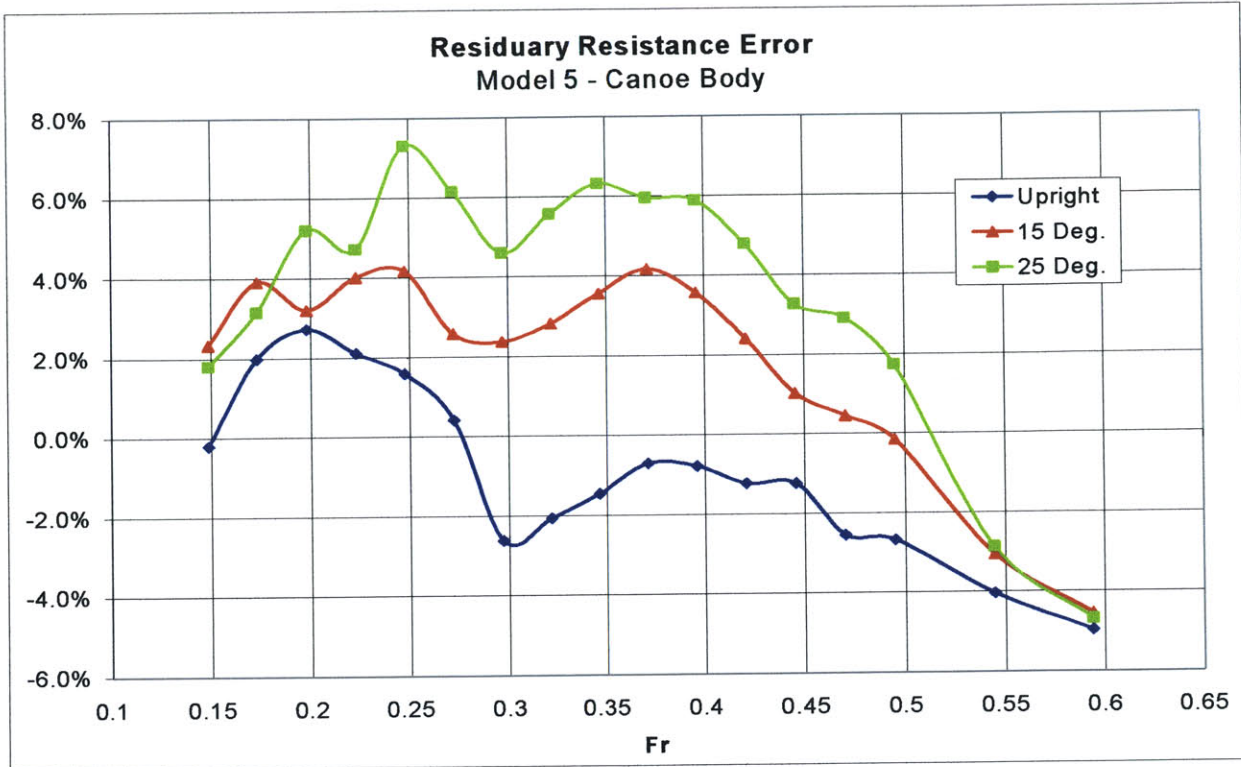
Figure 4.10 Canoe body residuary resistance error for Model 5.
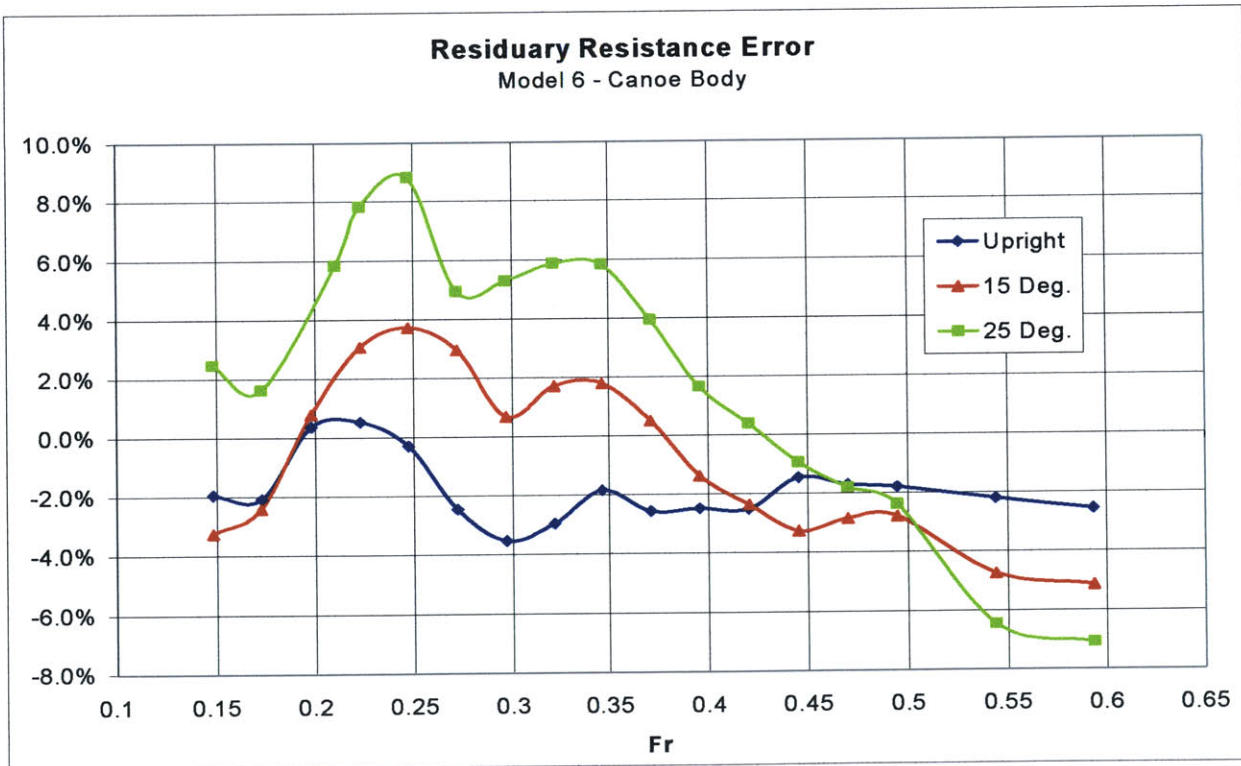
Figure 4.11 Canoe body residuary resistance error for Model 6.
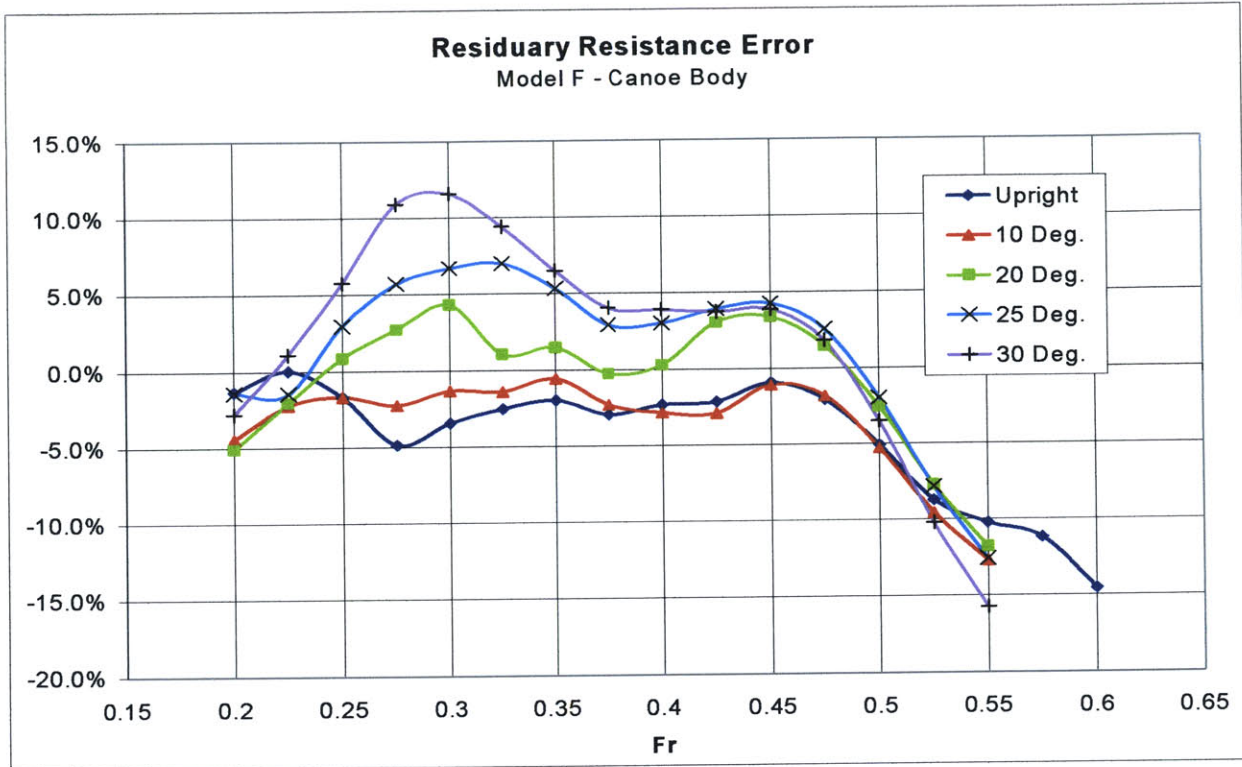
Figure 4.12 Canoe body residuary resistance error for Model F.
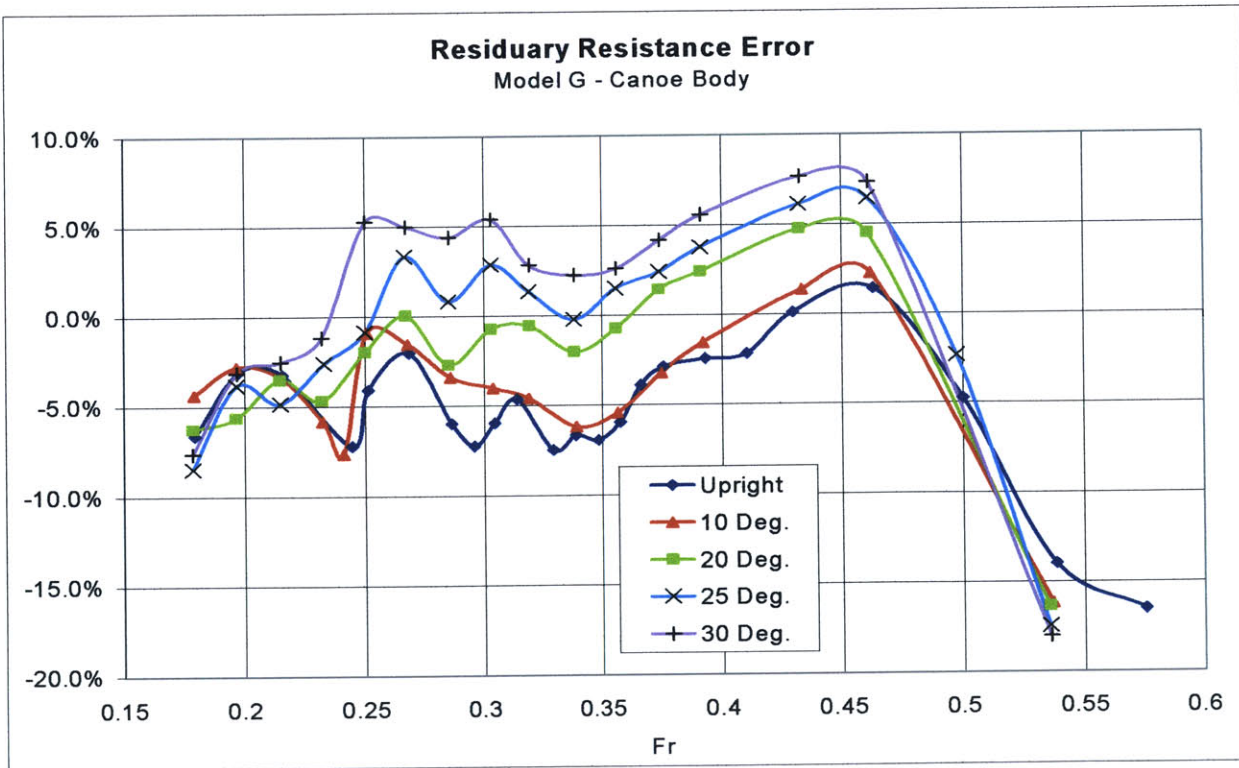
Figure 4.13 Canoe body residuary resistance error for Model G.
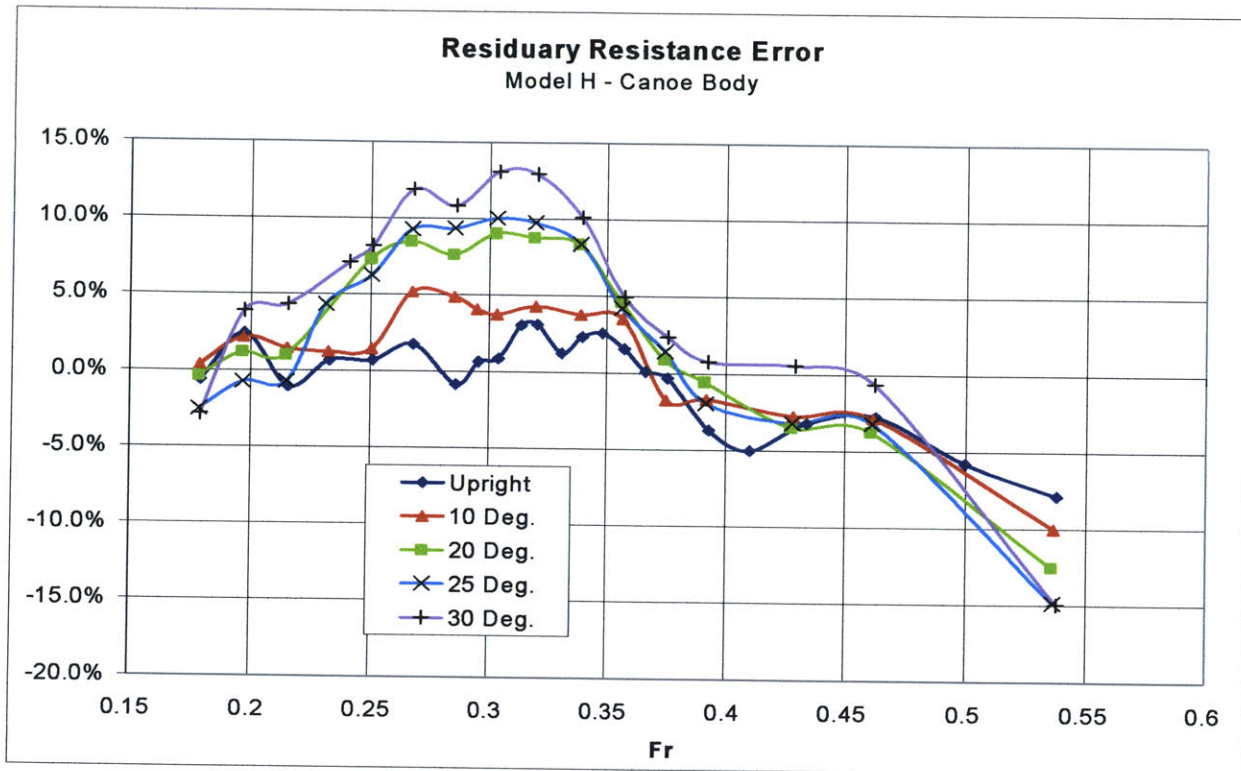
Figure 4.14 Canoe body residuary resistance error for Model H.

4.3 Heeled Canoe Body Residuary Resistance

The more the boats heel, the worse the VPP predictions become. Except at very low and very high Froude numbers, the predicted resistance, for all the models, is generally greater than the measured one. The error grows almost linearly with the heel angle up to even more than 10% in some cases. In heeled conditions, contrary to the upright, narrow boats seems to be predicted more accurately. It is though partly deceiving to look at the same figures to evaluate the heeled residuary resistance model. The VPP, in fact, obtains the heeled residuary resistance from the upright through the use of a multiplier (see Eq. 2.6), and it is known that the upright value is not correctly estimated. A better understanding of the performance of the heeled resistance model can be achieved by comparing heeled-upright residuary resistance ratios. These ratios are not affected by the error in the upright values, therefore differences between the predicted ratios and the measured ratios reflect only the error in the multipliers. As shown in the graphs from Figure 4.15 to Figure 4.20, the IMS VPP, except for some cases at very high Froude number, always predicts an increase of residuary resistance as the boat heels. And the more the boat heels, the larger the increase is believed to be. This is the main reason of the very poor performance of the heeled residuary resistance model, since in reality, modern designs can reduce, sometimes even significantly, the residuary resistance. Model 4, for example, is found from experiments to reduce the resistance by 3-5% at most speeds, while Model 6, around a Froude number of 0.3, needs about 10% less thrust than upright to maintain its speed.

37

Figure 4.15 Heeled-upright canoe body residuary resistance ratios for Model 4.

Figure 4.16 Heeled-upright canoe body residuary resistance ratios for Model 5.

38

Figure 4.17 Heeled-upright canoe body residuary resistance ratios for Model 6.

Figure 4.18 Heeled-upright canoe body residuary resistance ratios for Model F.

39

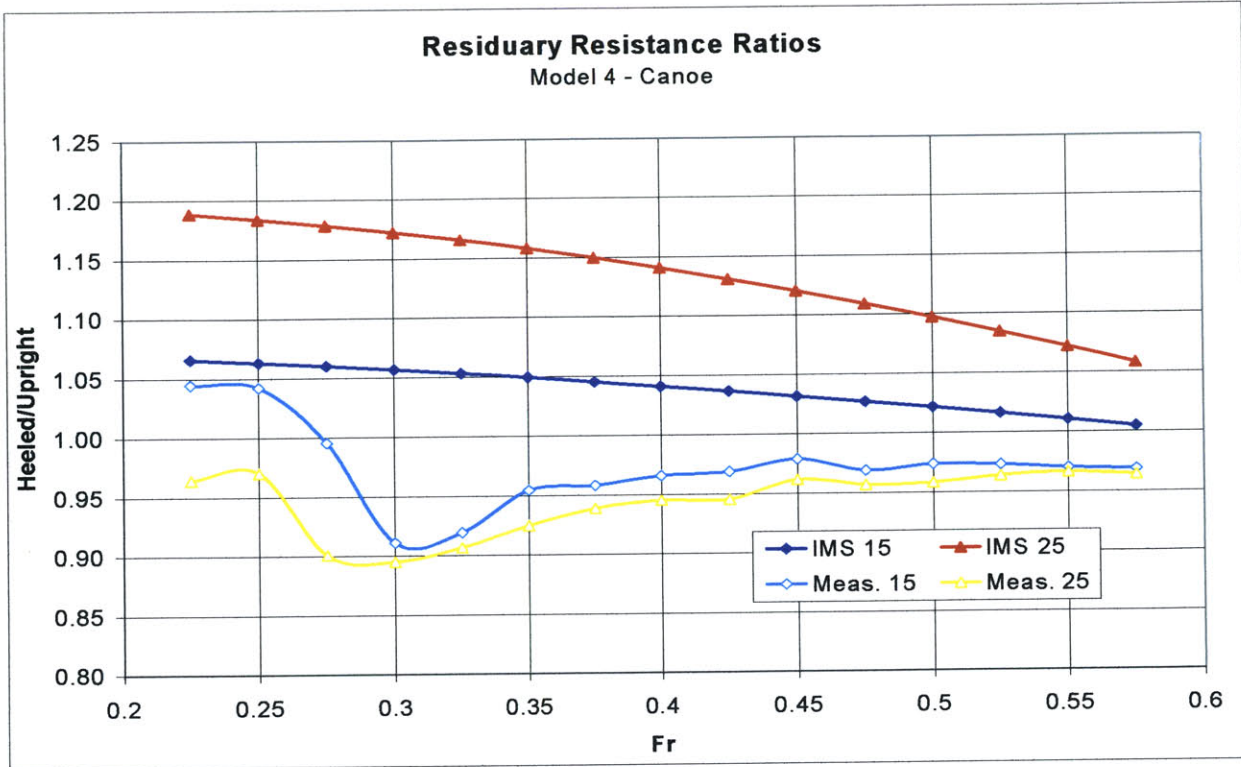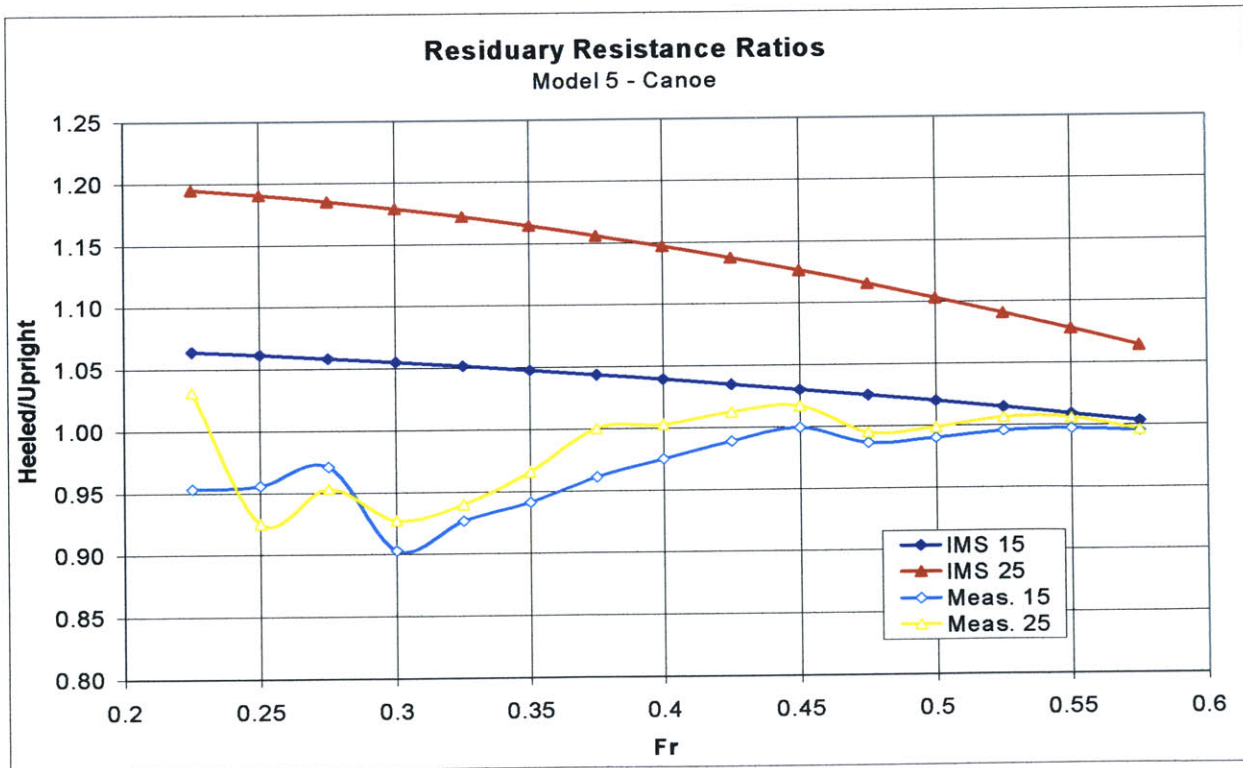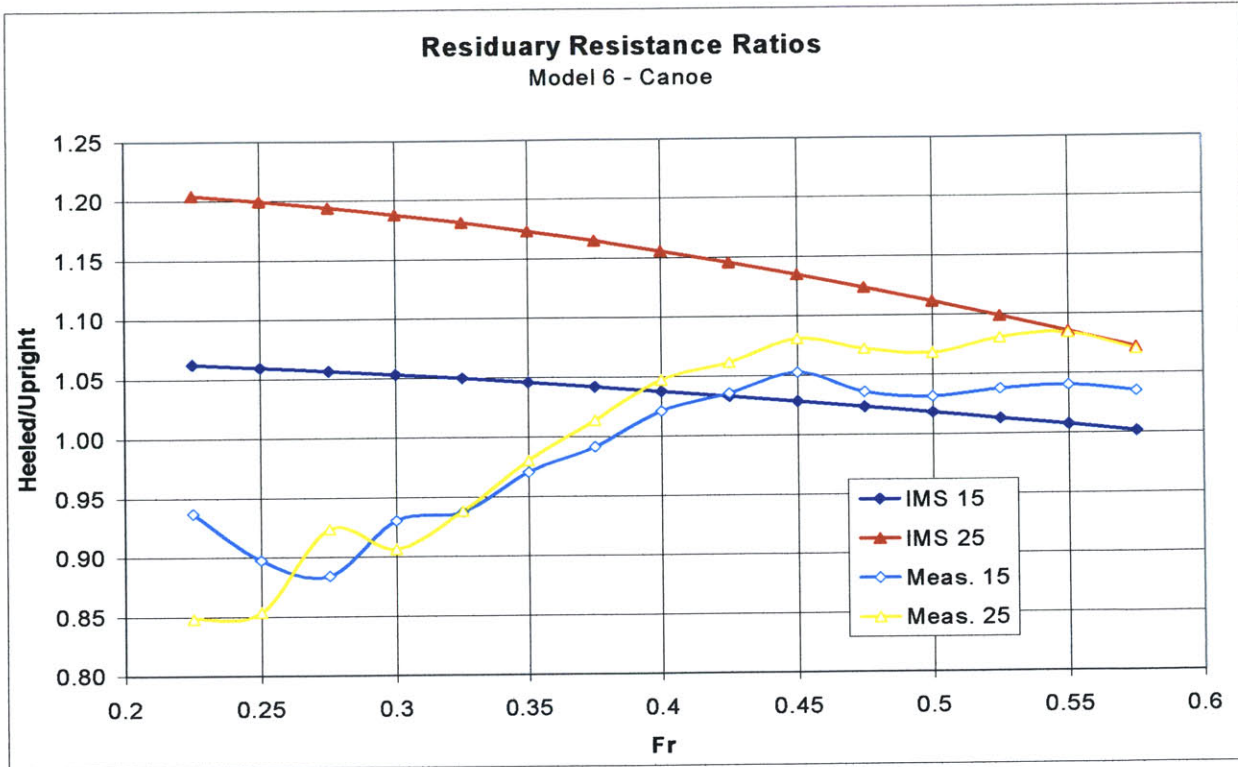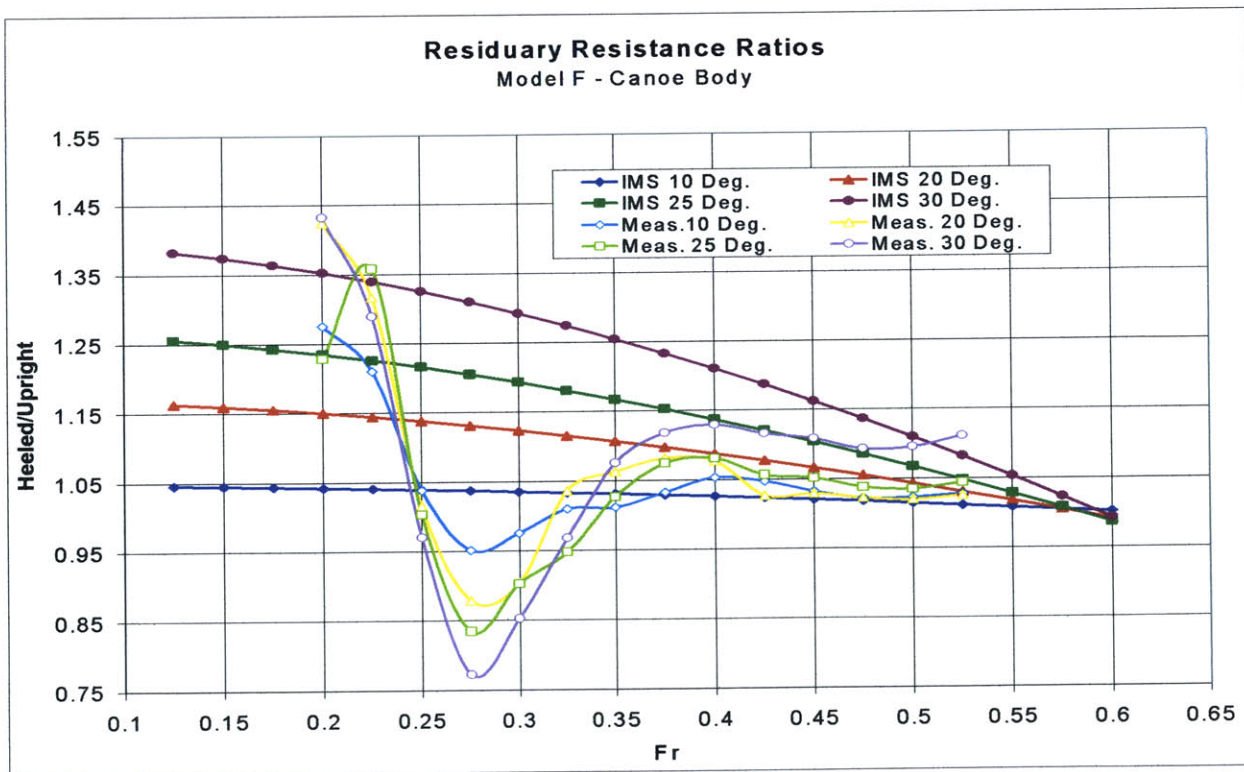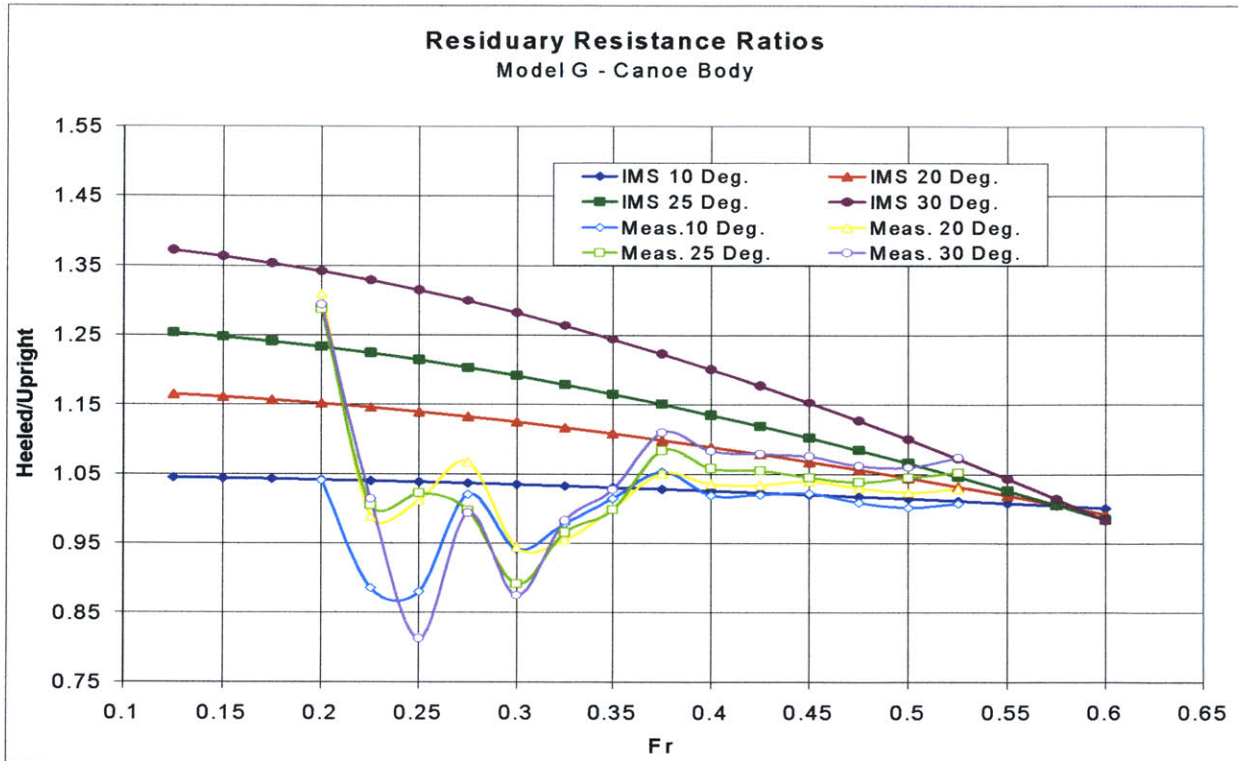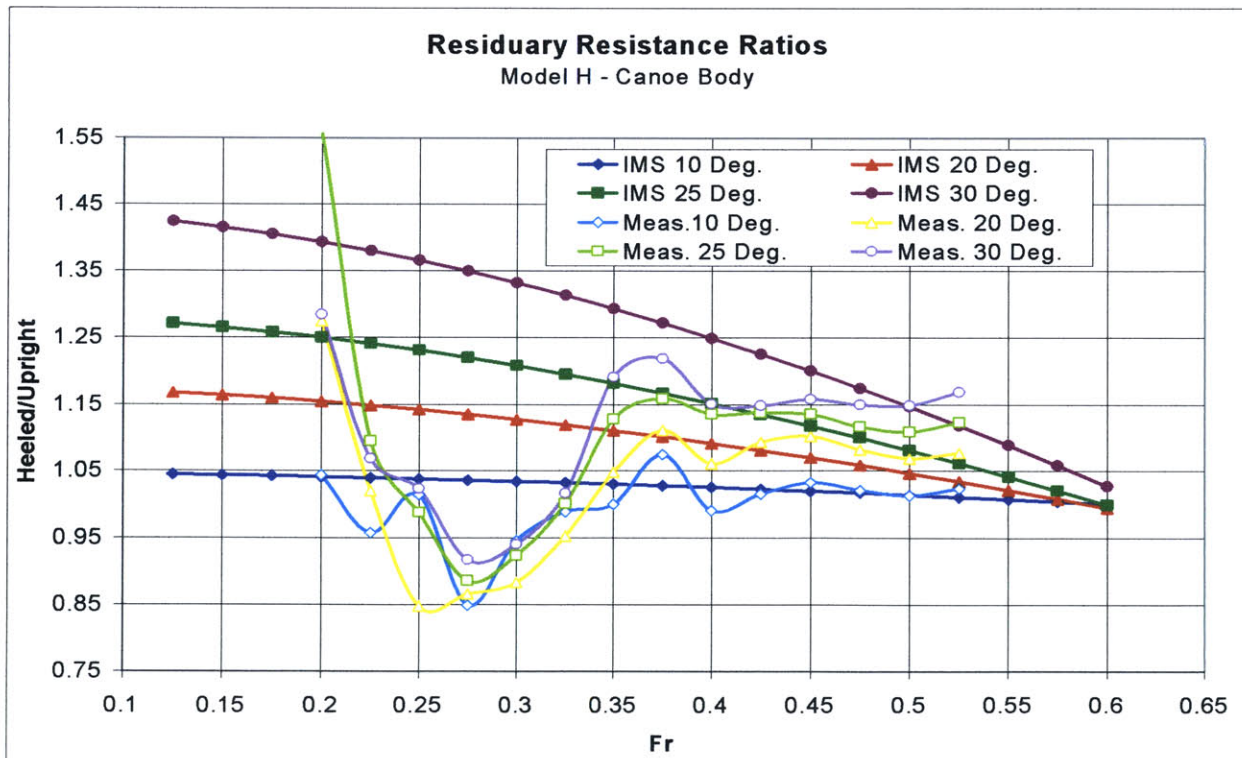**Figure 4.19 Heeled-upright canoe body residuary resistance ratios for Model G.**

Figure 4.20 Heeled-upright canoe body residuary resistance ratios for Model H.

The predicted ratios for the models of the second series agree better with the experiments, at least for Froude numbers above 0.35, where the measured ratios are larger than unity. Below that Fr, the situation worsens quickly. The extreme is reached for Model F at 25°, for which the IMS predicts a resistance 35% greater than the upright value, where the measurements give a ratio slightly larger than 0.75.

4.4 Appendages Resistance

In this section, the predictions for the resistance of the appendages are analyzed. As previously stated, the appendages resistance in the VPP is independent from the heel angle. So Figure 4.21 and Figure 4.22 compare estimates and measurements in the upright position. The error plotted in these figures is in percentage of the measured total resistance of the model considered. The experimental values of resistance are obtained by subtracting the measured resistance for the model in canoe body only configuration from the value recorded in appended configuration. The tests for the two different configurations were run at very similar speeds, even though not exactly the same, so the canoe body values were interpolated at the appended Froude numbers using natural cubic splines.

All the models, except in some sense for Model F, have their appendages drag overpredicted for Fr up to about 0.35. Around that Froude number, the error drops quickly to significant negative values to stabilize at about –3% for the models tested at IMD. The error for Model F and Model G reaches a minimum of –4% to recover to –2% at the highest speeds tested. The model that seems more accurately predicted by the VPP is Model H, the narrow model of the second series, for which the error, after very briefly exceeding 2% at $Fr \cong 0.22$, stays always within $\pm 2\%$.

For all the boats, most of the error shown is due to errors in the prediction of the residuary part of the resistance. However, a small part of it comes from a difference in the estimates of viscous resistance. This was very suspicious at first, since the algorithm used for the estimates for the experiments and inside the VPP, are substantially the same. The problem was found to be in the input data. For the experimental data, in fact, the viscous resistance is calculated using the actual dimensions of the appendages. The VPP algorithm, instead, uses dimensions derived from digitized sections of the hull generated, in the preprocessing, by the LPP. This introduces errors in the values of the dimensions that lead to errors in the viscous resistance. Compared to the actual values, which are shown in Table 3.2, the keel dimensions used by the VPP for Model 5, for example, are significantly different: the section chordlength varies from 1.647 m, at the junction with hull, to 1.194 m at the tip; the thickness to chord ratio is no longer constant and goes from a minimum of 10.35% to a maximum of 12.02%.

These differences lead to a predicted viscous drag that is up to 4% smaller than the estimate for the experiments. When considered in terms of total resistance error, this contribution is never bigger than –0.8%.
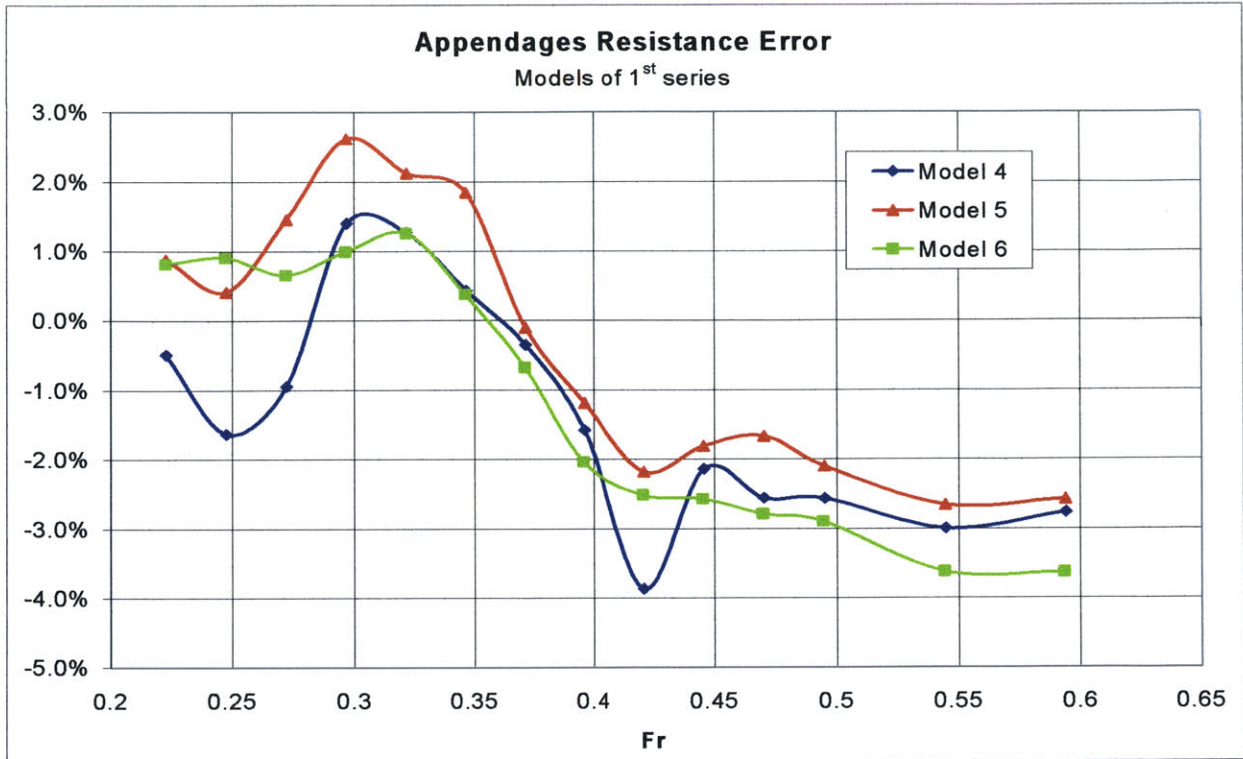
Figure 4.21 Appendages total resistance error for Model 4, Model 5 and Model 6.
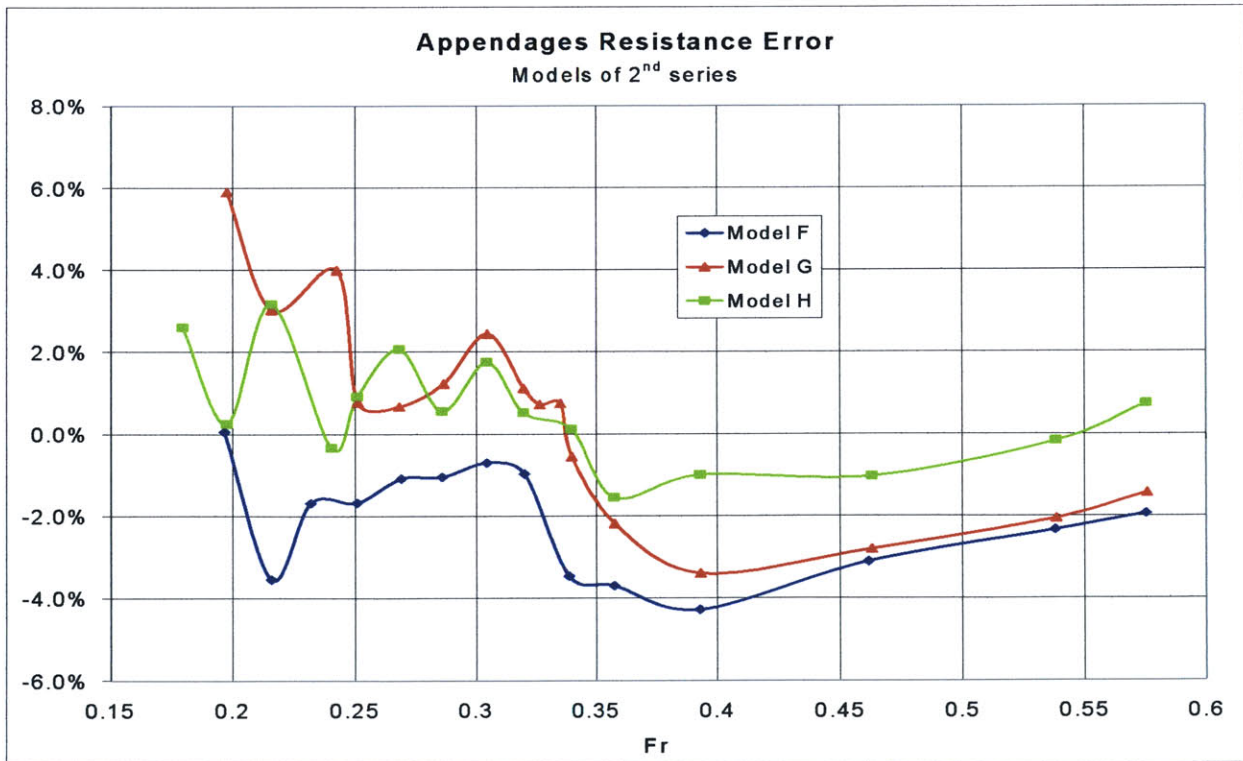
Figure 4.22 Appendages total resistance error for Model F, Model G and Model H.

4.5 Induced Drag

Figure 4.23 to Figure 4.25 show the increase in drag that Model 5 experienced as function of the side force compared to the prediction of the IMS program. Model 4 and Model 6 have very similar plots, so they are not included in this report. The induced drag is plotted in the form of a coefficient obtained by dividing the value of the increase in drag by the dynamic pressure and by the square of the IMS static draft T_{IMS}, as shown in Eq. 4.2.

$$\text{Induced Drag Coefficient} = \frac{\text{Induced Drag}}{\frac{1}{2}\rho V^2 T_{IMS}^2}$$

Eq. 4.2

The IMS value for the induced drag was obtained following the procedure described in Sec. 2.2.5. In this case the values for F_H used are the same recorded during the experiments. The experimental increase in drag due to the side force is obtained by subtracting the total resistance measured with no leeway from the values of resistance recorded when the boat and the appendages where producing a lifting force. In both cases the value of induced drag is then transformed into a coefficient using Eq. 4.2
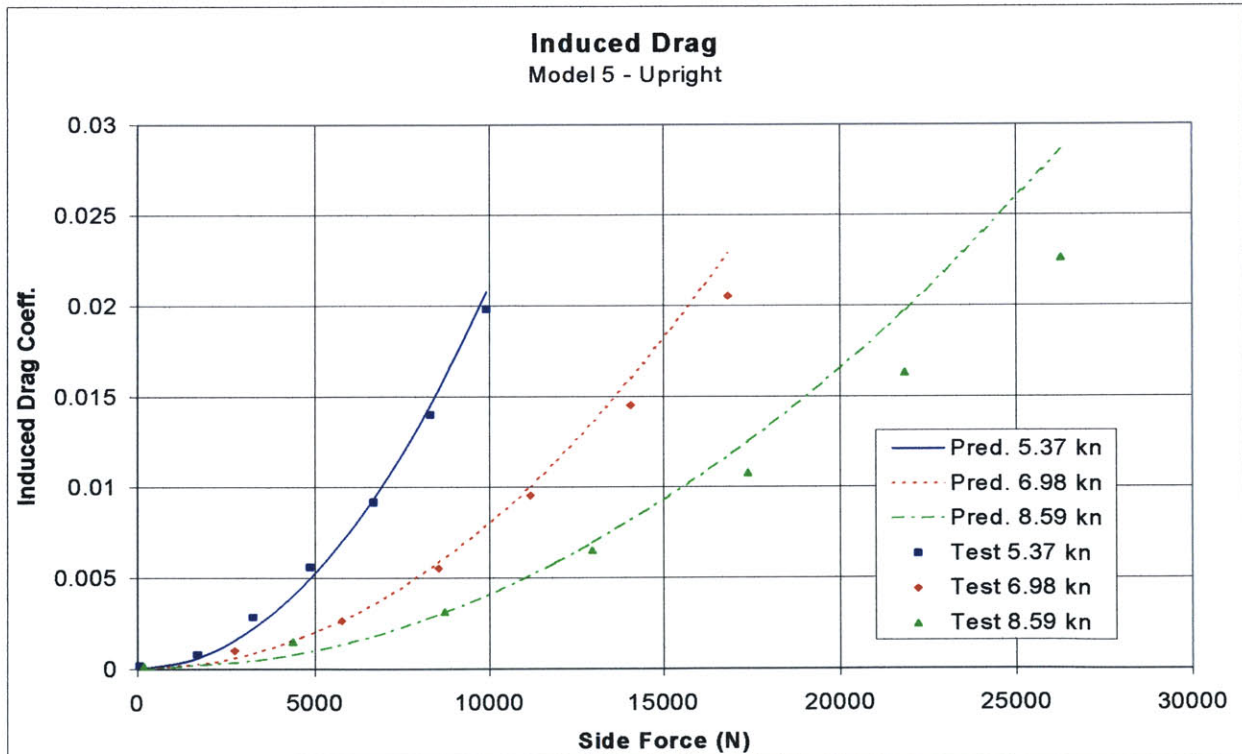
Figure 4.23 Measured and predicted induced drag coefficients For Model 5 upright.
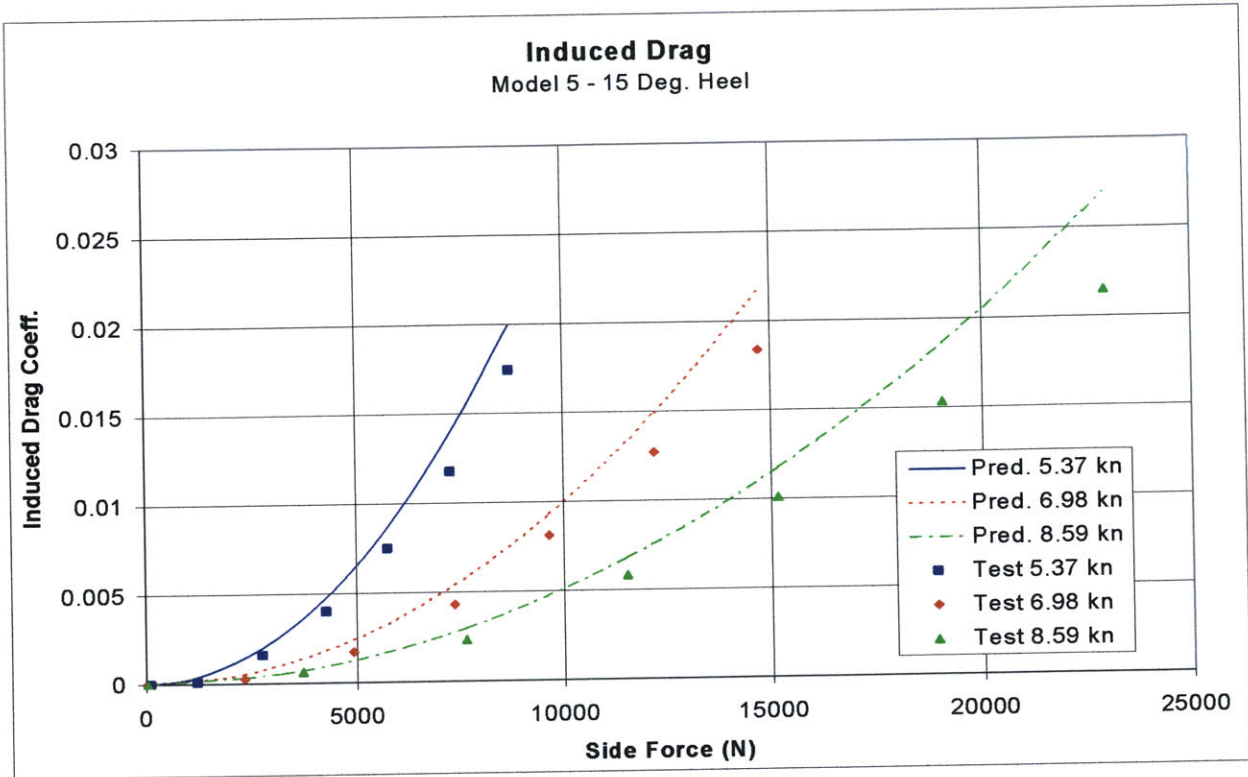
Figure 4.24 Measured and predicted induced drag coefficients For Model 5 at 15° heel.
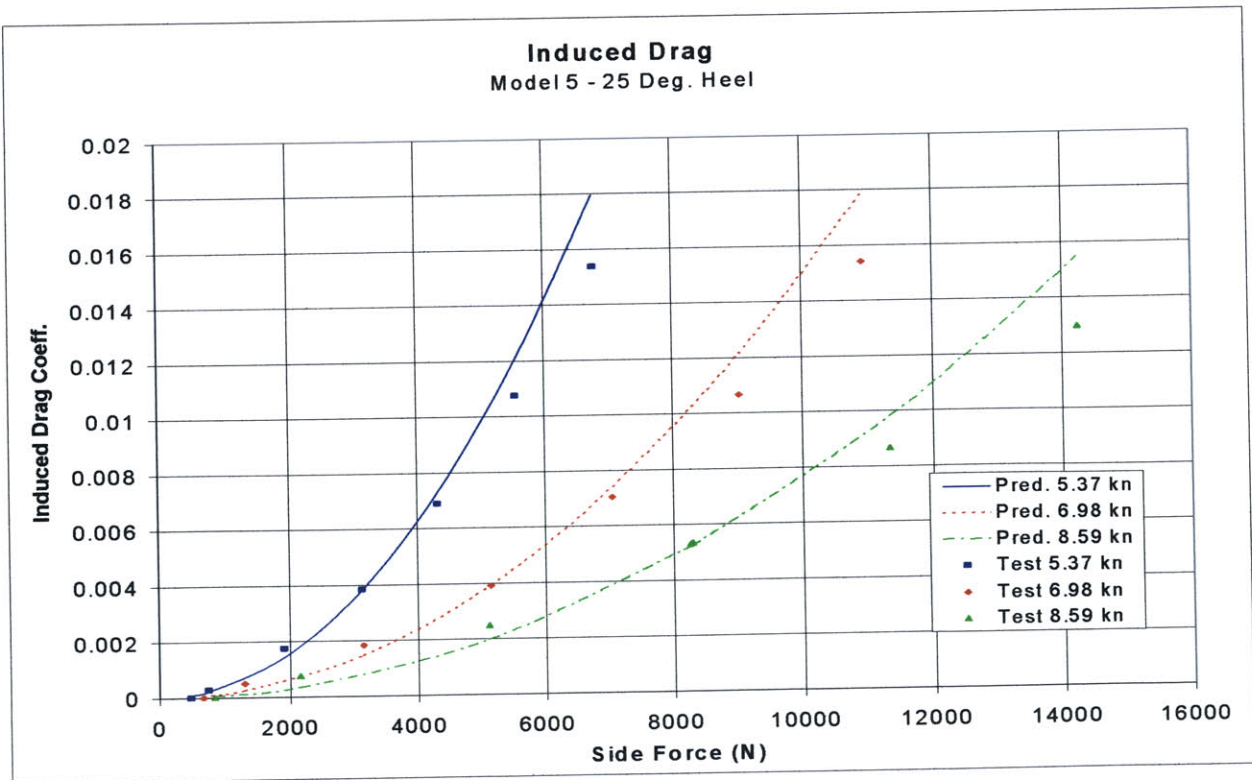
Figure 4.25 Measured and predicted induced drag coefficients For Model 5 at 25° heel.

44

Similar boats currently in production that participates in high-level IMS racing have an average sail area of 120 m². Using this value and considering a sail plan lift coefficient of 1.5, the maximum estimated side forces at the three speeds are about 900, 1425 and 2250 N respectively. These values are at the very low end of the range of side forces considered, where the errors are small, within ± 2%. However, in condition of high-lift coefficient, as coming out of a tack, the errors can increase considerably.

The error in total resistance associated with the predictions shown is reported in Figure 4.26. At high side force values, the VPP clearly overestimates the induced drag. At medium-low side forces, however, the goodness of the prediction depends on the velocity and heel angle considered. It is then important to know what is the maximum value of lift that a boat of this length generates in actual sailing. For this evaluation an approximation of the sail area is necessary, but the information available is only about the hull.
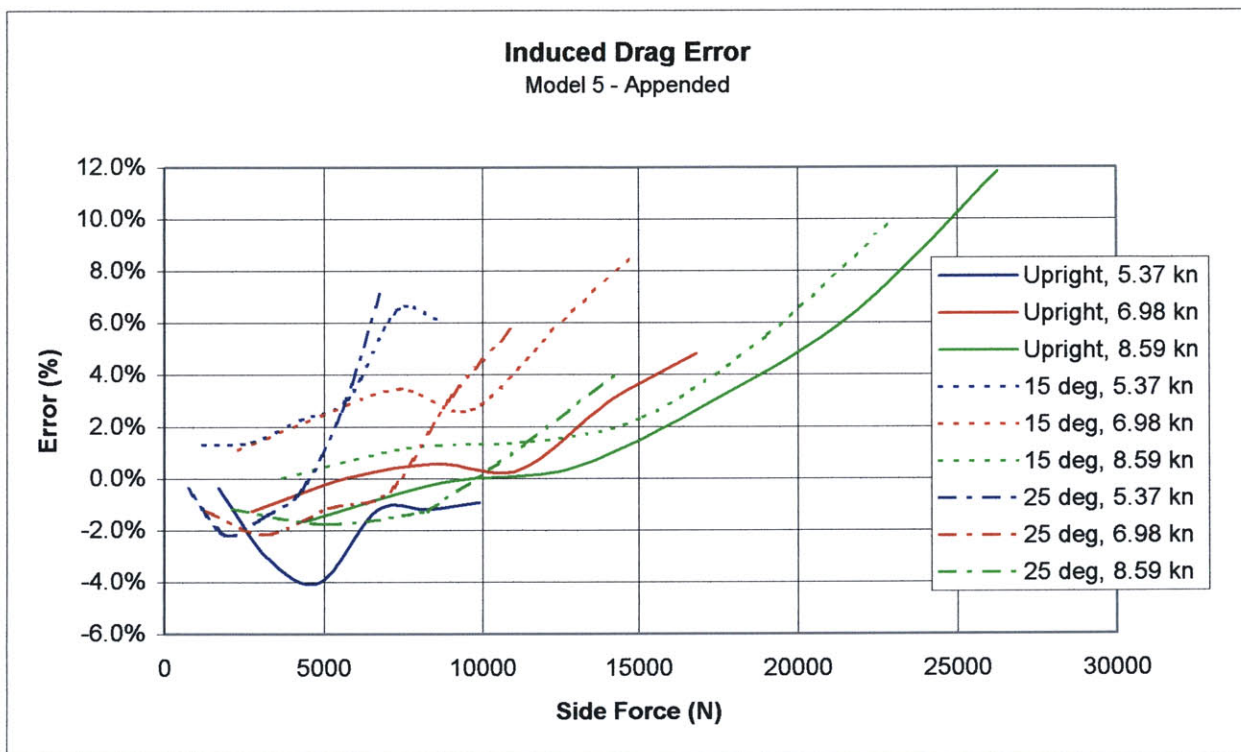
Figure 4.26 Induced drag error for Model 5

5. Developments of the IMS VPP

The IMS VPP hydrodynamic model was found, as described in Chapter 4, to be satisfactory is some parts, but deficient in others. The induced drag model is believed to be sufficiently accurate for normal sailing conditions and the viscous models, for both the appendages and the canoe body, are in good agreement with the experiments. Therefore most of the error in the estimation of the total resistance comes from inadequate modeling of the residuary resistance for the canoe body, in both upright and heeled conditions, and for the appendages.

In this Chapter, the possible sources of these errors are analyzed and, for the canoe body, an alternative model for the residuary resistance is proposed. The main difference with the currently used one is that the new model is intended to be valid for both upright and heeled condition, thus eliminating already one source of error. For the appendages, no specific improvements are proposed, mainly because the amount of available data was so small that it would have been impossible to test the changes.

5.1 Appendages Resistance Error

At first it was believed that the underprediction by the VPP, was due to the fact that it did not include any kind of resistance due to the interaction of the appendages with the hull or between parts of the appendages themselves (for example, between keel and bulb).

It was then decided to add these contributions to see if this reduced the error. The junctions between the fin keel and the hull and between the rudder and the hull can be approximated as junctions of a foil into a flat wall. The interference drag coefficient C_{INT} based on the square of the chordlength c is given by, [Hoerner]

$$C_{INT} = \frac{\Delta D}{\frac{1}{2}\rho V^2 c^2} = 0.8\left(\frac{t}{c}\right)^3 - 0.0003$$

Eq. 5.1

where $\frac{1}{2}\rho V^2$ is the dynamic pressure and t/c is the thickness-chord ratio. The increases in resistance due to the fin keel and the rudder were calculated using Eq. 5.1 and the using respective root chord length as c's. For models F, G and H, where a bulb is present at the tip of

the fin keel, a third term, based again on the coefficient C_{INT} was added, to account for the intersection of the keel and the bulb. In this case the chord length used was that of the keel tip chord.

Along the same lines, it was thought necessary to add the wing tip drag, the parasitic drag due to the presence of an edge. Again the coefficient C_{WT} formula, shown in Eq. 5.2, was taken from [Hoerner].

$$C_{WT} = \frac{\Delta D}{\frac{1}{2}\rho V^2 c^2} = 0.075\left(\frac{t}{c}\right)^2$$

Eq. 5.2

Models 4, 5 and 6 have two contributions, one for each foil, while the other models have only one term coming from the rudder since at the tip of the fin keel there is a bulb present.

Figure 5.1 and Figure 5.2 show the error in the appendages resistance predictions when interference and wing tip drag are added to them. Now, for all models, the error at high Froude numbers, say greater than about 0.4, is greatly reduced, but at the lower Fr the error skyrockets, in particular for the models of the second series. Therefore, it was concluded that in some way, implicitly, these contributions were already built in into the formulation.

The fact that for all the models in a series the error drops quickly to negative values at the same Froude number leads to the belief that it comes from an increase in measured resistance, and it suggests it could be due to some effect directly related to the length of the models.
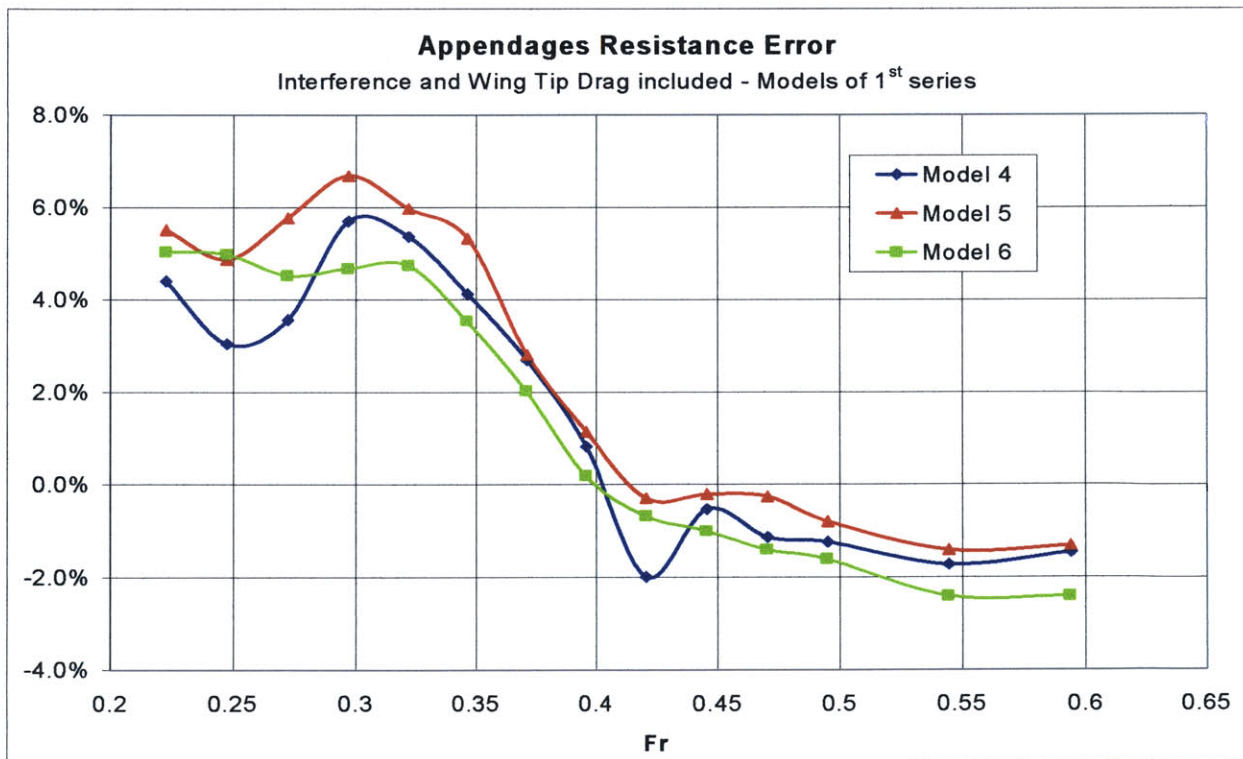
Figure 5.1 Error in appendages resistance when interference and wing tip drag are included.

47
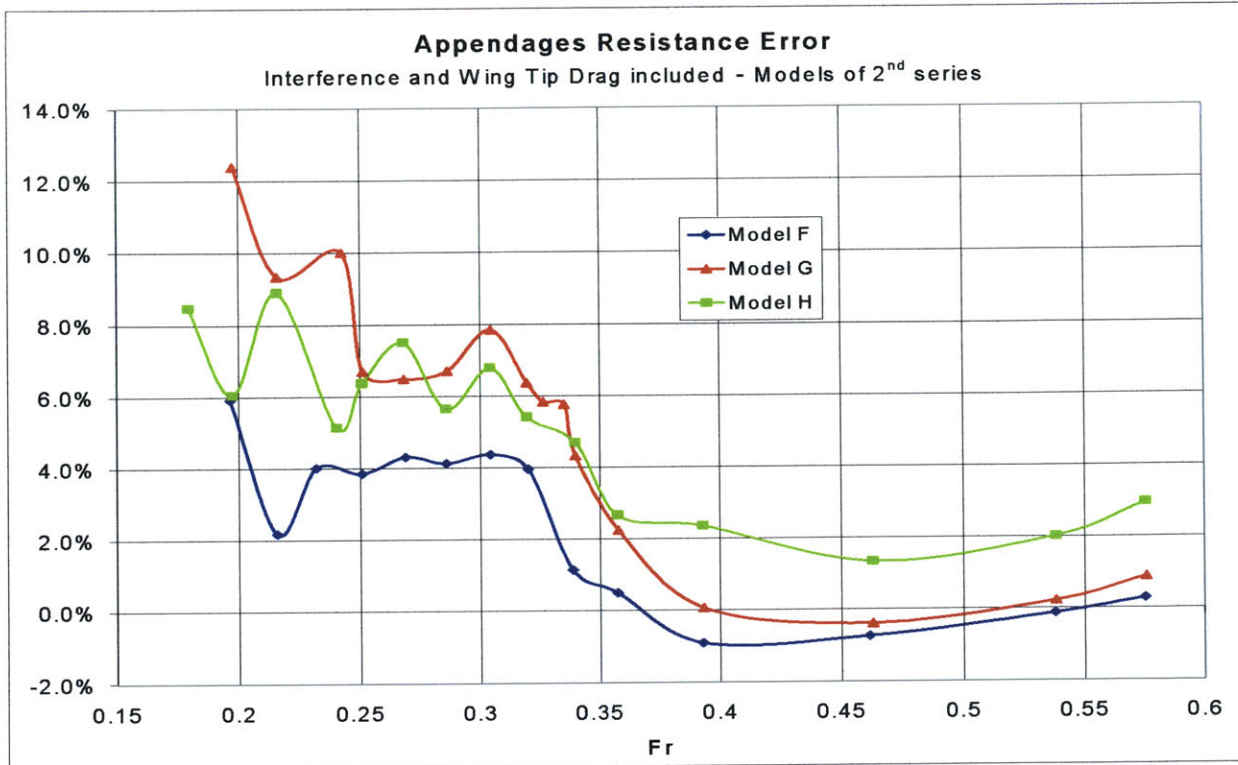
Figure 5.2 Error in appendages resistance when interference and wing tip drag are included.

In deep water, the length λ of a wave that is moving at speed U is given by

$$\lambda = \frac{2\pi U^2}{g}$$

Eq. 5.3

where g is the gravity acceleration. If Eq. 5.3 is divided by the boat length L, it becomes

$$\frac{\lambda}{L} = \frac{2\pi U^2}{gL} = 2\pi Fr^2$$

Fr being the Froude number. When the Froude number is equal to 0.375 and 0.4, the drop in error happens, and the wavelength-boat length ratio is equal to 0.88 and 1, respectively. The keel is located, in all the models, at about midship, which means at about 6.2 m full scale from the stern for the first series and about 10.4 m full scale for the second series. This means that, at that particular speed, the wave generated by the keel has a trough right under the stern, thus increasing considerably the total wave resistance of the boat. The increase, however, is not directly due to the appendage resistance, but rather to the interactions. Currently these interactions are not explicitly modeled in the prediction program.

5.2 Canoe Body Residuary Resistance

As described in 4.3 and shown in Figure 4.15 to Figure 4.20, the IMS residuary resistance multipliers are not able to predict with sufficient accuracy the change in residuary resistance due to heel. From a hydrodynamic point of view, two things happen when a boat heels: the value of the parameters that describe the hull shape changes, and the immersed hull is no longer symmetric with respect to the centerline. The change in wave drag due to heel, then, can be seen as the sum of two contributions: the first one caused by the change in the parameter values and the second caused by the asymmetry of the hull. If the latter contribution is assumed to be small in comparison with the first one, then a robust and reliable formula for the upright residuary resistance should give good predictions also for the heeled resistance when the heeled hull parameters are used as inputs. Based on this idea, the objective was set to find a unique formula that applies to both the upright and the heeled condition, where, however, the input parameters are those proper of the hull in the desired position.

The first step was to check how the current formulation performs when used in this manner. The necessary input parameters are calculated from the hull characteristic dimensions at different heel angles found in the LPP output. The results were not any better than the ones given by the multipliers, but it was thought that the poor agreement with the experiments might be caused by the fact that the coefficients were optimized for the upright case. So, it was decided to find a better set of coefficients, and to do this, a spreadsheet, a part of which is shown in Table 5.1, was created to look at the contribution to C_R of each single term in Eq. 2.5.

		Constant	Cp	BTR	L/Vol^(1/3)	WPA/Vol^(2/3)	LCB/Lvol	LCB^2/Lvol	Lvol^2	Total
					Current set of coefficients					
Model 5	Upright	54.511	-20.567	4.103	-14.939	-6.753	-2.700	1.055	1.842	16.551
	15 Deg.	54.511	-20.283	3.591	-15.066	-6.535	-4.517	2.977	1.873	16.552
	25 Deg.	54.511	-20.150	3.113	-15.077	-6.297	-4.160	2.527	1.876	16.343
Model 4	Upright	54.511	-20.529	3.292	-14.924	-5.997	-2.663	1.025	1.838	16.552
	15 Deg.	54.511	-20.321	3.067	-15.032	-5.928	-4.599	3.079	1.865	16.643
	25 Deg.	54.511	-20.150	2.840	-15.090	-5.876	-4.051	2.398	1.879	16.461
Model 6	Upright	54.511	-20.681	5.172	-14.968	-7.679	-2.431	0.857	1.849	16.630
	15 Deg.	54.511	-20.340	4.129	-15.115	-7.156	-4.181	2.559	1.886	16.293
	25 Deg.	54.511	-20.226	3.321	-15.063	-6.667	-3.660	1.955	1.873	16.043
Model F	Upright	54.511	-20.719	3.629	-17.530	-6.944	-3.914	2.601	2.536	14.171
	10 Deg.	54.511	-20.567	3.459	-17.606	-6.872	-6.256	3.816	2.558	13.042
	20 Deg.	54.511	-20.264	3.108	-17.703	-6.724	-6.256	3.816	2.587	13.074
	25 Deg.	54.511	-20.150	2.943	-17.699	-6.658	-6.256	3.816	2.586	13.091
	30 Deg.	54.511	-20.063	2.816	-17.659	-6.622	-6.123	3.816	2.574	13.248
Model G	Upright	54.511	-20.681	3.023	-17.527	-6.326	-3.906	2.589	2.535	14.219
	10 Deg.	54.511	-20.529	2.960	-17.610	-6.327	-6.256	3.816	2.560	13.123
	20 Deg.	54.511	-20.302	2.823	-17.688	-6.354	-6.256	3.816	2.582	13.133
	25 Deg.	54.511	-20.150	2.764	-17.698	-6.383	-6.256	3.816	2.585	13.187
	30 Deg.	54.511	-20.063	2.731	-17.677	-6.442	-6.184	3.816	2.579	13.270
Model H	Upright	54.511	-20.719	4.311	-17.510	-7.584	-3.945	2.639	2.531	14.234
	10 Deg.	54.511	-20.529	3.984	-17.596	-7.428	-6.256	3.816	2.555	13.057
	20 Deg.	54.511	-20.226	3.382	-17.657	-7.105	-6.256	3.816	2.573	13.037
	25 Deg.	54.511	-20.075	3.127	-17.621	-6.963	-6.256	3.816	2.563	13.101
	30 Deg.	54.511	-20.063	2.935	-17.533	-6.863	-6.256	3.816	2.537	13.084

Table 5.1 Calculated values for terms in Eq. 2.5 for $Fr = 0.4$.

a_0	54.5110
a_1	-37.8769
a_2	0.8530
a_3	-2.4344
a_4	-1.0685
a_5	-7.5650
a_6	1.3493
a_7	0.0489

Table 5.2 Values of the coefficients a_i of Eq. 2.5.

The reported values are for a Froude numberk of 0.4 (values have been computed for other Fr as well) and are the product of the boat parameter and the corresponding IMS coefficient given in Table 5.2. As shown, for this particular Froude number, the residuary resistance coefficient is obtained by starting from a constant term almost six times bigger and subtracting relatively large numbers. For some different Fr, the constant term a_0 has even a negative value. This is a poor numerical practice, which makes the errors propagate fast; in fact, for example, for Model 5 in upright position, an error in the evaluation of the prismatic coefficient of 0.0045 results in an error in the residuary resistance of more than 1%.

Since at a given Fr all the boat have a similar value of resistance per unit weight, it was decided, in the new set of coefficients, to assign to a_0 the average measured value of C_R, and then find the other a_i's that best fit the difference between the average resistance coefficient and the actual value for each boat. Because this difference is small for all the cases, it was hoped that, using a least squares method, the coefficients would have a value such that the corresponding contribution to C_R would be small compared to that of a_0. It turned out not to be the case, even though the results with the new coefficients were considerably better than the previous ones. Figure 5.3 and Figure 5.4 show the results for Model 5 for 15° and 25° heel, respectively. The lines labeled "IMS" are the multipliers currently used in the VPP, while the lines labeled as "New" are the ratios calculated using the upright formula with heeled parameters with the original coefficients. The "New Coeff" lines represent the ratios with the recalculated set of coefficients.

It appeared, at this point, that a more radical modification was needed to improve the VPP prediction capabilities. The two options available were either to keep on trying to modify the present formulation, maybe adding more terms to it, or to start from zero and come up with a new, more simple and intuitive formulation. It was decided for the second option.

5.2.1 New Formulation

The difference in residuary resistance (RR) per unit weight, at a given Froude number, between two boats, A and B, depends on the differences in the geometry of the hulls. Mathematically these differences are better represented by the change in value of the parameters rather than by their absolute values. So, it was decided to write

50

$$\left(1000\frac{RR}{\Delta}\right)_A - \left(1000\frac{RR}{\Delta}\right)_B = f\left(C_{P,A} - C_{P,B}, \left(\frac{B}{T}\right)_A - \left(\frac{B}{T}\right)_B, \left(\frac{L}{\nabla^{1/3}}\right)_A - \left(\frac{L}{\nabla^{1/3}}\right)_B\right)$$

Eq. 5.4

where only the prismatic coefficient, the beam-draft ratio, and the length-volume ratio are used as parameters because they are believed to be, together with weight, the main drivers of the wave drag. The reduced number of parameters allowed keeping the formulation, at least initially, as simple as possible. Again, because of simplicity, the function f was, at first, taken to be linear, leaving the possibility to correct it later with high order terms, if necessary. So, Eq. 5.4 was rewritten as

$$\left(1000\frac{RR}{\Delta}\right)_A = \left(1000\frac{RR}{\Delta}\right)_B + b_1\left(C_{P,A} - C_{P,B}\right) + b_2\left[\left(\frac{B}{T}\right)_A - \left(\frac{B}{T}\right)_B\right] + b_3\left[\left(\frac{L}{\nabla^{1/3}}\right)_A - \left(\frac{L}{\nabla^{1/3}}\right)_B\right]$$

Eq. 5.5

b_1, b_2, and b_3, represent the rates of change in residuary resistance per unit weight with prismatic coefficient, beam-draft ratio and length-volume ratio, respectively, and are function of the Froude number.
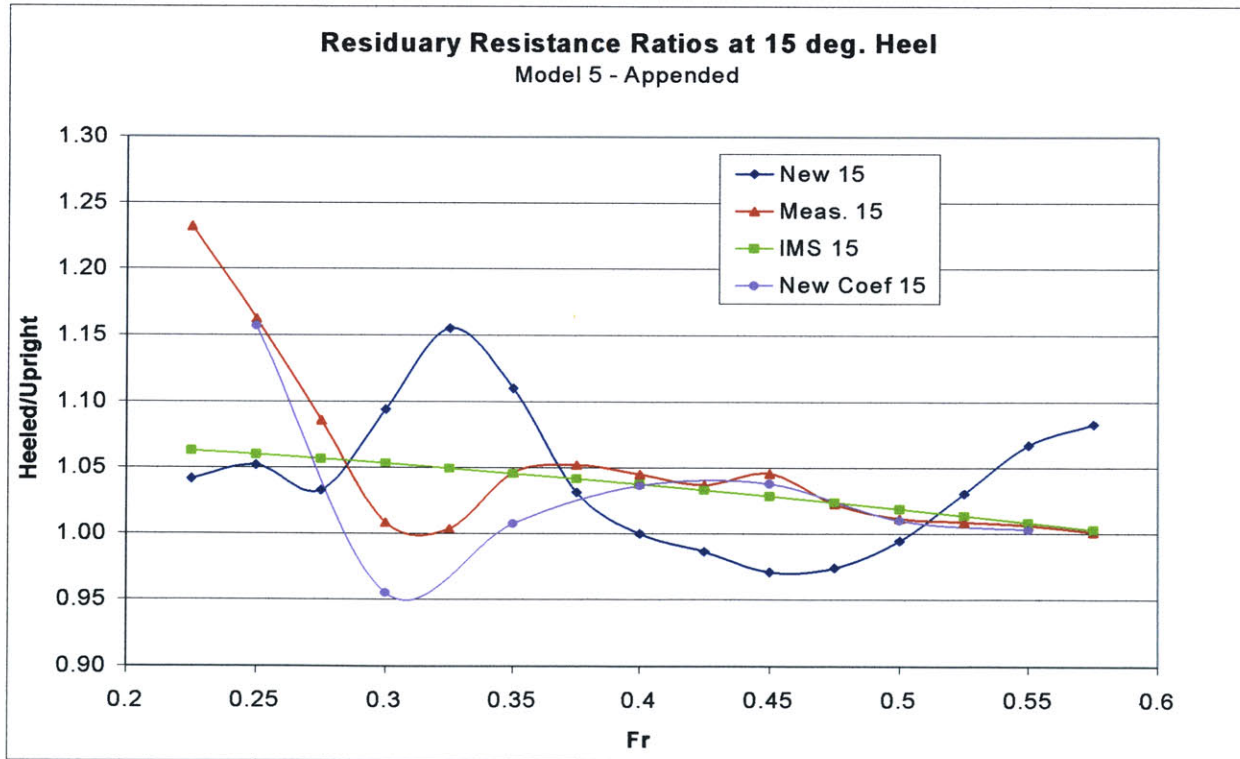

Figure 5.3 Comparison of heeled-to-upright residuary resistance ratios for Model 5.
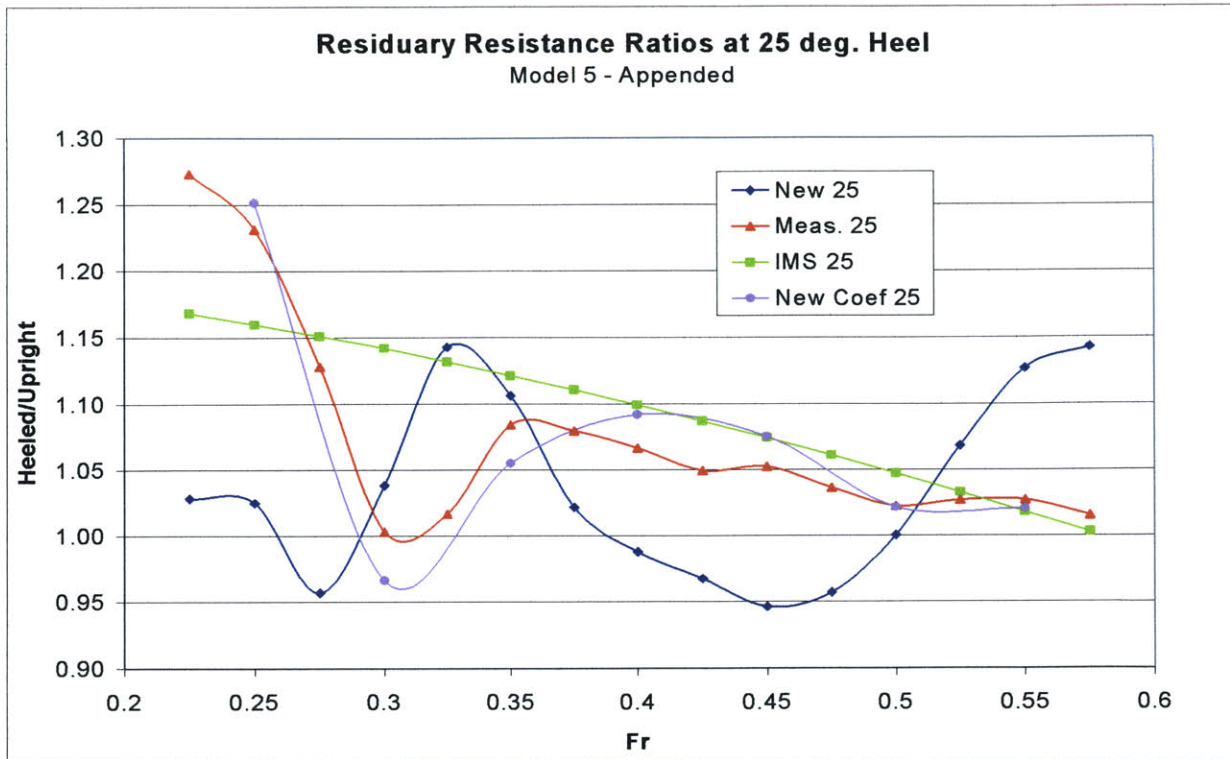
Figure 5.4 Comparison of heeled-to-upright residuary resistance ratios for Model 5.

Instead of using some statistically determined values for the three coefficients, it was decided to try to determine them from part of the experimental data available. On the same line, it was decided to use Model 5 in the upright position as boat B, or base boat, and to calculate the residuary resistance per unit weight for all the other models at any heel angle as a variation from the value for Model 5 upright.

The first coefficient to be determined was b_2. Mathematically, this coefficient can be thought as the partial derivative of the residuary resistance per unit weight with respect to beam-draft ratio, evaluated at B/T of the base boat B, while prismatic coefficient and length-volume ratio are held constant. Because for the three models of the IMD series, when upright, the latter two parameters assume similar values, as seen in Table 5.3. The experimental data of these models were used to find the best approximation for b_2. First the measured resistance was interpolated using cubic splines at the Froude numbers used by the VPP. Then the data points were fitted with parabolas, one for each Fr, whose equations, shown in Figure 5.5 next to the corresponding key in the legend, were used to determine the value of the derivative at the beam-draft ratio of Model 5. The calculated values are reported in the first column of Table 5.4.

The determination of the coefficient b_3 was even trickier and required making bigger approximations. In fact to find the dependency of the residuary resistance on the length-volume ratio from the experiments, it is necessary to correct the data for the same beam-draft ratio, as this parameter covers a wide range of values for the different boats. Moreover, the models of the IMD series have values of $L/\nabla^{1/3}$ too close to each other to give reliable results for the coefficient.

		Cp	BTR	L/Vol^(1/3)
Model 5	Upright	0.543	4.810	6.137
	15 Deg.	0.536	4.211	6.189
	25 Deg.	0.532	3.649	6.193
Model 4	Upright	0.542	3.859	6.131
	15 Deg.	0.537	3.596	6.175
	25 Deg.	0.532	3.329	6.199
Model 6	Upright	0.546	6.063	6.148
	15 Deg.	0.537	4.841	6.209
	25 Deg.	0.534	3.893	6.188
Model F	Upright	0.547	4.255	7.201
	10 Deg.	0.543	4.055	7.232
	20 Deg.	0.535	3.644	7.272
	25 Deg.	0.532	3.450	7.271
	30 Deg.	0.530	3.301	7.254
Model G	Upright	0.546	3.544	7.200
	10 Deg.	0.542	3.470	7.234
	20 Deg.	0.536	3.310	7.266
	25 Deg.	0.532	3.240	7.270
	30 Deg.	0.530	3.202	7.261
Model H	Upright	0.547	5.054	7.193
	10 Deg.	0.542	4.671	7.228
	20 Deg.	0.534	3.965	7.253
	25 Deg.	0.530	3.666	7.239
	30 Deg.	0.530	3.441	7.202

Table 5.3 Upright and heeled parameter for all the models.

So, it was decided to use the upright data for both series and to fit the points at each Fr with a straight line, as shown in Figure 5.6. The slope of the line, then, gives the desired value for the coefficient, as reported in the second column of Table 5.4. The derivative of residuary resistance with prismatic coefficient, b_1, could not be found using again the same data, since this time it would require two corrections. The values were then derived using data from Taylor Standard Series, but, once more, it meant making approximations. In fact all the models have a beam to draft ratio much larger than 3.75, which is the highest value available in Taylor's work. Also, because the derivatives had to be calculated from values read from a printed graph, the accuracy is not very high. Furthermore, the tables are given for speed-length ratios that often do not coincide with the Froude numbers used in this work, thus requiring some sort of interpolation. The values obtained, shown in the third column of Table 5.4, are for a limited range of Fr because the highest speed-length ratio available was 1.4, which corresponds to a Fr of 0.4163.

The experimental data for Model 1 has, so far, never been used so that, at this point, it can be used to verify the goodness and accuracy of the newly developed formulation. Starting from the measured residuary resistance per unit weight of Model 5, the values at each Froude number were corrected accordingly to Eq. 5.5, using the coefficients in Table 5.4. Figure 5.7 compares the measured resistance with IMS VPP prediction ("IMS" labeled line) and with the new model formulation before any correction ("Starting NM") and after each correction ("NM BTR", "NM LVR", and "New Model").
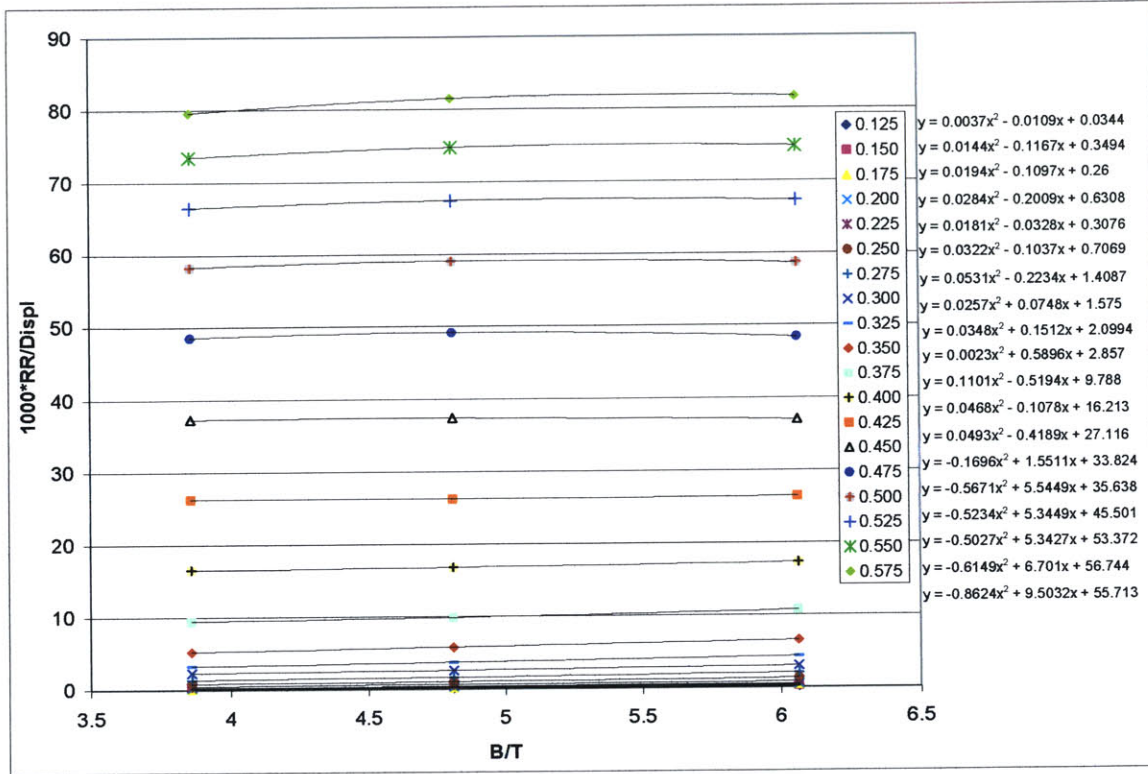
The legend for Figure 5.5 (markers):
- ♦ 0.125
- ■ 0.150
- ▲ 0.175
- ✕ 0.200
- ✳ 0.225
- ● 0.250
- + 0.275
- ✕ 0.300
- − 0.325
- ♦ 0.350
- ▢ 0.375
- + 0.400
- ■ 0.425
- △ 0.450
- ● 0.475
- ♦ 0.500
- + 0.525
- ✴ 0.550
- ♦ 0.575

Equations (Figure 5.5):

$y = 0.0037x^2 - 0.0109x + 0.0344$
$y = 0.0144x^2 - 0.1167x + 0.3494$
$y = 0.0194x^2 - 0.1097x + 0.26$
$y = 0.0284x^2 - 0.2009x + 0.6308$
$y = 0.0181x^2 - 0.0328x + 0.3076$
$y = 0.0322x^2 - 0.1037x + 0.7069$
$y = 0.0531x^2 - 0.2234x + 1.4087$
$y = 0.0257x^2 + 0.0748x + 1.575$
$y = 0.0348x^2 + 0.1512x + 2.0994$
$y = 0.0023x^2 + 0.5896x + 2.857$
$y = 0.1101x^2 - 0.5194x + 9.788$
$y = 0.0468x^2 - 0.1078x + 16.213$
$y = 0.0493x^2 - 0.4189x + 27.116$
$y = -0.1696x^2 + 1.5511x + 33.824$
$y = -0.5671x^2 + 5.5449x + 35.638$
$y = -0.5234x^2 + 5.3449x + 45.501$
$y = -0.5027x^2 + 5.3427x + 53.372$
$y = -0.6149x^2 + 6.701x + 56.744$
$y = -0.8624x^2 + 9.5032x + 55.713$

Figure 5.5 Residuary resistance per unit weight as function of B/T for different Fr.

The legend for Figure 5.6 (markers):
- ♦ 0.2
- ■ 0.225
- ▲ 0.25
- ✕ 0.275
- ✳ 0.3
- ● 0.325
- + 0.35
- ✕ 0.375
- ■ 0.4
- ◇ 0.425
- ▢ 0.45
- △ 0.475
- ✕ 0.5
- ✳ 0.525
- ● 0.55
- + 0.575

Equations (Figure 5.6):

$y = 0.0743x - 0.1121$
$y = 0.1316x - 0.2249$
$y = 0.1664x - 0.0418$
$y = 0.2556x + 0.036$
$y = 0.235x + 1.1081$
$y = 0.2154x + 2.3373$
$y = 0.0055x + 5.7126$
$y = -0.7263x + 14.385$
$y = -1.5857x + 26.551$
$y = -3.7493x + 49.299$
$y = -7.193x + 81.377$
$y = -11.132x + 117.06$
$y = -14.458x + 147.42$
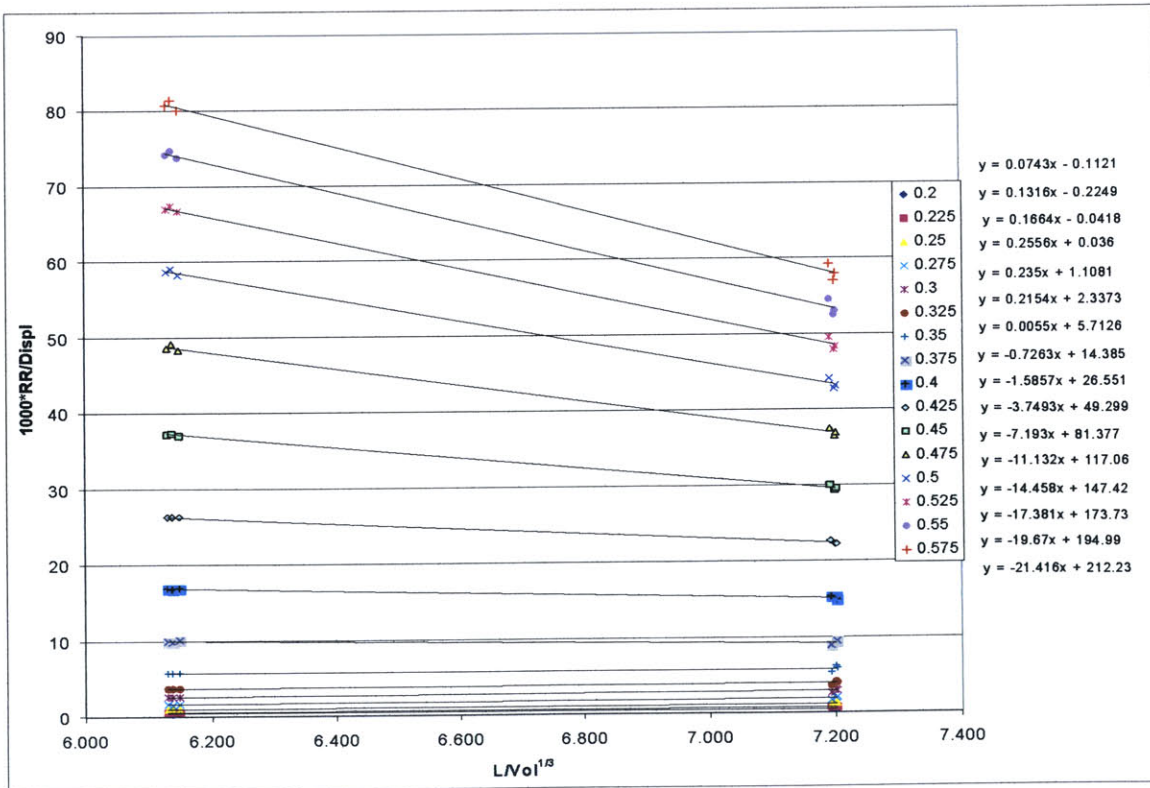$y = -17.381x + 173.73$
$y = -19.67x + 194.99$
$y = -21.416x + 212.23$

Figure 5.6 Residuary resistance dependence on length-volume ratio at different Fr.

Fr	D Cr / D BTR	D Cr / D LVR	D Cr / D Cp
0.125	2.469E-02		
0.15	2.183E-02		
0.175	7.693E-02		
0.2	7.231E-02	7.430E-02	-2.000E-01
0.225	1.413E-01	1.316E-01	-7.500E-01
0.25	2.061E-01	1.664E-01	-2.500E+00
0.275	2.874E-01	2.556E-01	0.000E+00
0.3	3.220E-01	2.350E-01	4.300E+00
0.325	4.860E-01	2.154E-01	1.550E+00
0.35	6.117E-01	5.500E-03	-7.400E+00
0.375	5.398E-01	-7.263E-01	-4.000E+01
0.4	3.424E-01	-1.586E+00	-1.175E+02
0.425	5.537E-02	-3.749E+00	
0.45	-8.045E-02	-7.193E+00	
0.475	8.940E-02	-1.113E+01	
0.5	3.098E-01	-1.446E+01	
0.525	5.067E-01	-1.738E+01	
0.55	7.857E-01	-1.967E+01	
0.575	1.207E+00	-2.142E+01	

Table 5.4 Values of b_1, b_2, and b_3 at different _Fr_.

The error plotted in the relative difference with respect to the measured residuary resistance; when calculated as percentage of the total resistance, especially at low and medium speed the values are much lower. As seen, the new model behaves considerably better than the current IMS formulation, in particular the beam-draft ratio and the length-volume ratio correction seems to go in the right direction.

As stated at the beginning of this section, the objective was to find a formula that applied to both upright and heeled condition. Verified that the new model is an improvement at zero heel angle, it still needed to be put to the test at heeled condition. Figure 5.8 shows that the new model is a definite improvement for the 15° heel angle case, in particular at low and medium speeds. For 25° heel angle, the new model predictions are not better than the IMS predictions.

Overall the method appears to be a step forward in the right direction. A partial confirmation of this comes from the comparison of the VPP prediction error (Lines in Figure 5.9 and Figure 5.10 labeled as "IMS – M...") with the error of the new model (lines labeled "Model ...") for all the other models in upright position. It was, in fact, somewhat expected that Model 4 and Model 6 would be better predicted, since their experimental data was used in finding the coefficients of Eq. 5.5. The models of the series tested in England, instead were used only for one of the coefficients, but still their predictions, in particular at medium and high speeds where most of the resistance is due to waves, are significantly better than the IMS predictions.

When looking at non-zero heel angle cases, the results are not as good. Figure 5.11 shows the results for 15° for the IMD series models, where it is still possible to see a small improvement. At 25° heel (Figure 5.12), the results are more difficult to interpret, in fact, while the prediction for Model 4 and Model 5 seem a step forward, the one for Model 6 is not better than the IMS one.
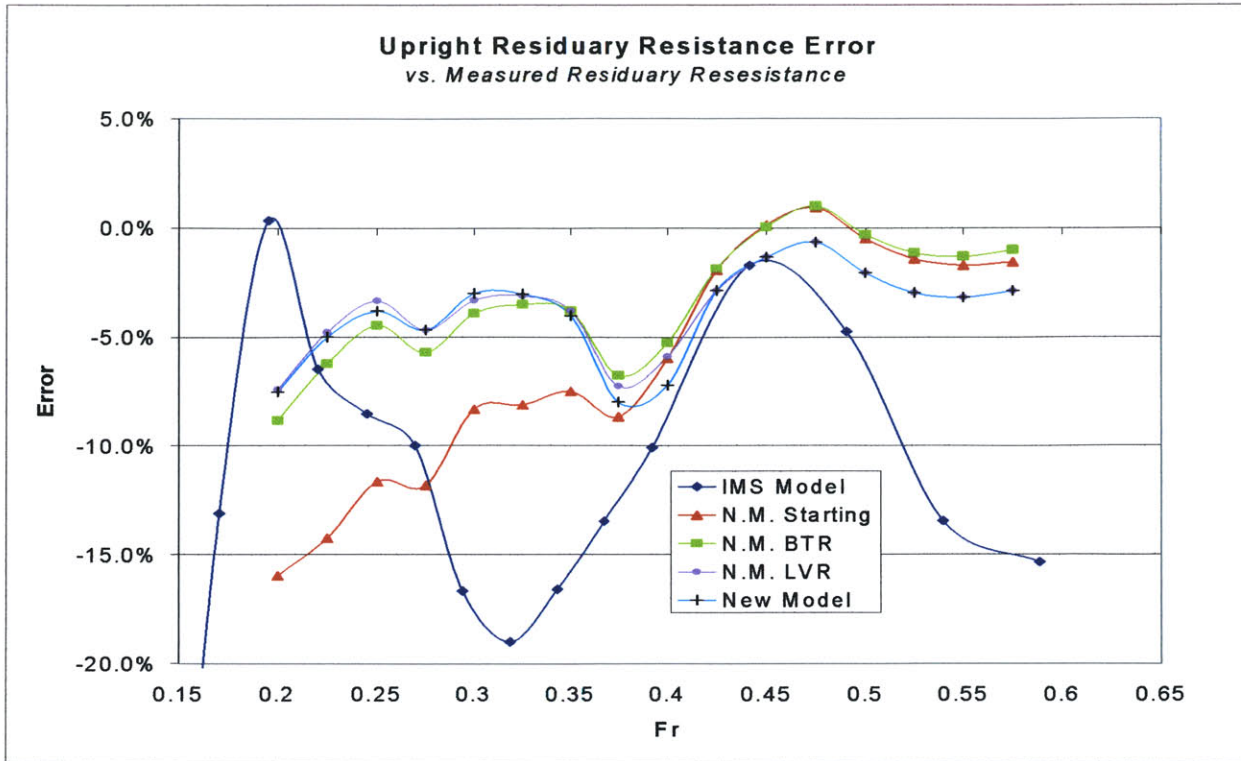
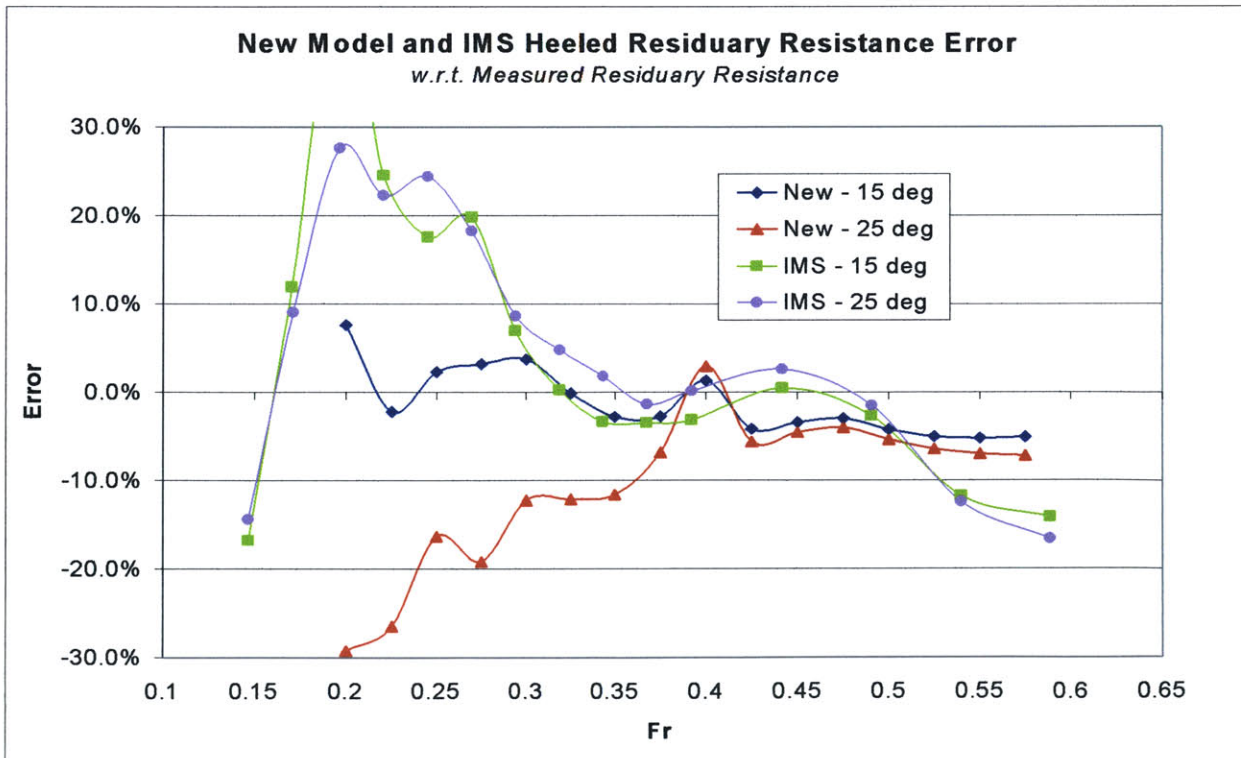**Figure 5.7 New model and IMS formulation comparison for Model 1.**

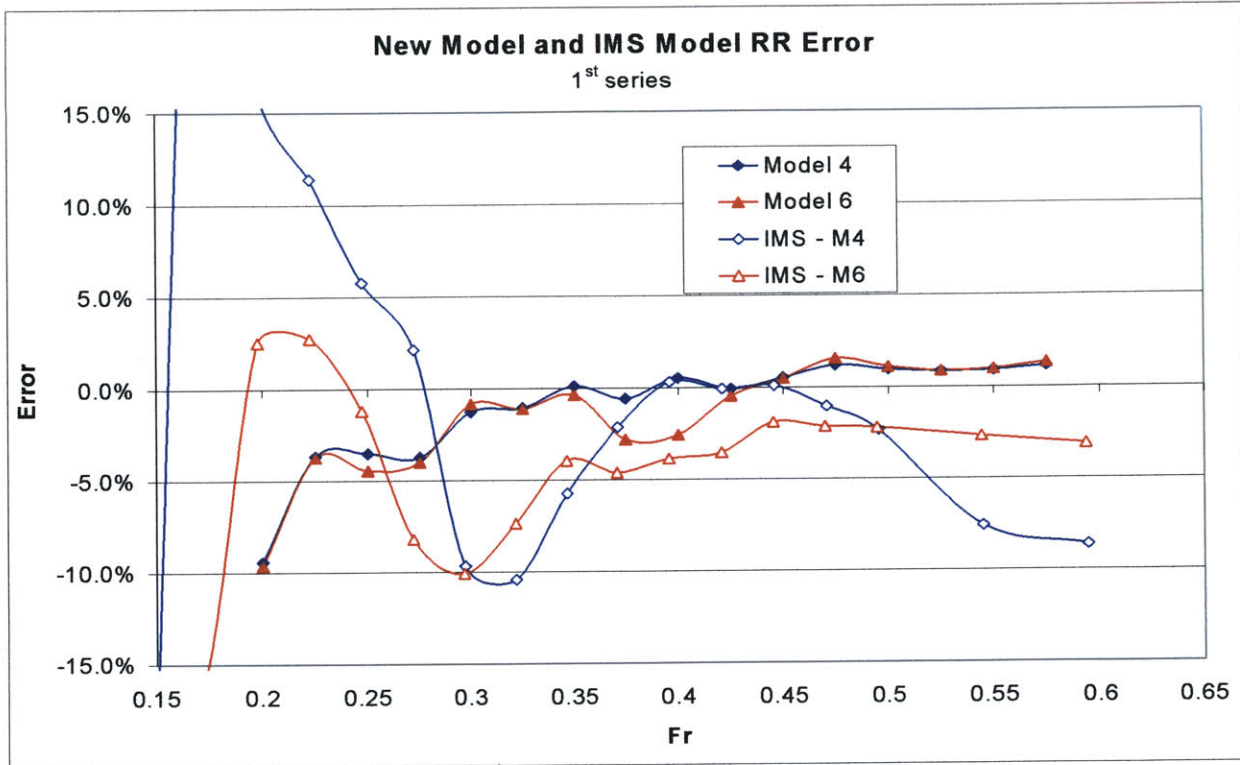**Figure 5.8 Heeled residuary resistance error for Model 1.**

56

Figure 5.9 Upright residuary resistance error comparison.
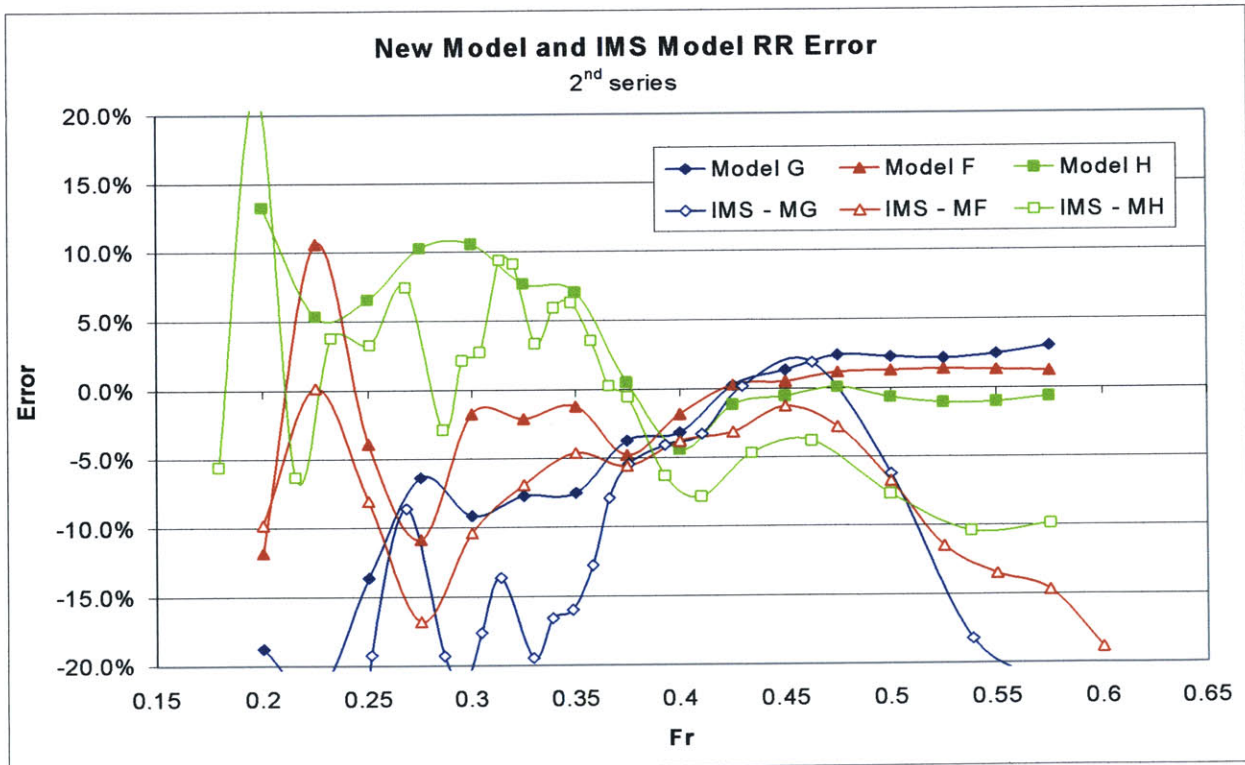

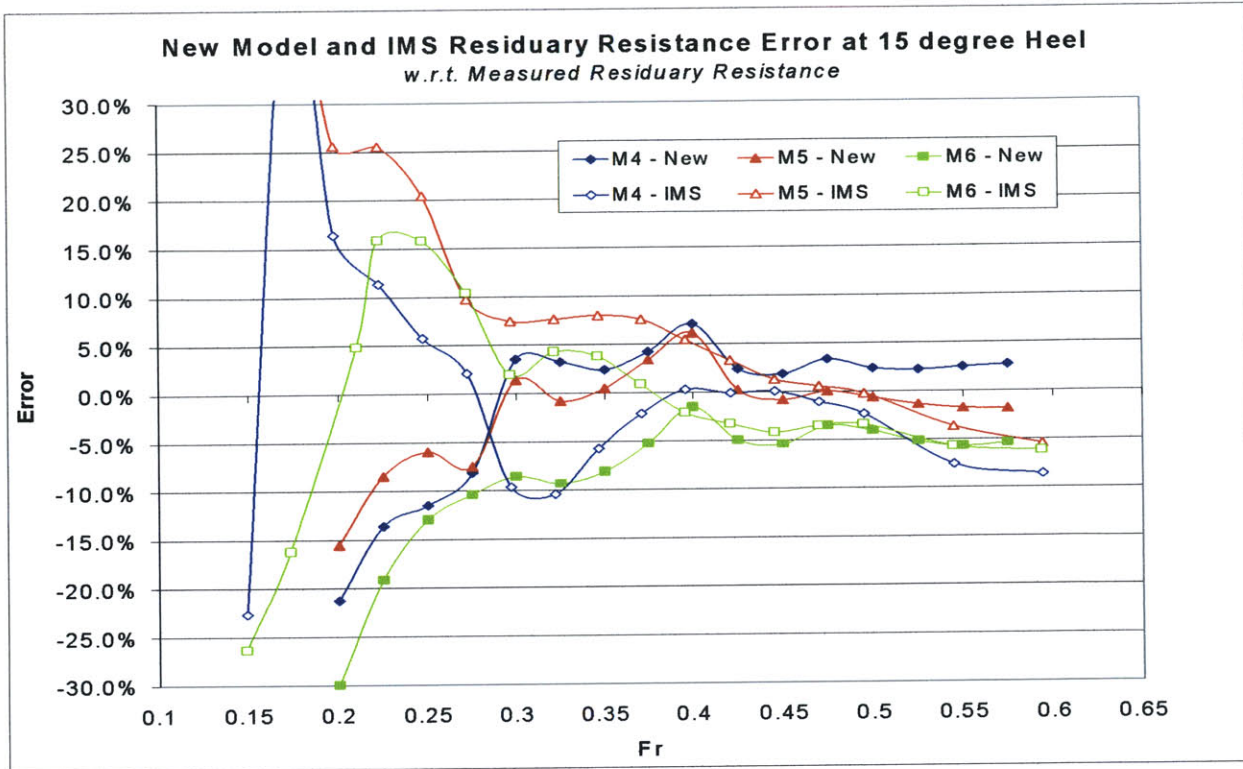**Figure 5.10 Upright residuary resistance error comparison.**

Figure 5.11 Residuary resistance error comparison at 15° heel.
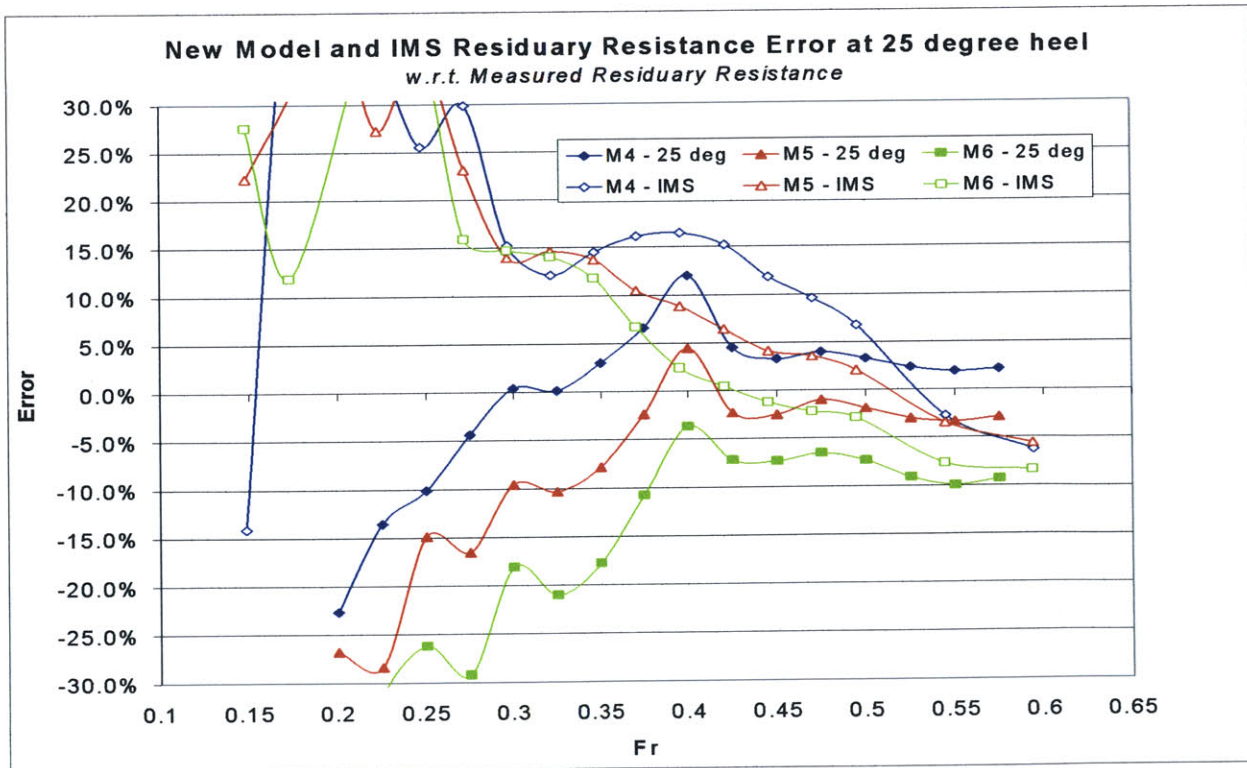

Figure 5.12 Residuary resistance error comparison at 25° heel.

6. Conclusions

The IMS Velocity Prediction Program has been, in this work, analyzed to the maximum extent allowed by the limited amount of experimental data available. A more complete set of measurements would have been particularly helpful in the development of the new formulation of the residuary resistance model.

6.1 Appendage Resistance

The viscous part of the resistance, for both appendages and canoe body, appears to be well represented in the VPP. In fact, the errors found in the portion of the appendage are not directly related to the model, but rather to imprecise evaluations of the keel and rudder characteristic dimensions by the LPP.

The appendage residuary resistance, instead, is usually overestimated by the IMS VPP at low speeds. When the Froude number is increased past 0.4, the error suddenly drop to negative values, suggesting that a rapid increased in resistance, possibly due to interactions between the appendages wave pattern and the canoe body wave pattern, is not captured sufficiently well.

The induced drag is predicted with fairly good accuracy in normal sailing conditions; however, in high-lift coefficient situations, such as coming out of a tack, the increase in drag calculated in the model is usually bigger than the measured, in particular at non-zero heel angles.

6.2 Canoe Body Resistance

The residuary resistance model for the canoe body is undoubtedly the major source of errors. For the heeled cases, the model always predicts an increase in resistance, except at very high speed when the multipliers can assume a value less than unity. The measurements, though, show that the change in resistance due to heel is not always positive nor is a monotonic decreasing function of the Froude number.

The upright formula is believed to have two flaws: the first one, of numerical nature, is that the residuary resistance per unit weight is obtained as a linear combination of several parameters, whose corresponding coefficients were determined statistically. The result is that rather large positive and negative numbers are added to obtain a smaller one. This allows the error to propagate fairly quickly. The second defect, somewhat related to the first one, is that some of the terms do not have a physical meaning. From a hydrodynamic point of view, the residuary

resistance per unit weight is largely dependent on speed with correction terms that depend on the geometry of the hull. However, this is not reflected in the VPP formulation, where the term that depends solely on speed (a_0) can even have negative values.

The approach taken in this study for the proposed new model was to try to translate the physics into mathematical terms. The result is a formula that is a sort of Taylor expansion of the resistance around a base boat, Model 5. Despite the crudeness of the new model and the numerous approximations made to find the necessary coefficients, this was found to perform at least as well as the IMS model, and in some cases, namely when the boat is in upright position, even considerably better. This, however, does not mean that the model is ready to be implemented in the VPP. It needs further development and testing, but it seems that with it a promising way to achieve a higher accuracy has been identified.

6.3 Future Work

As already stated, the biggest limitation in conducting this study has been the limited amount of data available. Both available series of models, in fact, are beam variation series, therefore the beam to draft ratio is the only parameter that had a wide range of tested values. The fact that the two series have very different displacements was used to get a feeling of the change in resistance with length-volume ratio. Certainly at least a series of sailing-yacht-shaped models with a systematic variation of the prismatic coefficient is needed to find a better set of coefficients than the one obtained for Taylor Standard Series, which is for battleship hull forms. More measurements in heeled conditions will help understand whether the residuary resistance formula needs to have a term directly dependent on the heel angle added. A more complete database would also give more confidence in the measurements themselves; in fact, if some of the larger oscillations, seen in some of the error plots, are caused by imprecise measurements that would be easily identified.

6.4 Acknowledgements

Bibliography

- A. Claughton. *"Developments in the IMS VPP formulations"*. In Proceedings of the Fourteenth Chesapeake Sailing Symposium, Society of Naval Architects and Marine Engineers, 1997...9
- IMS Velocity Prediction Program. From source files of the official IMS VPP 10
- J.E. Kerwin. *"A velocity prediction program for ocean racing yachts, revised to June 1978"*. H. Irwing Pratt Project Report n. 78-11, Massachusetts Institute of Technology, Cambridge, MA, 1978. 10
- J.K. Milgram. *"Naval architecture technology used in winning the 1992 America's Cup match"*. Society of Naval Architects and Marine Engineers Transactions, 1993 6
- ORC, Ocean Racing Council. *"History of the IMS"*. From the Offshore Racing Council website, www.orc.org. 6
- S.F. Hoerner. *"Fluid Dynamic Drag"*. Hoerner, 1965. 22
- T.A. Hodgson. *"History of the Class: shape takes form"*. from the National C Scow Sailing Association website, www.ncssa.org. 5